The Kitaev Model on Surfaces with Lattice Defects and of Higher Genus

John Brennan

B.Sc.

Thesis presented for the degree of

Doctor of Philosophy

to the

National University of Ireland Maynooth

Department of Theoretical Physics

February 2018

Department Head

Dr. Jon-Ivar Skullerud

Research advisor

Dr. Jiří Vala

To my parents

Contents

Declaration

This thesis has not been submitted in whole, or in part, to this or any other university for any other degree and is, except where otherwise stated, the original work of the author.

John Brennan, 28 February 2018

Acknowledgements

Firstly, I would like to express my appreciation to my supervisor Jiří Vala for his help and advice over the last four years. I would like to thank Graham Kells, Paul Watts and Mikael Fremling for many inspiring discussions and insightful comments. My sincere thanks also go to Jon-Ivar Skullerud and Monica Hart for their hard work in running the department. I also acknowledge financial support from the Science Foundation Ireland through the Principal Investigator Award 10/IN.1/I3013.

I would like to thank Aoife Kelly, Darragh Miller, Aonghus Hunter-McCabe and Stephen Nulty for providing a fun office, which often felt like a second home, and many interesting scientific and unscientific conversations. I also thank Domenico Pellegrino, Aaron Conlon, Kevin Kavanagh, Kenneth Granahan and James Smith for making the department a great and friendly place to work.

I thank my friends Alan Heffernan, Lorcan Moore, Brian Kelly, Neil O'Donnell, Sean O'Connor, Barry Murphy, Criag Carri and Gordon Bond for all the fun times we have had over the years. A special thank you goes to Gary O'Connor and Róisín Mhaoláin for being great house mates on top of being good friends. My thanks also go to my friends and classmates: Jack McDonnell, Alexei Kudryashov, Aisling McGlinchey, Emma Berry, Eoin Rock and Joe Flavin for all the good times we have had. I would also like to thank my close friend Petar Stefanov for all the time spent over the years eating dinner and watching the big bang theory.

Last but not least, I would like to thank my family: Matthew, Veronica, Conor, Pauric, Joe and Christopher for always supporting me in everything I do.

Chapter 1

Introduction

The quantum phase of a physical system is defined as its ground state. As examples of quantum phases we mention superfluids, superconductors, Bose-Einstein condensates and quantum Hall states. Different phases of a system originate from the different ways a systems' constituents can be organised or, in other words, the different orders of the system. Landau had the insight that the difference between two phases can be attributed to the corresponding orders having different symmetries [1]. Also, the transition between phases can be associated with the breaking of symmetries. This insight led to Ginzburg and Landau describing orders using local order parameters and developing a general theory of phase transitions based on symmetry breaking. This theory was successful in describing a large number of observed phases of matter. However, phases of matter have been discovered which cannot be described using a local order parameter and Landau's theory of symmetry breaking known as topological phases.

For example, in 1982 Robert Laughlin, Horst Störmer, and Daniel Tsui discovered that a two dimensional electron gas confined to the interface of two different semiconductors at low temperatures and under a strong magnetic field form a highly correlated state [2]. However, due to the small mass of electrons, quantum fluctuations are strong enough to prevent the electrons from forming a crystal lattice and so this highly correlated state behaves more like a liquid. This phase of a system of electrons is known as a fractional quantum

hall state and it is an example of a phase whose internal ordering cannot be described using a local order parameter. Such phases are said to possess a topological order [3, 4, 5, 6] and are called topological phases. Topological order was proposed in a study of chiral spin liquids [7] and the first experimentally observed topological phase was the superconducting phase of helium discovered in 1911 [8].

Specifically, for lattice models, topological order is defined to describe gapped quantum phases that cannot be deformed into a product state without a gap-closing phase transition [9]. Such quantum phases are said to have long range entanglement which is the microscopic origin of topological order. A gapped state that can be smoothly deformed into a product state is short range entangled and has no topological order. In particular, a product state has no topological order. We define topological order via observable characteristics which are generally non-local and are called topological invariants.

One of the key characteristics of systems in topological order is a ground state degeneracy that depends on the topology of the manifold the system is defined on and is robust under continuous deformations of that manifold. This is usually referred to as topological degeneracy. Unlike other degeneracies that may occur in the spectrum of a system, topological degeneracy is not necessarily the result of a symmetry of the system's Hamiltonian since it must be robust under small perturbations that can break any symmetry of the system. Therefore the ground state degeneracy is a quantum number that can be used to characterize a system's topological order.

However, the degeneracy of the ground state may only partially characterise a system's topological order. To completely characterise it one may also need to examine defects of the order. The types of defects that can occur and the properties they can have depend on the internal order of the system. So we can make a more complete measurement of topological order by examining its defects as well as the ground state degeneracy. Defects in a topological order are quasiparticles which can have a variety of interesting properties, particularly

if the system under consideration is two dimensional like fractional quantum hall systems mentioned above. In this case, the quasiparticles of the system can carry an electric charge that is a fraction of the charge carried by the constituent electrons. On top of that, these quasiparticles obey unusual statistics known as fractional statistics. Unlike regular bosons or fermions whose quantum state is multiplied by 1 or -1 under an exchange of two particles, the state of the system may be multiplied by any complex phase $e^{i\theta}$ under the exchange of two quasiparticles. Quantum numbers like these (fractional charge and fractional statistics) reflect the internal structure of a quasiparticle. Thus topological orders can also be characterised by the quantum numbers of their quasiparticles.

While the general mathematical theory behind topological orders is still an active area of research, progress has been made which reveals a deep connection between these topological orders and areas of mathematics which are still under development [10, 11]. Witten discovered a new class of field theories in 1989 whose behaviour is independent of the metric of the underlying space-time [12]. The metric independence of these theories implies their behaviour can only depend on the topology of the underlying space-time and so these theories are called topological quantum field theories. Topological quantum field theories turn out to effectively describe the low energy regime of matter in a topological phase [13] and can be defined axiomatically as a functor from the category of n-cobordisms to the category of Hilbert spaces [14, 15, 16]:

$$F : n\text{-}\mathbf{Cob} \to \mathbf{Vect},$$

where n is the number of dimensions in the theory. To specify a category, we have to identify its objects and morphisms (or arrows) between them. Objects of the category of n-cobordisms n-**Cob** are closed oriented $(n-1)$-dimensional manifolds. These form the boundaries of oriented n-dimensional manifolds, called cobordisms, which constitute the morphisms between the objects of the category. Topological quantum field theory is a rule that associates finite-dimensional Hilbert spaces with $(n-1)$-manifolds and a linear map between

these Hilbert spaces with each cobordism. Furthermore, this rule is subject to certain axioms which for example ensure that the Hilbert spaces originating from topologically equivalent manifolds are isomorphic and that the disjoint union of $(n-1)$-manifolds carries over to a tensor product of Hilbert spaces. Functors satisfying these axioms are called modular and the underlying categories are called monoidal [10]. We point out that realizing a topological phase of a physical system on a closed oriented surface of some genus represents a realization of an important part of this functor. Specifically it assigns to the surface a Hilbert space spanned by the ground states of the relevant physical system.

1.1 The toric code

To illustrate the properties mentioned thus far we will consider one of the simplest models that exhibits topological order, which was introduced by Kitaev [17] and is known as the toric code. The toric code is a lattice model whose ground state is described by a TQFT making it an important model where the abstract concepts of TQFT could be explored in the context of an exactly solvable system. The toric code is defined on a square lattice with a spin 1/2 particle attached to each edge of the lattice. The Hamiltonian of the model is a sum of four body interactions, one for each vertex and plaquette of the lattice. It can be written as

$$H = -\sum_s A_s - \sum_p B_p, \tag{1.1}$$

where the first sum is over the vertices of the lattice and the second sum is over the plaquettes of the lattice. The four body interactions for the vertices and plaquettes, denoted by A_s and B_p respectively, are the following products of Pauli operators:

$$A_s = \sigma_1^x \sigma_2^x \sigma_3^x \sigma_4^x \text{ and } B_p = \sigma_1^z \sigma_2^z \sigma_3^z \sigma_4^z. \tag{1.2}$$

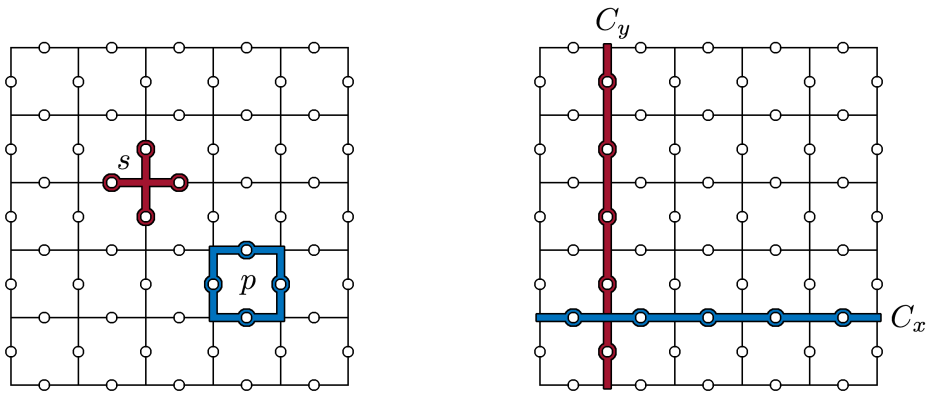

(a) (b)

Figure 1.1: For every vertex s of the toric code lattice we can define an operator that acts on the four spin 1/2 particles neighbouring s as highlighted in (a) in red. Similarly, we can define an operator for every plaquette p of the lattice that acts on the four particles attached to the edges of the plaquettes boundary as highlighted in blue in (a). If we impose periodic boundary conditions on the lattice, we can define two operators that each act as σ^z on different strings of particles, denoted C_x and C_y, that form a homologically non-trivial loop as highlighted in (b). These loop operators commute with each other, and the Hamiltonian.

These operators act on the spin 1/2 particles associated with each vertex or plaquette (see Fig. 1.1a). The eigenvalues of each four body interaction are ± 1

We will first look at the ground state degeneracy of this model when the square lattice is defined on an infinite plane. We will then compare it with ground state degeneracy when the lattice is defined on a surface with a different topology, namely a torus. Firstly, we note that since each plaquette shares either two or no edges with the set of edges linked to any one vertex, all of the A_s and B_p operators commute with each other and thus with the Hamiltonian. Hence the A_s and B_p operators can be simultaneously diagonalised, providing a basis of eigenstates of the Hamiltonian that are also eigenstates of the A_s and B_p operators. Not all of the A_s and B_p operators are independent however, since the product of all operators of the same kind is equivalent to the identity operation ($\prod_s A_s = \prod_p B_p = 1$). These conditions imply that all but one A_s operator can be considered as independent and likewise for the B_p operators. For the case where the lattice tiles an infinite plane, the independent A_s and B_p operators form a complete set of commuting observables and so the set of

common eigenstates form an orthonormal basis for the system's Hilbert space. Clearly the eigenstate of (1.1) with the lowest possible energy is the common eigenstate with eigenvalue +1 for each four body interaction. Therefore, when the system is defined on an infinite plane, the model has a single, non-degenerate ground state.

On the other hand, when the lattice tiles the surface of a torus, the independent A_s and B_p operators no longer form a complete set of commuting observables. This is because, for a $N \times N$ lattice with periodic boundary conditions, the Hilbert space for the model has 4^{N^2} dimensions while we only have $2N^2-2$ independent operators and hence only 4^{N^2-1} distinct combinations of A_s and B_p eigenvalues with which to label basis states.

This issue is rectified by the fact that, on a torus, the Hamiltonian (1.1) has two additional symmetries. These new symmetries are a result of the existence of homologically non-trivial loops on a torus (See the appendix A for a review of the basic concepts, terminology and notation used in homology theory of lattices). If we consider either one of the two closed 1-cycles shown in Fig. 1.1b, the following products of Pauli operators:

$$L_x = \prod_{i \in C_x} \sigma_i^z, \qquad L_y = \prod_{i \in C_y} \sigma_i^z. \tag{1.3}$$

act on the particles attached to the edges of the 1-cycle. We have used C_α to denote the set of particles attached to a cycle as well as the cycle itself. These operators commute with the Hamiltonian and all of the A_s and B_p operators. We call these symmetries loop operators, they have eigenvalues ± 1 and together with the independent A_s and B_p operators they form a complete set of commuting observables for the model on a torus. Just like the model on an infinite plane, the states with minimum energy are the common eigenstates with eigenvalue +1 corresponding to the A_s and B_p operators. Unlike the model on an infinite plane however, we can now identify four orthogonal states with this property and we may write them as follows:

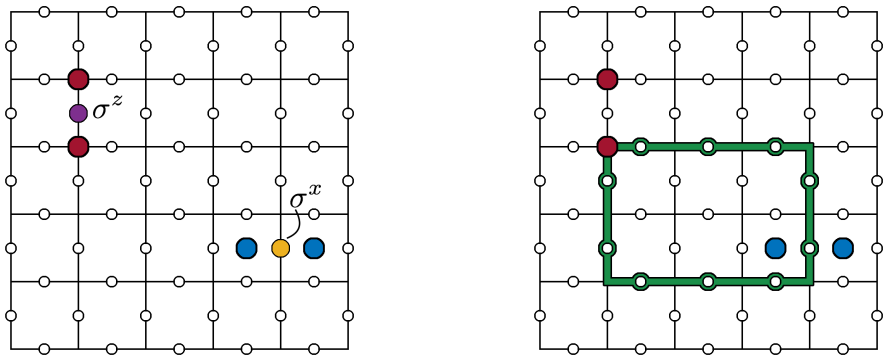

(a) (b)

Figure 1.2: If we consider the ground state of the toric code and apply a σ^z operator to one of the spin 1/2 particles, the resultant state will have excitations located on the neighbouring vertices since σ^z anti-commutes with the A_s operators for those vertices. We graphically represent these quasiparticle excitations by a red dot drawn on the vertices they occupy as shown in (a). Similarly, applying a σ^x operator to a site while the system is in the ground state will create a pair of excitations located on the neighbouring plaquettes which we graphically represent as a blue dot drawn over the occupied plaquettes. Excitations occupying a vertex can be transported to a neighbouring vertex by applying a σ^z operator to the spin 1/2 particle attached to the edge connecting those vertices. It follows that applying a σ^z operator to a string of spin 1/2 particles forming a closed loop beginning and ending at a quasiparticle, like the one highlighted in green in (b), effectively transports the quasiparticle around the closed loop.

$$\left\{ \ |\{a_s = 1\}, \{b_p = 1\}, l_x, l_y\rangle \ \ \middle| l_x, l_y = \pm 1 \ \right\} \tag{1.4}$$

where we have used a_s to denote the eigenvalue of A_s, b_p to denote the eigenvalue of B_p and l_x and l_y to denote the eigenvalues of L_x and L_y respectively. Hence, the model has a four fold degenerate ground state when it is defined on a torus. Comparing the ground state degeneracy of the model in the two different cases highlights the dependence of the model's ground state degeneracy on the topology of the underlying lattice which characterises the model's topological order.

The other characteristic of topological order we mentioned was the structure of the system's quasiparticle defects. Excited quasiparticle states can be created from the ground state of the toric code by applying a Pauli operator that acts on one of the spin 1/2 particles. Every spin 1/2 particle of the model is acted

on by exactly two A_s operators and two B_p operators. The action of a Pauli operator on a particle will anti-commute with either two or all four of those A_s and B_p operators. This follows from the anti-commutation relations of the Pauli operators. The application of a σ^z operator to a particular particle for example will anti-commute with the two A_s operators that also act on that particle. So if we apply a σ^z operator to a spin 1/2 particle while the model is in its ground state, the resultant state will be another eigenstate of the Hamiltonian but with the eigenvalues of two A_s operators flipped from $+1$ to -1. When the model is in such a state we say both of the vertices corresponding to these A_s operators are occupied by a quasiparticle. Similarly, a single σ^x operator will anti-commute with the two B_p operators acting on the same particle and we say acting on the ground state with the σ^x operator occupies the plaquettes corresponding to these B_p operators with a quasiparticle (see Fig. 1.2a).

These quasiparticles can be transported around the lattice by an appropriate application of Pauli operators. We note that a quasiparticle occupying a vertex cannot be moved to a plaquette or vice versa. For this reason the model has two kinds of quasiparticles: those that live on the vertices of the lattice and those that live on the plaquettes. Kitaev called these electric and magnetic charges respectively. We also note, these quasiparticles can only be created in pairs due to the relation satisfied by the A_s and B_p operators $\prod_s A_s = \prod_p B_p = 1$. This shows that the first excited states above the ground state are excited states with two quasiparticles and the energy gap between the ground state and the first excited states is 4. This gap exists in the thermodynamic limit of the model.

We can measure the statistics of the quasiparticles by moving them around the lattice, as described above, in order to perform particle exchanges. Since σ^z operators commute with themselves, transporting electric charges around each other in a way that results in the exchange of two electric charges will map the system's state to itself. So electric charges behave as bosons. Likewise, since σ^x operators commute with themselves, a similar argument implies that

magnetic charges also behave as bosons under exchange. We find a different result, however, when we look at the exchange of an electric charge and a magnetic charge. We are unable to perform an exchange of quasiparticles of different types directly since electric charges cannot be transported from a vertex to a plaquette and a magnetic charge cannot be transported from a plaquette to a vertex. Despite this, we can still measure their mutual statistics by encircling one quasiparticle with another, an operation which is equivalent to two consecutive exchanges. If we create a pair of electric charges and a pair of magnetic charges and then consider a string of Pauli operators which will transport them around each other (see Fig. 1.2b) we will find that the state of the system is multiplied by -1 as a consequence of the anticommutativity of the Pauli operators involved. Therefore we can conclude the state of the system must be multiplied by $\sqrt{-1} = \pm i$ when an electric charge and a magnetic charge are exchanged. This behaviour of quasiparticles under exchange differs from the usual behaviour of bosons or fermions under exchange and particles that exhibit such statistical phases are known as anyons (their statistical phase can be *any* complex phase $e^{i\theta}$).

1.2 Remarks and outline

The anyons that appear in the toric code are also sometimes called Abelian anyons since the quantum state of the system only changes by a complex phase and the group of complex phases $U(1)$ is an Abelian group. Kitaev also introduced another model in [18] known as the Kitaev honeycomb model which exhibits a topological order distinct from the toric code phase. The quasiparticles of the honeycomb model in this phase exhibit non-Abelian statistics and are known as non-Abelian anyons. We will formally introduce the honeycomb model in the next chapter but like the toric code, the honeycomb model is a lattice system of spin 1/2 particles and the quasiparticles of the model are excitations that live on the plaquettes of the model. These are quasiparticle states that belong to some degenerate subspace with the same

energy; the exchange of quasiparticles then acts as a unitary matrix which mixes states within the degenerate subspace. The matrices that arise from different particle exchanges need not commute with one another, hence the name non-Abelian anyons.

Topological orders and their properties are relevant to the development of quantum computing [19]. For instance, the fact that topologically degenerate ground states are robust under small continuous deformations of the system make materials that exhibit topological order useful for creating devices that can store and process information in a way that is resilient against noise which might lead to errors. When Kitaev introduced the toric code in fact, he thought of the model as a quantum memory device where the degenerate ground state on the torus code be used to store two qubits of information. The advantage of storing information with a system like the toric code rests with the fact that a ground state can only be lifted into one of the orthogonal ground states by quasiparticle excitations that are created at one point of the torus and then annihilating at some other point such that the closed trajectory of both particles form a homologically non-trivial loop. Such excitations are exponentially suppressed with system size and are absent in the thermodynamic limit. This means that any information encoded in a ground state is resilient against local thermal excitations and the stability of the stored information is attained at the physical level without the need for any implementation of an error correction procedure. Kitaev also suggested that non-Abelian anyons could be used for a fault tolerant implementation of a quantum computer called topological quantum computation. This method of quantum computation involves using the degenerate subspace spanned by quasiparticle states as a computational space and using the unitary matrices produced by particle exchanges to implement quantum gates [18].

There are different kinds of phases which are also referred to as topological, such as topological insulators and topological superconductors [20]. These are called symmetry protected topological phases and display 'symmetry protected

topological order'. While the topological phases we discuss in this thesis are phases originating from long range entanglement which cannot be removed by local perturbations, symmetry protected topological phases have short range entanglement and are only well defined if the Hamiltonian has a certain symmetry. These systems are 'topological' in the sense that the ground states of these phases cannot be deformed into each other without breaking the symmetry of the Hamiltonian or going through a phase transition. Such phase will not be discussed in this thesis.

In the next chapter, we formally introduce the Kitaev honeycomb model and a solution of the model developed by Kells et al [21]. This solution will allow us to numerically calculate the ground state of the model and its topological degeneracy. In chapter 3 we will use this solution to study the model with a lattice defect. We will investigate how the presence of a lattice defect affects the spectrum of the model and its topologically degenerate ground state. In chapter 4 we will discuss the Kitaev honeycomb model on lattices with different topologies. The solution of the model presented in the next chapter was developed on lattices with Euler characteristic $\chi = 0$ which are only relevant to a torus and an infinite plane. We will show how this solution can be extended to lattices that can be realised on surfaces of genus $g \geq 2$ and then use it to numerically calculate the ground state degeneracy of the model on various surfaces.

Chapter 2

The Kitaev Honeycomb Model

2.1 The Kitaev honeycomb model

The Kitaev honeycomb model is a hexagonal lattice model with a spin half particle attached to each vertex. Therefore its Hilbert space is the n-fold tensor product of two dimensional Hilbert spaces describing a single spin: $\mathcal{H} = \mathcal{H}_{1/2}^{\otimes n}$, where n is the number of vertices of the lattice. Each spin interacts only with its nearest neighbours via an interaction term that depends on the orientation of the link (x, y or z) connecting them. Then, if i and j label neighbouring vertices connected by a link of orientation α, these spins interact via a term of the form $J_\alpha K_{i,j}^\alpha = J_\alpha \sigma_i^\alpha \sigma_j^\alpha$. Here J_α is a coupling constant determining the strength of interactions along links of orientation α. The model's Hamiltonian is the sum of all such interactions:

$$H_0 = -J_x \sum_{x-links} \sigma_i^x \sigma_j^x - J_y \sum_{y-links} \sigma_i^y \sigma_j^y - J_z \sum_{z-links} \sigma_i^z \sigma_j^z. \tag{2.1}$$

We can place the system in a uniform magnetic field $\vec{h} = (h_x, h_y, h_z)$ by adding the following potential to the Hamiltonian:

$$V_m = -\sum_{j \in sites} (h_x \sigma_j^x + h_y \sigma_j^y + h_z \sigma_j^z). \tag{2.2}$$

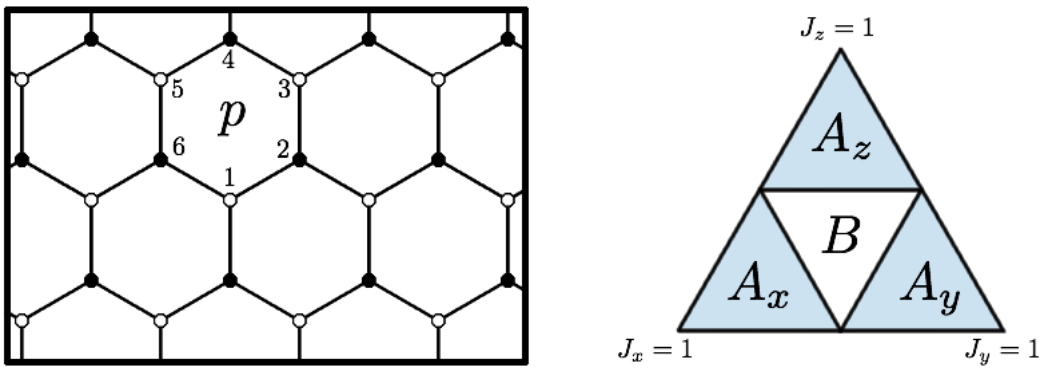

Figure 2.1: We number the sites 1 to 6 for a plaquette p of the honeycomb lattice as depicted on the left. On the right we show the phase diagram of the Kitaev honeycomb model. The three A phases can all be shown to be equivalent to the toric code phase. The B phase is gapless. However in a weak magnetic field the system in this phase acquires a gap and is equivalent to the Ising topological phase.

We will only be interested in the case where the model experiences a weak magnetic field. In this case, the third order of perturbation theory gives an effective potential $V = \sum_p V_p$ where the sum is over the plaquettes of the system and each hexagonal plaquette p makes the following contribution to the potential:

$$\begin{aligned} V_p = \sigma_6^y \sigma_1^z \sigma_2^x + \sigma_1^x \sigma_2^y \sigma_3^z + \sigma_2^z \sigma_3^x \sigma_4^y \\ + \sigma_3^y \sigma_4^z \sigma_5^x + \sigma_4^x \sigma_5^y \sigma_6^z + \sigma_5^z \sigma_6^y \sigma_1^x, \end{aligned} \tag{2.3}$$

where the sites of the plaquette p have been numbered as in Fig. 2.1. Hence, the full Hamiltonian of the model is

$$H = H_0 + \kappa \sum_p V_p, \tag{2.4}$$

where κ is a coupling constant.

This model was introduced by Kitaev [18] who solved the system by a reduction to free fermions in a static $\mathbb{Z}_2$ gauge field. He was able to show that the model exhibits four distinct topological phases A_x, A_y, A_z and B for

different values of the couplings J_x, J_y, J_z. The different A phases occur when the corresponding inequality holds for the couplings and the others do not:

$$\begin{aligned} A_x &: |J_y| + |J_z| \leq |J_x| \\ A_y &: |J_z| + |J_x| \leq |J_y| \\ A_z &: |J_x| + |J_y| \leq |J_z| \end{aligned} \tag{2.5}$$

The B phase occurs when all three inequalities are violated. The three A phases were shown to be equivalent to the toric code phase and so they are called the Abelian phases. In the absence of the magnetic field the B phase is gapless, but in the presence of a weak magnetic field it acquires a gap. The model's quasiparticle excitations in the B phase, which are formed by Majorana fermions attached to vortices, show non-Abelian fractional statistics and are known as Ising anyons. Hence, we call the B phase the non-Abelian phase.

The full Hamiltonian has a number of integrals of motion which depends on both the size and topology of the underlying lattice. To illustrate this, we note that to every $\mathbb{Z}_2$ 1-chain C of the underlying lattice we can associate an operator (up to a minus sign) by composing the link interactions $K^{\alpha}_{i,j}$ for each link in the 1-chain. The resultant operator will be a composition of Pauli operators acting on the vertices connected to the links of the 1-chain times some phase $(1, -1, i, -i)$ depending on the length (number of links) of the 1-chain and the order in which the interactions are composed in. In general, these operators may not commute with each other or the Hamiltonian. However, it is easy to check that the operators associated in this way to closed 1-chains (or 1-cycles) not only commute with the interaction terms, and thus with the Hamiltonian, but they also commute with themselves. To make this association of operators to 1-cycles unambiguous we will always fix the phase of the assigned operator by choosing to compose the interactions in the following way (see Fig. 2.2 for an example): For a connected 1-cycle C of length n, the links are labelled 1 to n so that adjacent links are either labelled with consecutive integers or with

1 and n. We then compose the associated link interactions in the same order the links are numbered ($K_n K_{n-1} \cdots K_2 K_1$). It is a property of the honeycomb lattice that any 1-cycle will always consists of an even number of links. It follows from this and the anti-commutativity of the Pauli operators that the resultant operator is independent of the way the links are numbered, provided adjacent links are numbered with consecutive integers or with 1 and n. For disconnected 1-cycles we just apply this procedure to each connected piece. The order in which the cycles are taken does not matter since the associated operators will act on different spins and so will commute with each other. This means the resultant operator we have just associated with C is well defined. We denote the constructed operator by $K(C) = \prod_{i=1}^{n} K_i^{\alpha_i}$. To the zero 1-chain we associate the identity operator. This defines a mapping $K : Z_1 \to C_{\mathrm{Aut}(\mathcal{H})}(H)$ from the group of 1-cycles Z_1 to the centraliser of the Hamiltonian in $\mathrm{Aut}(\mathcal{H})$, where $\mathrm{Aut}(\mathcal{H})$ is the automorphism group of $\mathcal{H}$. It is easy to show this mapping is a group homomorphism.

$$K(a+b) = K(a)K(b), \quad \forall a, b \in Z_1 \tag{2.6}$$

Therefore, since the mapping K is one to one, we have one symmetry for every element of Z_1, the number of which depends on the size and topology of the underlying lattice.

It will prove useful to choose a set of generators for Z_1 and regard the associated operators via K as the elementary symmetries of the system. The smallest 1-cycles on the honeycomb lattice are the boundaries of single plaquettes, i.e. $C = dP$ where P is a 2-chain consisting of a single plaquette and $d : Z_2 \to Z_1$ is the homological boundary operator. We refer to the symmetries associated to such 1-cycles as vortex operators and denote them by W_P. So, for a plauette P, if we label the sites and edges as in the Fig. 2.3, we can write the vortex operator as follows:

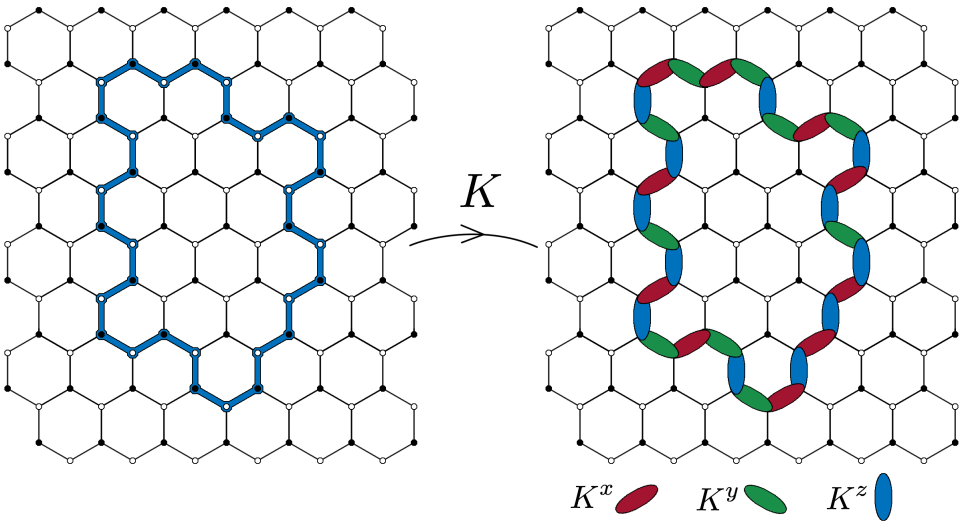

Figure 2.2: An example of a 1-cycle C, indicated by the highlighted links (Left). The operator $K(C)$ is depicted (Right) by a sequence of coloured ovals. Each oval represents a link interaction and covers the associated link. The colour of the oval indicates the orientation of link and hence the type of interaction it represents. Overlapping ovals indicate interactions acting on the same site. If one oval covers another, it means the interaction represented by the former comes before that of the latter in the composition defining the operator $K(C)$.

$$\begin{aligned} W_P &\equiv K(dP), \\ &= K_1^x K_2^z K_3^y K_4^x K_5^z K_6^y, \\ &= \sigma_a^z \sigma_b^y \sigma_c^x \sigma_d^z \sigma_e^y \sigma_f^x. \end{aligned} \tag{2.7}$$

The vortex operators have eigenvalues ± 1. We will say the plaquette P is occupied by a vortex if the state of the system is an eigenstate of W_P with eigenvalue -1 and it is unoccupied if the state is an eigenstate of W_P with eigenvalue $+1$.

Using the fact that K is a group homomorphism it is easy to show that the operator associated with the boundary of a 2-chain is the product of vortex operators for the plaquettes that constitute the 2-chain. If S denotes some 2-chain of length n (the length being the number of plaquettes making up the 2-chain) and $\{P_i \mid i = 1, 2, \cdots n\}$ is the set of plaquettes that constitute S, we have

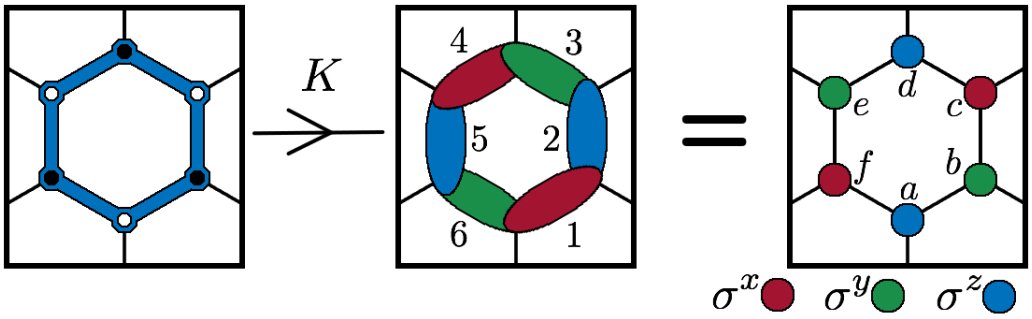

Figure 2.3: The smallest 1-chain on a honeycomb lattice is the boundary of a plaquette. The operator assigned to such a 1-chain by the homomorphism K is shown in the centre image using the graphical representation described in Fig. 2.2. This operator is equivalent to acting on each of the six sites surrounding the plaquette with the Pauli operators shown on the right.

$$\begin{aligned} K(dS) &= K(d(\sum_{i=1}^{n} P_i)), \\ &= K(\sum_{i=1}^{n} dP_i), \\ &= \prod_{i=1}^{n} K(dP_i), \\ &= \prod_{i=1}^{n} W_{P_i}. \end{aligned} \tag{2.8}$$

This means if C_1 and C_2 are both homologous 1-cycles then, as operators, $K(C_1)$ is equivalent to $K(C_2)$ times some product of vortex operators since C_1 and C_2 being homologous means there exists a 2-chain S such that $dS = C_1 + C_2$. Explicitly, we have

$$\begin{aligned} K(C1)K(C_2) &= K(C_1 + C_2), \\ &= K(dS), \\ &= \prod_{i=1}^{n} W_{P_i}, \\ \text{therefore} \quad K(C_1) &= K(C_2) \prod_{i=1}^{n} W_{P_i}. \end{aligned} \tag{2.9}$$

On the last line we have used the fact that the operator $K(C_2)$ squares to the identity. Being able to express operators associated to 1-cycles as being equivalent to operators associated with homologically equivalent 1-cycles like this will prove to be useful when we write down the solution of the model. It is also worth noting that since every 2-chain has the same boundary as its complement and $K(0)$ is the identity operator, equation (2.8) implies $\prod_{i=1}^{n} W_{P_i} = 1$, where the product is over all plaquettes of the lattice.

The boundaries of plaquettes generate the homologically trivial elements of Z_1 which, in the case that our system is a honeycomb lattice tiling an infinite plane, are all of the elements of Z_1. However, if the lattice has a topology other than an infinite plane, there may be homologically non-trivial 1-cycles which provide additional symmetries under K that can not be formed as a product of vortex operators alone. From now on, we will consider the case were our hexagonal lattice tessellates the surface of a torus (See Fig. 2.4). On a torus there are three classes of non-trivial 1-cycles which are homologically distinct from each other. A non-trivial 1-cycle from any one of these three classes is homologically equivalent to a sum of two non-trivial 1-cycles from each of the other two classes. This means the set of boundaries of plaquettes and any two non-trivial cycles from two different classes form a full set of generators for Z_1. We will choose C_x and C_y shown in Fig. 2.4 as generators for the non-trivial cycles and name the associated operators under K loop operators denoted L_x and L_y respectively.

$$L_x \equiv K(C_x), \qquad L_y \equiv K(C_y). \tag{2.10}$$

The loop operators clearly have eigenvalues ± 1.

The vortex and loop operators form a set of commuting observables, and so the Hilbert space can be decomposed as follows. (We use $\{w_p\}$ to denote a particular configuration of vortex operator eigenvalues and l_x and l_y to denote the eigenvalues of L_x and L_y respectively. We use $\{\{w_p\}, l_x, l_y\}$ to denote the set of all configurations of vortex and loop eigenvalues)

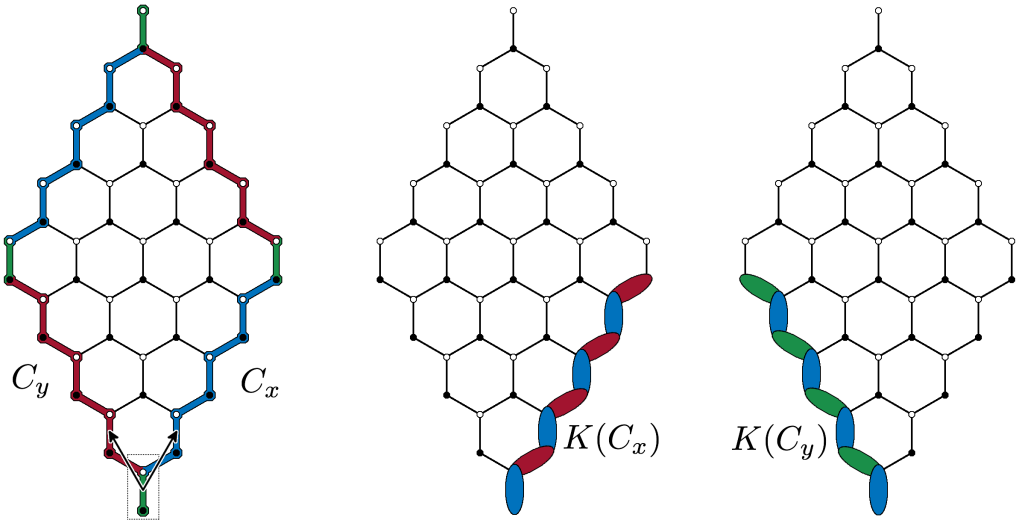

Figure 2.4: The lattice shown on the left will cover a torus once the boundaries have been glued together appropriately. The edges of the lattice with the same colour are to be identified. Hence, the links coloured in red (blue) on the bottom half of the lattice represent the same 1-chain as the links coloured in red (blue) on the top of the lattice. Similarly, the four green links all represent the same link. We can construct two homologically non-trivial 1-cycles by adding the coloured chains together. We will use C_x to denote the cycle obtained by adding the blue and green chains together. We will use C_y to denote the cycle obtained by adding the red and green chains together. Both of these cycles are homologically distinct from each other. The operator $K(C_x)$ (centre) and $K(C_y)$ (right) are also shown.

$$\mathcal{H} = \bigoplus_{\{\{w_p\},l_x,l_y\}} \mathcal{H}_{\{w_p\},l_x,l_y}. \tag{2.11}$$

Here we have used $\mathcal{H}_{\{w_p\},l_x,l_y}$ to denote the common eigenspace of all vortex and loop operators corresponding to the configuration of eigenvalues $\{w_p\}, l_x, l_y$. The method we will use to solve the model involves restricting the Hamiltonian to one of these subspaces where it can be expressed as a combination of terms that are quadratic in fermionic operators. The restricted Hamiltonian can then be diagonalised by an appropriate Bogoliubov transformation.

2.2 The effective spin/hardcore boson representation

There exists a large number of methods to solve the Kitaev honeycomb model [22, 23, 24, 25, 26, 27]. We will use a method presented by Kells et al [21] which relies on representing the degrees of freedom of the honeycomb lattice by the degrees of freedom of a square lattice with both spins and hardcore bosons living on the vertices. To construct this representation we should first think of a quantum state of the system as a tensor product of paired spin states. We choose to pair the spins of the model connected by z-links and view a state of the system as a tensor product of two-spin states over all the z-links. For example, the state where every spin is pointing up can be written as

$$|\uparrow\uparrow\cdots\uparrow\rangle = \prod_{z-links} |\uparrow_\bullet\uparrow_\circ\rangle \otimes \cdots \otimes |\uparrow_\bullet\uparrow_\circ\rangle. \tag{2.12}$$

This notation takes advantage of the fact that the honeycomb lattice consists of two square sub-lattices, the vertices of which can be labelled by filled and empty circles respectively as in Fig. 2.4. Here, $\circ$ denotes the spin the top spin of the z-link and $\bullet$ denotes the bottom spin.

We replace each z-link of the honeycomb lattice, with its two spins attached, by a single site of a square lattice with a spin and a boson which is either present or absent from the site. This change in perspective can be visualised by taking the honeycomb lattice and shrinking the length of the z-links to a point-like object. The x and y-links will line up during this process to form a square lattice as depicted in Fig. 2.5. We relabel the spin states of the z-links with the degrees of freedom of the new square lattice as follows:

$$\begin{aligned} |\uparrow_\bullet\uparrow_\circ\rangle &= |\Uparrow 0\rangle, \quad |\downarrow_\bullet\uparrow_\circ\rangle = |\Downarrow 1\rangle, \\ |\uparrow_\bullet\downarrow_\circ\rangle &= |\Uparrow 1\rangle, \quad |\downarrow_\bullet\downarrow_\circ\rangle = |\Downarrow 0\rangle. \end{aligned} \tag{2.13}$$

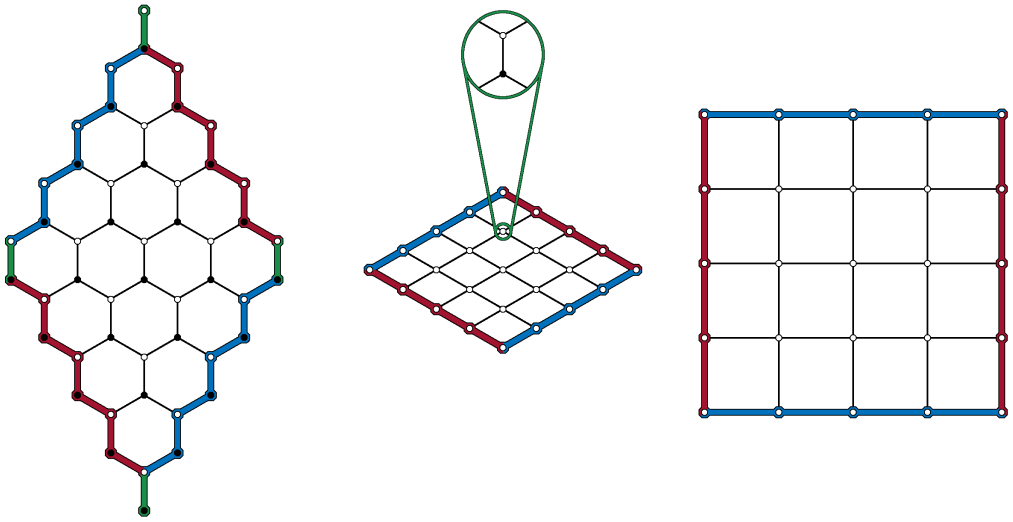

Figure 2.5: Shrinking the z-links of the honeycomb lattice (left) results in a skewed square lattice (middle) which we will depict as a regular square lattice (right)

Namely, we say the state has effective spin up ($\Uparrow$) if the $\bullet$ spin is up and has effective spin down ($\Downarrow$) if the $\bullet$ spin is down. We say there is a boson present (represented by the occupation number 1) if the $\circ$ spin is anti-parallel to the $\bullet$ spin and a boson is absent (represented by the occupation number 0) if the $\circ$ spin is parallel to the $\bullet$ spin. Note, the $\circ$ spin can only be parallel or anti-parallel to the $\bullet$ spin and so the occupation number of the boson can only be 0 or 1. Hence we think of the boson as having a 'hardcore' since there can be no more than 1 boson on a site.

So far we have only relabelled basis sates of the form (2.12) using effective spins and hardcore bosons. However, this relabelling entices us to re-express observables, which up until now have been expressed in terms of Pauli operators independently acting on different spins, in terms of new operators which act on the effective spin and boson degrees of freedom separately.

To this end, we can define creation and annihilation operators for the boson degree of freedom for each site q as follows:

$$b_q^\dagger = \frac{1}{2}(\sigma_{q,\circ}^x - i\sigma_{q,\bullet}^z\sigma_{q,\circ}^y) \tag{2.14}$$

$$b_q = \frac{1}{2}(\sigma^x_{q,\circ} + i\sigma^z_{q,\bullet}\sigma^y_{q,\circ})$$

It is easy to check, using (2.13), that the defined operators have the desired action of creating and annihilating a boson on the site q with the appropriate commutation and anti-commutation relations and without affecting the state of the effective spin.

$$\begin{aligned} &b_q^\dagger \,|\Uparrow 0\rangle = |\Uparrow 1\rangle, \quad b_q \,|\Uparrow 0\rangle = 0, \qquad [b_q^\dagger, b_{q'}] = [b_q^\dagger, b_{q'}^\dagger] = [b_q, b_{q'}] = 0, \\ &b_q^\dagger \,|\Uparrow 1\rangle = 0, \qquad b_q \,|\Uparrow 1\rangle = |\Downarrow 0\rangle, \quad \{b_q, b_q^\dagger\} = 1. \end{aligned} \tag{2.15}$$

The fact that the creation and annihilation operators for the same site anti-commute reflects the fact these are hardcore bosons. This a site can only be occupied by a single boson.

We can also define Pauli operators for the effective spin at a site q, which do not affect the boson degree of freedom as follows:

$$\tau^x_q = \sigma^x_{q,\bullet}\sigma^x_{q,\circ}, \qquad \tau^y_q = \sigma^y_{q,\bullet}\sigma^x_{q,\circ}, \qquad \tau^z_q = \sigma^z_{q,\bullet}. \tag{2.16}$$

We note that since $\sigma^\alpha_{q,\bullet}$ and $\sigma^\alpha_{q,\circ}$ act on different spins, it is clear that the τ^α_q operators satisfy the same commutation relations as the Pauli matrices:

$$[\tau^a_q, \tau^b_q] = 2i\epsilon_{abc}\tau^c_q. \tag{2.17}$$

We also note that since the effective spin and boson occupation are independent degrees of freedom at each site, the creation and annihilation operators commute with the τ^α operators.

The transformation that gives the two spin representation from the effective spin/ hardcore boson representation of the model is found by inverting the above definitions:

$$\begin{aligned}
\sigma^x_{q,\bullet} &= \tau^x_q(b^\dagger_q + b_q), \quad & \sigma^x_{q,\circ} &= (b^\dagger_q + b_q), \\
\sigma^y_{q,\bullet} &= \tau^y_q(b^\dagger_q + b_q), \quad & \sigma^y_{q,\circ} &= i\tau^z_q(b^\dagger_q - b_q), \\
\sigma^z_{q,\bullet} &= \tau^z_q, & \sigma^z_{q,\circ} &= \tau^z_q(1 - 2b^\dagger_q b_q),
\end{aligned} \tag{2.18}$$

We now want to express the defined observables in terms of these creation/annihilation and effective spin operators. In terms of these new operators the Hamiltonian (2.1) becomes

$$\begin{aligned}
H_0 = &- J_x \sum_{x-links} (b^\dagger_{q_l} + b_{q_l})\tau^x_{q_r}(b^\dagger_{q_r} + b_{q_r}) \\
&- J_y \sum_{y-links} i\tau^z_{q_b}(b^\dagger_{q_b} - b_{q_b})\tau^y_{q_t}(b^\dagger_{q_t} + b_{q_t}) \\
&- J_z \sum_q (I - 2N_q),
\end{aligned} \tag{2.19}$$

where q_l and q_r denote the sites attached to the left and right hand ends of a $x - link$. Similarly, q_b and q_t denote the sites attached to the bottom and top ends of a $y - link$. While the summations over the x and y-links of the honeycomb lattice translate into the summations over the x and y-links of the square lattice, the sum over z-links, appearing in (2.1), translates into a sum over sites of the square lattice in this representation.

The contribution to the time-reversal and parity-breaking potential from each plaquette (2.3) can be expressed in terms of these new operators as follows:

$$\begin{aligned}
V_p = \tau^y_d\tau^z_a\tau^x_b(I - 2N_a)(b^\dagger_d + b_d)(b^\dagger_b + b_b) \quad & + i\tau^x_b(b^\dagger_a + b_a)(b^\dagger_b - b_b) \\
+ \tau^z_b\tau^y_c(b^\dagger_b + b_b)(b^\dagger_c + b_c) \quad & + i\tau^z_b\tau^z_c(b^\dagger_b - b_b)(b^\dagger_d + b_d) \\
+ i\tau^x_c(b^\dagger_c + b_c)(b^\dagger_d - b_d) \quad & + \tau^y_d\tau^z_a(b^\dagger_d - b_d)(b^\dagger_a - b_a)
\end{aligned} \tag{2.20}$$

Note, we have labelled the sites of the square plaquette as shown in Fig. 2.6a.

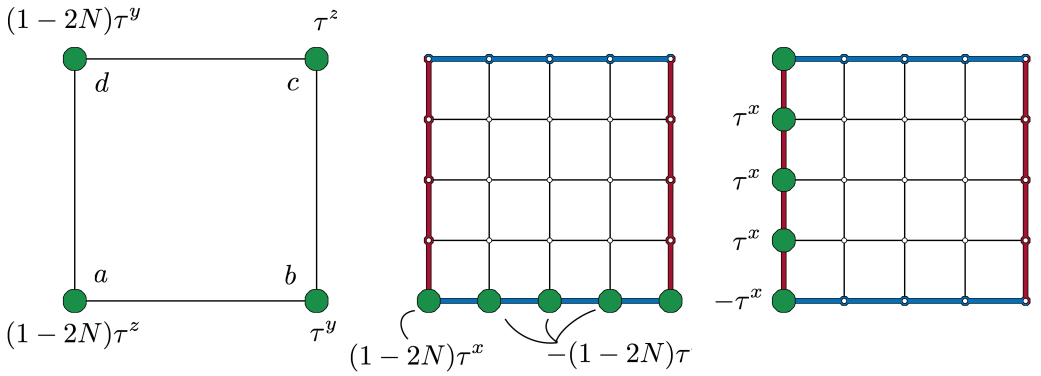

(a) (b) (c)

Figure 2.6: We label the sites of each plaquette by a, b, c and d as shown in (a). We also show how the vortex operator W_P in equation (2.21) acts on the sites of P in the hardcore boson/effective spin representation in (a). We show how the loop operators L_x and L_y act on the sites of the cycles C_x and C_y in (b) and (c) respectively.

In terms of the bosonic creation and annihilation operators $b^\dagger, b$ and the Pauli spin operators τ^α, the vortex operators (2.7) become

$$\begin{aligned} W_P &= \sigma_1^z\sigma_2^y\sigma_3^x\sigma_4^z\sigma_5^y\sigma_6^x \\ &= [\tau_a^z(I-2N_a)][\tau_b^y(b_b^\dagger+b_b)][b_b^\dagger+b_b][\tau_c^z][i\tau_d^z(b_d^\dagger-b_d)][\tau_d^x(b_d^\dagger+b_d)] \\ &= (I-2N_a)(I-2N_d)\tau_a^z\tau_b^y\tau_c^z\tau_d^y \\ &= (I-2N_a)(I-2N_d)Q_P, \end{aligned} \tag{2.21}$$

where $Q_P = \tau_a^z\tau_b^y\tau_c^z\tau_d^y$.

The loop operators become

$$L_x = -\prod_{i\in C_x} -(1-2N_i)\tau_i^x, \qquad L_y = -\prod_{i\in C_y}\tau_i^x \tag{2.22}$$

where C_x and C_y are loops around the meridian and longitude of the torus. (See Fig. 2.6b and Fig. 2.6c)

We now want to change to a basis in the Hilbert space which reflects the decomposition (2.11). To do this we will come up with a complete set of

commuting observables, which include the vortex and loop operators, and use the corresponding set of common eigenvectors as our basis. For such a complete set of commuting observables, one might try to use the collection of vortex and loops operators along with the boson number operator ($N_q = b_q^\dagger b_q$) for each site q of the square lattice. However, if we count the number of distinct combinations of eigenvalues for all the operators in this set, we will find there are too many for each of them to label distinct orthogonal states. If there are N spins in the honeycomb lattice, the model clearly has 2^N spin configurations. Yet there are $N/2$ vortex operators, $N/2$ boson number operators (one for each site of the square lattice) and 2 loop operators, all of which have eigenvalues ± 1. So there appears to be $2^{N/2} \times 2^{N/2} \times 2 \times 2 = 2^{N+2}$ distinct combinations of eigenvalues which a common eigenvector might have. However, the vortex and number operators are not completely independent operators as they satisfy two conditions.

The first condition is the fact that the product of all vortex operators is equivalent to the identity operator. That is,

$$\prod_P W_P = 1, \tag{2.23}$$

where the product is over all the plaquettes of the lattice. Since a product of vortex operators can be thought of as counting the parity of vortices occupying the associated plaquettes, this essentially means there can only be an even number of vortices in total occupying plaquettes of the model. So the number of independent vortex operators is $N/2-1$ and hence the number of configurations of vortices in the model is $2^{N/2-1}$.

The second condition follows from an identity satisfied by the Q_q operators in (2.21). For a lattice that has an even number of plaquettes both in the x and y directions, we can consider a set of plaquettes forming a checkerboard pattern as depicted in the top left picture of Fig. 2.7 by the coloured squares. It is easy to check that since the Pauli operators square to the identity, the product of the Q_p operators associated with the coloured (or uncoloured) plaquettes is the

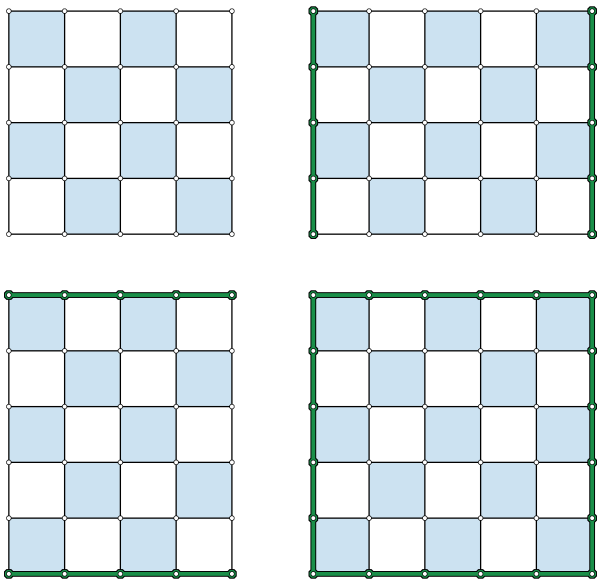

Figure 2.7: The plaquettes of a square lattice with an even number of sites in both the horizontal and vertical directions can be coloured with a checkerboard pattern as in the top left image. For lattices with an odd number of sites in either the horizontal or vertical directions, as in the other three images, the plaquettes can be coloured with a checkerboard pattern where the pattern is misaligned along one of the boundaries of the lattice where periodic boundary conditions are to be imposed as highlighted in green.

identity operation.

$$\prod_{coloured} Q_P = \prod_{uncoloured} Q_P = 1. \tag{2.24}$$

If we compose vortex operators for the corresponding coloured plaquettes we get an operator which counts the parity of vortices on the coloured plaquettes. However, using the above identity for the Q_p operators and (2.21) we find

$$\begin{aligned} \prod_{coloured} W_P &= \prod_q (1 - 2N_q) \prod_{coloured} Q_P \\ &= \prod_q (1 - 2N_q), \end{aligned} \tag{2.25}$$

where q runs over all the sites of the lattice. In other words, this product of vortex operators counts the parity of the number of bosons in the system. Therefore, the parity of the bosons must be the same as the parity of vortices

occupying coloured plaquettes (or equivalently uncoloured plaquettes). Since the parity of bosons is fixed to be 1 or -1 depending on the configuration of vortices, the number of independent boson number operators N_q is $N/2-1$ and hence the number of configurations of bosons in the model is $2^{N/2-1}$.

For lattices with an odd number of plaquettes in either the x or y direction or both, we have a similar dependence of the boson parity on the vortex configuration. For such lattices, we cannot colour the plaquettes with a perfect checkerboard pattern but we can consider sets of plaquettes as depicted in Fig. 2.7, which have a line of plaquettes sharing edges with other plaquettes of the same colour. The pattern can be chosen so that the line coincides with the 1-cycle C_x or C_y or both. If we compose the corresponding vortex operators, the Pauli operators for sites away from C_x and C_y will cancel out as they did before. However, along C_x or C_y or both, the resultant operator will act with a string of Pauli operators and may not act with the parity operator $(1-2N_q)$ for some sites. We can cancel the action of these Pauli operators and replace any missing single site parity operators we need to obtain the full boson parity operator by composing this product of vortex operators with one or both of the loop operators. Using the fact that the loop operators square to the identity, we can write the boson parity operator for a lattice with N_x plaquettes in the x direction and N_y plaquettes in the y direction as

$$\prod_q (1-2N_q) = (-1)^{N_x N_y}(-L_x)^{N_y}(-L_y)^{N_x} \prod_{coloured} W_P. \tag{2.26}$$

These conditions mean we can form a complete set of commuting observables reflecting the decomposition (2.11) by taking all vortex and loop operators with every single site boson number operator and then excluding one vortex operator and one number operator. For example, if we identify a plaquette of the square lattice by the coordinates of the site in the lower left hand corner of the square, we could choose to exclude both the vortex operator and number operator that are identified by the origin $q=(0,0)$. We will use ω_q to denote the eigenvalue of the vortex operator W_P when q denotes the site we associate

with the plaquette P. We will use η_q to denote the eigenvalue of the number operator N_q. Excluding the operators mentioned above, we can now change to the basis of common eigenvectors of this complete set of commuting observables and write it down as follows:

$$B = \Big\{ |\{\omega_q, \eta_q : q \neq (0,0)\}, l_x, l_y\rangle \ : \ \omega_q, \eta_q, l_x, l_y \in \{1, -1\}, \ \forall q \Big\}. \tag{2.27}$$

2.3 Fermionization

The next step of the solution is to use a 'Jordan-Wigner' type transformation to fermionize the bosons of the model. This will result in a Hamiltonian which is quadratic in fermionic operators which we will then be able to solve using the Bogoliubov-de Gennes (BdG) technique.

To fermionize the bosons, we will define a Jordan-Wigner type string operator for each site q of the lattice which we denote by S_q. The composition of these string operators with the boson creation and annihilation operators will be fermionic creation and annihilation operators. Expressing the Hamiltonian and other observables in terms of these new operators will effectively transform the hardcore bosons of the model into fermions, i.e. we will define

$$c_q^\dagger = b_q^\dagger S_q, \qquad c_q = b_q S_q, \tag{2.28}$$

for some S_q such that $\{c_q, c_{q'}^\dagger\} = \delta_{q,q'}$ and $\{c_q, c_{q'}\} = \{c_q^\dagger, c_{q'}^\dagger\} = 0$. We will first define the string operators in the honeycomb picture of the model and then translate it into the effective spin/hardcore boson representation. Since in the honeycomb picture of the model, a site q is really a z-link we will need to define a string operator for each z-link of the hexagonal lattice.

To begin defining string operators for the z-links of the honeycomb lattice we first need to choose a reference z-link whose spins will be acted on by every string operator. For convenience, we will choose a coordinate system to identify

each z-link by a pair of integers (q_x, q_y), which will range from 0 to $N_x - 1$ and 0 to $N_y - 1$ respectively for a N_x by N_y lattice (N_x and N_y are the number of plaquettes in the x and y directions respectively). We identify our chosen reference z-link with the origin $(0, 0)$. The z-link identified by (q_x, q_y) is then the z-link reached by starting at the origin and moving up the lattice along q_x consecutive x-links and then moving up q_y consecutive y-links.

The operator S_q, for the z-link $q = (q_x, q_y)$, is defined as the following composition of operators. First, we act on the $\bullet$ spin of the reference z-link $(0, 0)$ with a σ^x operator. We then apply the z-link interaction K^z to the $(0, 0)$ link followed by the x-link interaction K^x to the link connecting $(0, 0)$ to $(1, 0)$. We then apply K^z to the $(1, 0)$ link followed by K^x on the link connecting $(1, 0)$ to $(2, 0)$. We continue applying K^z and K^x operators like this until we have applied K^x to the x-link connecting $(q_x - 1, 0)$ and $(q_x, 0)$. Then, if $q_y > 0$, we apply K^z and K^y operations in a similar fashion until we have acted on all the links connecting (q_x, q_y) and $(q_x, 0)$. Finally, once we have acted on a string of sites connecting the reference link $(0, 0)$ to (q_x, q_y) we act on the $\circ$ spin of the link (q_x, q_y) with a σ^x. The definition of S_q is visually summarised in Fig. 2.8. So for the site q, we have

$$\begin{aligned} S_q &= \sigma^x_{\bullet,(0,0)} && \text{reference link} \\ &\times K^z_{(0,0)} K^x_{(0,0)} K^z_{(1,0)} K^x_{(1,0)} \cdots K^z_{(q_x-1,0)} K^x_{(q_x-1,0)} && \text{the } x \text{ part} \\ &\times K^z_{(q_x,0)} K^y_{(q_x,0)} K^z_{(q_x,1)} K^y_{(q_x,1)} \cdots K^z_{(q_x,q_y-1)} K^y_{(q_x,q_y-1)} && \text{the } y \text{ part} \\ &\times \sigma^x_{\circ,(q_x,q_y)} && \text{end} \end{aligned} \tag{2.29}$$

where the x part refers to the z and x links connecting the sites $(0, 0), \bullet$ and $(q_x, 0), \bullet$, and the y part refers to the z and y links connecting the sites $(q_x, 0), \bullet$ and $(q_x, q_y), \bullet$.

To translate this definition into the effective spin/hardcore boson representation we can use (2.18). In the context of the square lattice, we find the

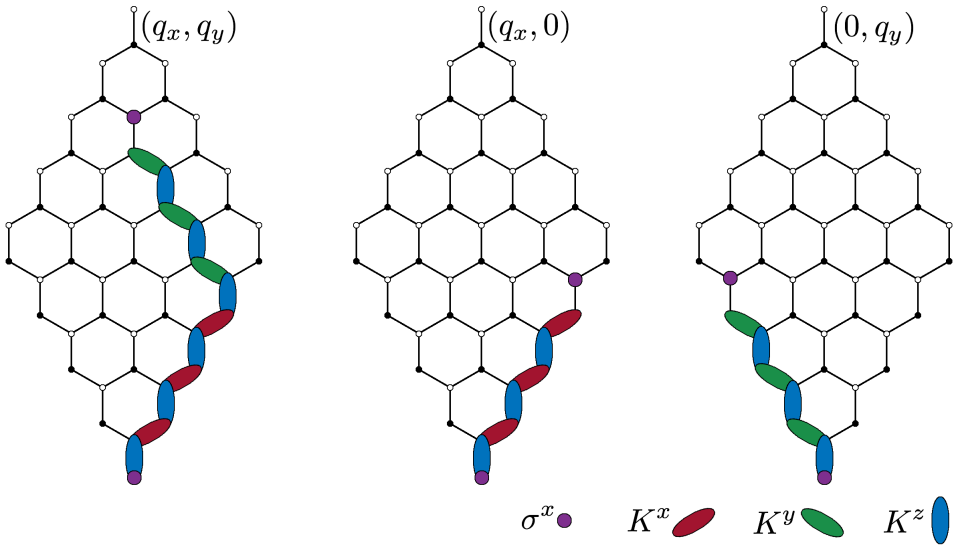

Figure 2.8: The String operator for a z-link $q = (q_x, q_y)$ is depicted on the left using the graphical representation of operators described in Fig. 2.2. We have chosen the z-link appearing at the bottom of the image as the reference link. The string operators for the z-links $q = (q_x, 0)$ and $q = (0, q_y)$ are shown in the middle and on the right respectively. The string operator for the origin consists of a single σ^x operator acting on the $\bullet$ spin of the origin link.

operator S_q acts on a string of sites connecting q to the origin, which we can consider as being made of four segments: a horizontal piece, a corner, a vertical piece and the end point as depicted in Fig. 2.9 The string operator acts on each site i making up the horizontal piece with $-(1 - N_i)\tau_i^x$ and on the corner site with $-\tau^y$. It acts on each site j of the vertical piece with τ_i^x and on the site q with τ^y. So, in terms of the effective spin and hardcore boson degrees of freedom, the string operator becomes

$$\begin{aligned} S_q &= [-(1 - 2N_{(0,0)})\tau^x_{(0,0)}] \times \cdots \times [-(1 - 2N_{(q_x-1,0)})\tau^x_{(q_x-1,0)}] && \text{horizontal part} \\ &\times -\tau^y_{(q_x,0)} && \text{corner} \\ &\times \tau^x_{(q_x,1)} \times \cdots \times \tau^x_{(q_x,q_y-1)} && \text{vertical part} \\ &\times \tau^y_{(q_x,q_y)} && \text{end} \end{aligned} \tag{2.30}$$

If we compose the string operator S_q with the bosonic creation and annihilation operators for the site q we create fermionic creation and annihilation

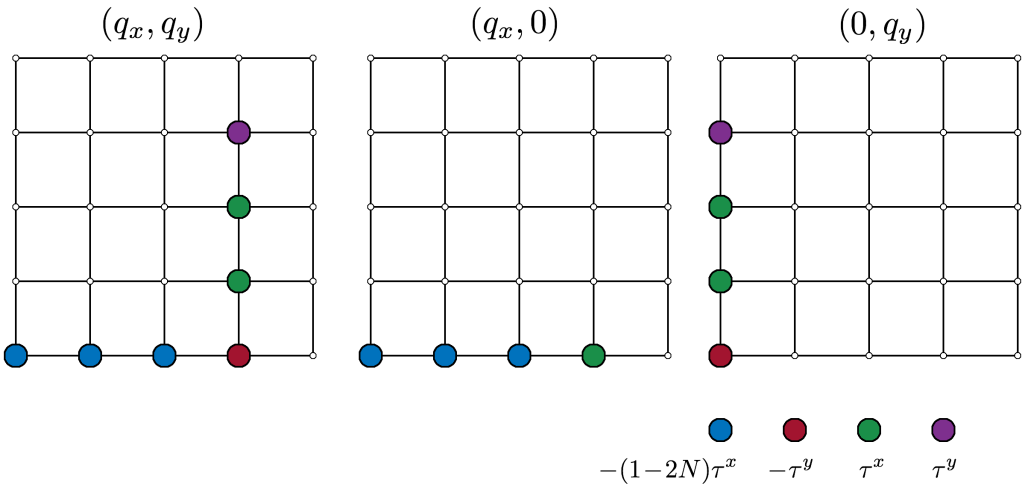

Figure 2.9: In the square lattice picture, the reference link we chose is mapped to the site on the bottom left corner of the above images. The operator S_q acts on a string of sites connecting q to the reference site, which we can consider as being made of a horizontal piece (coloured in blue in the left image), a corner (red), a vertical piece (green) and an end point (purple). The string operators for sites identified by $(q_x, 0)$ and $(0, q_y)$ are shown in the middle and right hand images respectively. The string operator for the reference site consists of a single τ^x operator acting on the reference site.

operators for q. These new operators are denoted by $c_q^\dagger$ and c_q. To see these operators are fermionic, we can consider the two operators $b_q S_q$ and $b_{q'} S_{q'}$ such that $q \neq q'$. There will be a single site, acted on by both operators, where the action of these operators anti-commute. Depending on the exact choices for q and q', the reason these operators anti-commute may either be because they act on the same site with different Pauli operators for the effective spin, or because one of the bosonic annihilation operators anti-commutes with one of the boson parity factors $(1 - 2N)$ from the other operator. Given that the two operators act identically on any other shared site, it follows that the operators obtained by compositing string and boson operators in this way satisfy the fermionic anti-commutation relations. So we have the following:

$$c_q^\dagger \equiv b_q^\dagger S_q, \qquad c_q \equiv b_q S_q.$$
$$\{c_q^\dagger, c_{q'}\} = \delta_{q,q'}, \quad \{c_q^\dagger, c_{q'}^\dagger\} = 0, \quad \{c_q, c_{q'}\} = 0. \tag{2.31}$$

We now want to re-express the observables of the model in terms of these new fermionic creation and annihilation operators.

The expression for the vortex operators in terms of c_q and $c_q^\dagger$ is largely unchanged from (2.21). This is because the string operators all square to the identity operator, and so the fermion number operator is equivalent to the boson number operator: $c_q^\dagger c_q = b_q^\dagger S_q b_q S_q = b_q^\dagger b_q$ (we note that this equivalence means the parity of fermions inherits the same dependence on the vortex configuration the parity of bosons has). Hence, the vortex operator is (we continue to label the sites of the plaquette q as in Fig. 2.6.)

$$\begin{aligned} W_q &= (I - 2c_a^\dagger c_a)(I - 2c_d^\dagger c_d)\tau_a^z \tau_b^y \tau_c^z \tau_d^y \\ &= (I - c_a^\dagger c_a)(I - 2c_d^\dagger c_d)Q_q. \end{aligned} \tag{2.32}$$

Expressing the basic Hamiltonian in terms of the fermionic creation and annihilation operators yields,

$$\begin{aligned} H_0 =& J_x \sum_{x-links} X_{q_1,q_2}(c_{q1}^\dagger - c_{q1})(c_{q2}^\dagger + c_{q2}) \\ &+ J_y \sum_{y-links} Y_{q_1,q_2}(c_{q1}^\dagger - c_{q1})(c_{q2}^\dagger + c_{q2}) \\ &+ J_z \sum_q (2N_q - I), \end{aligned} \tag{2.33}$$

where, if q_1 and q_2 are sites on the left and right hand side of a x-link respectively, $X_{q_1,q_2} = -(I - 2N_{q_1})S_{q_1}\tau_{q_2}^x S_{q_2}$ and, if q_1 and q_2 are sites at the bottom and top of a y-link respectively, $Y_{q_1,q_2} = i\tau_{q_1}^z S_{q_1}\tau_{q_2}^y S_{q_2}$. If we restrict our attention to a particular eigenspace of the X and Y operators, we can replace these operators by their eigenvalues and obtain a Hamiltonian which is quadratic in the fermionic creation and annihilation operators. We will then be able to use the BdG formalism to study the spectrum and eigenstates of the system within this eigenspace. However, before we move onto the BdG formalism we will

discuss the X and Y operators in more detail and see how their eigenvalues are related to vortex and loop configurations.

The X (or Y) operator associated with a particular link of the lattice turns out to be proportional to the operator assigned by the homomorphism K to a certain 1-cycle which can be associated with the link via the definition of string operators. We note, that since the two string operators in X (or Y) cancel each others actions on sites where they act similarly, the operator X (Y) acts on a set of sites forming a closed loop on the lattice. Hence, we can associate a 1-cycle to the link by considering the set of links connecting the sites being acted on. For the moment, we consider a the x-link connecting sites q_1 and q_2 and will denote the associated 1-cycle by C. The exact nature of the assigned 1-cycle (shape, homology class etc.) depends on the choice of definition for the string operators. In general, a different choice of string operators used to fermionise the bosons will result in a different assignment of 1-cycles to links. The operator X_{q_1,q_2} will turn out to be equal to $K(C)$. To see why we can use the fact that the string operators and the single site parity operator $(1-2N)$ all square to the identity to re-write the interaction along an x-link as follows:

$$\begin{aligned} K^x &= S_{q_1}S_{q_1}(I-2N)(I-2N)K^xS_{q_2}S_{q_2} \\ &= -S_{q_1}S_{q_1}(I-2N)K^xS_{q_2}(I-2N)S_{q_2} \\ &= -S_{q_1}(I-2N)K^xS_{q_2}S_{q_1}(I-2N)S_{q_2} \\ &= K(C)(c^\dagger_{q_1}-c_{q_1})(c^\dagger_{q_2}+c_{q_2}) \end{aligned} \tag{2.34}$$

where on the last line we used $K(C) = -S_{q_1}(I-2N)K^xS_{q_2}$ and $(c^\dagger_{q_1}-c_{q_1})(c^\dagger_{q_2}+c_{q_2}) = S_{q_1}(I-2N)S_{q_2}$. This shows that $X_{q_1,q_2} = K(C)$. A similar argument shows that $Y_{q_1',q_2'} = K(C)$ where C denotes the 1-cycle associated with the y-link connecting sites q_1' and q_2'.

The fact that $X_{q_1,q_2} = K(C)$ allows us to express X as a product of vortex and loop operators. Using (2.9) we can write $K(C)$ as being equal to $K(C')$,

where C' is any 1-cycle homologically equivalent to C, times an appropriate product of vortex operators. We can create such a $K(C')$ by taking a product of loop operators. In general, if the homology class of C is (a_x, a_y) in the basis we have chosen for the 1st homology group $\{C_x, C_y\}$, then such an operator will be $L_x^{a_x} L_y^{a_y} = K(C')$ where $C' = a_x C_x + a_y C_y$ and Cx and C_y are the 1-cycles defining the loop operators. Hence, if we use $S(C)$ to denote a 2-chain such that $d(S(C)) = C + C'$, then we can write the following

$$X_{q_1,q_2} = K(C) = L_x^{a_x} L_y^{a_y} \prod_{P \in S(C)} W_P. \tag{2.35}$$

We note that while there are always two 2-chains with $C + C'$ as a boundary, namely $S(C)$ and its complement $\bar{S}(C)$, the operator obtained by multiplying vortex operators corresponding to each plaquette in $S(C)$ is the same operator obtained by multiplying vortex operators corresponding to each plaquette in $\bar{S}(C)$. This follows from the fact that the product of all vortex operators is the identity operator and means the second equivalence in (2.35) is well defined.

$$\prod_P W_P = I \implies \prod_{P \in S(C)} W_P = \prod_{P \in \bar{S}(C)} W_P \tag{2.36}$$

To write down what the X and Y operators are more explicitly, we will need to better understand which links of the lattice are assigned 1-chains that are not homologically trivial and which ones are. All the x-links that are positioned away from the boundary ($q_x = N_x - 1$) of the coordinate system are the links that are assigned homologically trivial 1-cycles. That is the x-links whose coordinates for the connected left hand sites (q_x, q_y) satisfy $q_x < N_x - 1$. We note that when $q_x < N_x - 1$ and $q_y = 0$ the corresponding x-link is not assigned any 1-cycle (or is assigned the zero 1-cycle) and so for these links X is just the identity. If $q_x = N_x - 1$ however, the homology class of the 1-cycle assigned to this link will be $(1, 0)$ and so X will be proportional to L_x. For y-links away from the boundary $q_y < N_y - 1$ no 1-cycle is assigned and so the operator Y acts as the identity. For y-links with $q_y = N_y - 1$ the assigned 1-cycle is in the

homology class $(0,1)$ and so the operator Y will be proportional to L_y. All of this means we can write the X and Y operators as follows:

$$X_{(q_x,q_y)} = \begin{cases} \prod_{q_i=0}^{q_y-1} W_{(q_x,q_i)} & \text{if } q_y \neq 0 \text{ and } q_x \neq N_x - 1 \\ 1 & \text{if } q_y = 0 \text{ and } q_x \neq N_x - 1 \\ L_x \prod_{q_i=0}^{q_y-1} W_{(q_x,q_i)} & \text{if } q_y \neq 0 \text{ and } q_x = N_x - 1 \\ L_x & \text{if } q_y = 0 \text{ and } q_x = N_x - 1 \end{cases} \tag{2.37}$$

$$Y_{(q_x,q_y)} = \begin{cases} 1 & \text{if } q_y \neq N_y - 1 \\ L_y \prod_{q_i=0}^{N_y-1} \prod_{q_j=0}^{q_x-1} W_{(q_j,q_i)} & \text{if } q_y = N_y - 1 \end{cases} \tag{2.38}$$

Now that the X and Y operators are expressed purely in terms of vortex and loop operators, it is easy to see that simultaneous eigenstates of the X and Y operators are simultaneous eigenstates of all vortex and loop operators. If we restrict our attention to one of the subspaces in (2.11), we can replace the vortex and loop operators in (2.37) and (2.38) by their eigenvalues for that subspace. This leads to replacing the X and Y operators in (2.33) by their eigenvalues, resulting in an effective Hamiltonian that is quadratic in fermion creation and annihilation operators for the chosen subspace.

We can write the effective Hamiltonian as follows

$$H_0 = \frac{1}{2} \sum_{q,q'} \begin{bmatrix} c_q^\dagger & c_q \end{bmatrix} \begin{bmatrix} \xi_{q,q'} & \Delta_{q,q'} \\ \Delta_{q,q'}^\dagger & -\xi_{q,q'}^T \end{bmatrix} \begin{bmatrix} c_{q'} \\ c_{q'}^\dagger \end{bmatrix}, \tag{2.39}$$

where

$$\begin{aligned} \xi_{q,q'} &= J_z \delta_{q,q'} + J_x X_{q,q'} \left(\delta_{q,q'}^{(x)} + \delta_{q',q}^{(x)} \right) + J_y Y_{q,q'} \left(\delta_{q,q'}^{(y)} + \delta_{q',q}^{(y)} \right), \\ \Delta_{q,q'} &= J_x X_{q,q'} \left(\delta_{q,q'}^{(x)} - \delta_{q',q}^{(x)} \right) + J_y Y_{q,q'} \left(\delta_{q,q'}^{(y)} - \delta_{q',q}^{(y)} \right). \end{aligned} \tag{2.40}$$

Here, $\delta_{q,q'}$ is the usual Kronecker delta and $\delta_{q,q'}^{(x)}$ is defined to be 1 if q and q'

are the sites on the left and right hand side of an x-link respectively and zero otherwise. Similarly, $\delta^{(y)}_{q,q'}$ is 1 if q and q' are the sites on the bottom and top of a y-link respectively and zero otherwise.

The potential also becomes quadratic in fermionic operators in this representation and can be written as

$$V = \sum_p V_p = \frac{1}{2} \sum_{q,q'} \begin{bmatrix} c_q^\dagger & c_q \end{bmatrix} \begin{bmatrix} \bar{\xi}_{q,q'} & \bar{\Delta}_{q,q'} \\ \bar{\Delta}^\dagger_{q,q'} & -\bar{\xi}^T_{q,q'} \end{bmatrix} \begin{bmatrix} c_{q'} \\ c^\dagger_{q'} \end{bmatrix}, \tag{2.41}$$

where

$$\bar{\xi}_{q,q'} = i \sum_\rho X_{q,\rho} Y_{q',\rho} \left(-\delta^{(x)}_{q,\rho}\delta^{(y)}_{q',\rho} + \delta^{(x)}_{q',\rho}\delta^{(y)}_{q,\rho} + \delta^{(x)}_{\rho,q'}\delta^{(y)}_{\rho,q} - \delta^{(x)}_{\rho,q}\delta^{(y)}_{\rho,q'} \right), \tag{2.42}$$

and

$$\begin{aligned} \bar{\Delta}_{q,q'} = i \sum_\rho X_{q,\rho} Y_{q',\rho} & \left(\delta^{(x)}_{q,\rho}\delta^{(y)}_{q',\rho} - \delta^{(x)}_{q',\rho}\delta^{(y)}_{q,\rho} + \delta^{(x)}_{\rho,q'}\delta^{(y)}_{\rho,q} - \delta^{(x)}_{\rho,q}\delta^{(y)}_{\rho,q'} \right) \\ & - 2iX_{q,q'} \left(\delta^{(x)}_{q,q'} - \delta^{(x)}_{q',q} \right) + 2iY_{q,q'} \left(\delta^{(y)}_{q,q'} - \delta^{(y)}_{q',q} \right). \end{aligned} \tag{2.43}$$

Hence, the full Hamiltonian is

$$H = \frac{1}{2} \sum_{q,q'} \begin{bmatrix} c_q^\dagger & c_q \end{bmatrix} \begin{bmatrix} \xi_{q,q'} + \kappa\bar{\xi}_{q,q'} & \Delta_{q,q'} + \kappa\bar{\Delta}_{q,q'} \\ \Delta^\dagger_{q,q'} + \kappa\bar{\Delta}^\dagger_{q,q'} & -\xi^T_{q,q'} - \kappa\bar{\xi}^T_{q,q'} \end{bmatrix} \begin{bmatrix} c_{q'} \\ c^\dagger_{q'} \end{bmatrix}. \tag{2.44}$$

Now, if we were to choose to restrict our attention a particular common eigenspace of the vortex and loop operators appearing in (2.11), we may replace the X and Y operators appearing in the above Hamiltonian by their eigenvalues. This would reduce in the square matrix appearing (2.44) to a square matrix whose entries are all real numbers. This new square matrix can then be diagonalised numerically to find the energy spectrum of the full Hamiltonian

within the subspace we chose.

2.4 Calculating the ground state

Once we have restricted the Hamiltonian (2.44) to a particular sector in (2.11), diagonalising the BdG matrix (i.e. the single particle Hamiltonian) results in a unitary matrix T whose columns hold the coefficients of quasiparticle modes in the c-fermion basis (the basis formed by the states $c_q^\dagger|-\rangle$, where $|-\rangle$ is the vacuum state with respect to the c_q operators). The spectrum of this Hamiltonian will be symmetric about zero due to the particle-hole symmetry intrinsic to the BdG formalism. Explicitly, if U_i denotes a column vector containing the c_q coefficients of an operator γ_i that creates a quasiparticle with eigenvalue E_i, and V_i denotes a column vector containing the $c_q^\dagger$ coefficients, then we have

$$\begin{bmatrix} \xi + \kappa\bar{\xi} & \Delta + \kappa\bar{\Delta} \\ \Delta^\dagger + \kappa\bar{\Delta}^\dagger & -\xi^T - \kappa\bar{\xi}^T \end{bmatrix} \begin{bmatrix} U_i \\ V_i \end{bmatrix} = E_i \begin{bmatrix} U_i \\ V_i \end{bmatrix}. \tag{2.45}$$

By multiplying the above equation by a permutation matrix, conjugating, negating and using the fact that ξ is hermitian and Δ is anti-symmetric, one can easily show that

$$\begin{bmatrix} \xi + \kappa\bar{\xi} & \Delta + \kappa\bar{\Delta} \\ \Delta^\dagger + \kappa\bar{\Delta}^\dagger & -\xi^T - \kappa\bar{\xi}^T \end{bmatrix} \begin{bmatrix} V_i^\star \\ U_i^\star \end{bmatrix} = -E_i \begin{bmatrix} V_i^\star \\ U_i^\star \end{bmatrix}. \tag{2.46}$$

Hence, for every eigenstate with energy E_i there is an orthogonal eigenstate with energy $-E_i$. So we have

$$H = \frac{1}{2} \begin{bmatrix} c^\dagger & c \end{bmatrix} \begin{bmatrix} \xi + \kappa\bar{\xi} & \Delta + \kappa\bar{\Delta} \\ \Delta^\dagger + \kappa\bar{\Delta}^\dagger & -\xi^T - \kappa\bar{\xi}^T \end{bmatrix} \begin{bmatrix} c \\ c^\dagger \end{bmatrix},$$

$$
\begin{aligned}
&= \frac{1}{2}\begin{bmatrix}\gamma^\dagger & \gamma\end{bmatrix}\begin{bmatrix}E & \\ & -E\end{bmatrix}\begin{bmatrix}\gamma \\ \gamma^\dagger\end{bmatrix}, \\
&= \frac{1}{2}\sum_i (E_i\gamma_i^\dagger\gamma_i - E_i\gamma_i\gamma_i^\dagger), \\
&= \sum_i E_i\gamma_i^\dagger\gamma_i - \frac{1}{2}\sum_i E_i.
\end{aligned} \tag{2.47}
$$

with

$$
\begin{bmatrix}\gamma \\ \gamma^\dagger\end{bmatrix} \equiv \begin{bmatrix}T^\dagger\end{bmatrix}\begin{bmatrix}c \\ c^\dagger\end{bmatrix}. \tag{2.48}
$$

Here, E is a real $(N_{tot}) \times (N_{tot})$ diagonal matrix with non-negative eigenvalues and N_{tot} is the total number of sites of the lattice. The diagonal entries of E are denoted by E_i. We note the spectrum is symmetric about zero due to the particle-hole symmetry of BdG Hamiltonians.

The ground state of the system in a particular vortex/homology sector is the quasiparticle vacuum defined by the property that it is annihilated by all quasiparticle annihilation operators (which we can number 1 to N_{tot})

$$
\gamma_i|GS\rangle = 0, \quad \text{for all } i = 1, .., N_{tot}. \tag{2.49}
$$

If we denote the c fermion vacuum by $|-\rangle$, it is easy to check that the state $|\phi\rangle = \mathcal{N}\prod_k \gamma_k|-\rangle$ satisfies the above condition, where the product runs over all the occupied quasiparticle modes of $|-\rangle$ and $\mathcal{N}$ is a normalisation constant. Depending on the parity of the number of occupied c-fermions modes, this state may or may not be the true ground state of the system. We need to make sure the c-fermion parity of $|\phi\rangle$ satisfies the condition (2.26) for the particular vortex/homology sector we have restricted to. If this condition is satisfied, $|\phi\rangle$ is the true ground state of the system. If the condition is not satisfied, $|\phi\rangle$ represents an unphysical state. However, we can rectify the situation by applying $\gamma_1^\dagger$, the minimum positive energy quasiparticle creation operator, to $|\phi\rangle$ to create the true ground state. Hence, if we denote the ground state by

$|GS\rangle$, we have

$$|GS\rangle = \begin{cases} |\phi\rangle = \mathcal{N}\prod_k \gamma_k|-\rangle & \text{if } |\phi\rangle \text{ satisfies (2.26)} \\ \gamma_1^\dagger|\phi\rangle & \text{otherwise} \end{cases} \tag{2.50}$$

It follows from (2.50) and (2.47) that the ground state energy for which ever homology/vortex sector we have restricted to is

$$E_{GS} = \begin{cases} -\frac{1}{2}\sum_i E_i, & \text{if } |\phi\rangle \text{ satisfies (2.26)}, \\ E_1 - \frac{1}{2}\sum_i E_i & \text{otherwise.} \end{cases} \tag{2.51}$$

To be able to calculate the ground state energy numerically for a particular vortex/homology sector, we need to understand how the matrix T represents the state $|\phi\rangle$ and how it can tell us the parity of the of the number of occupied c-fermions modes it has. In general, T will be of the following form:

$$T = \begin{bmatrix} U & V^\star \\ V & U^\star \end{bmatrix}. \tag{2.52}$$

where U and V are $N_{tot} \times N_{tot}$ matrices which, since T must be unitary, must satisfy.

$$\begin{aligned} U^\dagger U + V^\dagger V = 1, \quad UU^\dagger + V^\star V^T = 1, \\ U^T V + V^T U = 0, \quad UV^\dagger + V^\star U^T = 0. \end{aligned} \tag{2.53}$$

Bloch and Messiah were able to show that a unitary matrix of the form (2.52) can be decomposed as follows [28, 29]:

$$T = \begin{bmatrix} U & V^\star \\ V & U^\star \end{bmatrix} = \begin{bmatrix} D & \\ & D^\star \end{bmatrix} \begin{bmatrix} \bar{U} & \bar{V} \\ \bar{V} & \bar{U} \end{bmatrix} \begin{bmatrix} C & \\ & C^\star \end{bmatrix}. \tag{2.54}$$

where the $N_{tot} \times N_{tot}$ matrices D and C are unitary and both $\bar{U}$ and $\bar{V}$ are real

matrices of the following block diagonal form:

$$\bar{U} = \begin{bmatrix} 0 & & & & & & & & & & \\ & \ddots & & & & & & & & & \\ & & 0 & & & & & & & & \\ & & & u_1 & 0 & & & & & & \\ & & & 0 & u_1 & & & & & & \\ & & & & & \ddots & & & & & \\ & & & & & & u_n & 0 & & & \\ & & & & & & 0 & u_n & & & \\ & & & & & & & & 1 & & \\ & & & & & & & & & \ddots & \\ & & & & & & & & & & 1 \end{bmatrix}, \tag{2.55}$$

$$\bar{V} = \begin{bmatrix} 1 & & & & & & & & & & \\ & \ddots & & & & & & & & & \\ & & 1 & & & & & & & & \\ & & & 0 & v_1 & & & & & & \\ & & & -v_1 & 0 & & & & & & \\ & & & & & \ddots & & & & & \\ & & & & & & 0 & v_n & & & \\ & & & & & & -v_n & 0 & & & \\ & & & & & & & & 0 & & \\ & & & & & & & & & \ddots & \\ & & & & & & & & & & 0 \end{bmatrix}. \tag{2.56}$$

In light of this decomposition of T, the transformation (2.48) defining the

quasiparticle excitations can be considered as consisting of the following three parts:

1. A unitary transformation of the c-fermion creation and annihilation operators among themselves. This transformation does not mix creation operators with annihilation operators and defines a set of operators, which we will denote by a, known as the canonical basis

$$\begin{bmatrix} a \\ a^\dagger \end{bmatrix} \equiv \begin{bmatrix} D^\dagger & \\ & D^T \end{bmatrix} \begin{bmatrix} c \\ c^\dagger \end{bmatrix} \tag{2.57}$$

2. A Bogoliubov transformation which defines three classes of energy levels:

$$\begin{bmatrix} \alpha \\ \alpha^\dagger \end{bmatrix} \equiv \begin{bmatrix} \bar{U} & \bar{V}^T \\ \bar{V}^T & \bar{U} \end{bmatrix} \begin{bmatrix} a \\ a^\dagger \end{bmatrix} \tag{2.58}$$

   - paired levels with $u_p, v_p > 0$:

$$\alpha_p^\dagger = u_p a_p^\dagger - v_p a_{\bar{p}} \qquad \alpha_{\bar{p}}^\dagger = u_p a_{\bar{p}}^\dagger + v_p a_p \tag{2.59}$$

     where the pairs $(p, \bar{p})$ are defined by the 2×2 blocks in (2.56).

   - occupied levels where $v_i = 1, u_i = 0$:

$$\alpha_i^\dagger = a_i \qquad \alpha_i = a_i^\dagger \tag{2.60}$$

   - empty levels where $v_m = 0, u_m = 1$:

$$\alpha_m^\dagger = a_m^\dagger \qquad \alpha_m = a_m \tag{2.61}$$

3. A unitary transformation of the α operators among themselves

$$\begin{bmatrix} \gamma \\ \gamma^\dagger \end{bmatrix} \equiv \begin{bmatrix} C^\dagger & \\ & C^T \end{bmatrix} \begin{bmatrix} \alpha \\ \alpha^\dagger \end{bmatrix} \tag{2.62}$$

We can now express the state $|\phi\rangle$ in the canonical basis defined above as follows

$$\begin{aligned} |\phi\rangle &= \mathcal{N} \prod_k \gamma_k |-\rangle = \mathcal{N} \prod_k \alpha_k |-\rangle, \\ &= \mathcal{N} \prod_i \alpha_i \prod_p (\alpha_p \alpha_{\bar{p}}) |-\rangle, \\ &= \prod_i a_i^\dagger \prod_p (u_p + v_p a_p^\dagger a_{\bar{p}}^\dagger) |-\rangle, \end{aligned} \tag{2.63}$$

where in the first line we have used the fact that the γ operators are obtained by transforming the α operators among themselves. In the second line we have split the product of α operators into a product over the occupied levels and paired levels defined by the Bogoliubov transformation. The empty levels are omitted by definition of $|\phi\rangle$. In the last line we use (2.59) and (2.60) to write $|\phi\rangle$ in the canonical basis. The normalising constant is cancelled by a product of v coefficients over the paired levels $\prod_p v_p$.

From (2.63) it is easy to see that $|\phi\rangle$ is a superposition of states with an even or odd particle number, depending on the parity of occupied levels $\alpha_i^\dagger$. Since the occupied levels in the canonical basis have coefficients $v_i = 1, u_i = 0$, the number of occupied states is given by the number of zeros on the diagonal of $\bar{U}$. As implied by the Bloch-Messiah theorem (2.54), we can compute $\bar{U}$ by calculating the singular value decomposition of U,

$$U = D\bar{U}C. \tag{2.64}$$

Hence, we can calculate the parity of occupied states by calculating the parity of the zero singular values of U and then decide which formula in (2.51) is the appropriate one to use in calculating the ground state energy of the system.

As well as (2.63), the matrix T also enables us to describe $|\phi\rangle$ via its density operator and pairing tensor. Using the matrices U and V we can construct the generalised density operator,

$$R = \begin{bmatrix} \rho & k \\ -k^\star & 1-\rho^\star \end{bmatrix} \equiv \begin{bmatrix} V^\star \\ U^\star \end{bmatrix} \begin{bmatrix} V^T & U^T \end{bmatrix}, \\ = \begin{bmatrix} V^\star V^T & V^\star U^T \\ U^\star V^T & U^\star U^T \end{bmatrix}. \tag{2.65}$$

The matrices ρ and k (known as the single particle density operator and the abnormal density operator or pairing tensor respectively) determine the state $|\phi\rangle$ uniquely [28]. In this sense $|\phi\rangle$ is represented by the matrix T.

Given that T represents $|\phi\rangle$ as described above, we can construct a matrix $\widetilde{T}$ that represents the state $\gamma_1^\dagger|\phi\rangle$ by exchanging the first column of U and V with the first column of $V^\star$ and $U^\star$ respectively [28]. In general, we can represent any many-quasiparticle state $\gamma_{i_1}^\dagger \cdots \gamma_{i_n}^\dagger|\phi\rangle$ by interchanging columns $i_1 \cdots i_n$ of U and V with the corresponding columns of $V^\star$ and $U^\star$ respectively.

2.5 Ground state degeneracy

We can now use the formulation we have decribed in the last section to restrict attention to a particular common eigenspace of the vortex and loop operators and obtain an effective Hamiltonian for the fermions within that subspace. The unique ground state of this effective Hamiltonian can be found using the BdG formalism and we call it the fermionic ground state for the associated subspace. According to the generalised flux phase conjecture mentioned by Lieb [30], the ground state of the model should be in the common eigenspace of the vortex operators where all the corresponding eigenvalues are 1 (the vortex free sector of the Hilbert space). Within the vortex free sector, we refer to the different common eigen-subspaces of the loop operators as homology sectors. The degeneracy arises from the different homology sectors having fermionic ground states with the same energy. Hence, to calculate the ground state degeneracy of the system we need to calculate the fermionic ground state

energy in each homology sector of the vortex free sector and see which ones have ground states with the same energy.

We first consider the model on a $N_x \times N_y$ lattice where both N_x and N_y are **even** numbers, namely $N_x = N_y = 16$. Applying the analysis described above we find that the system has a ground state degeneracy of 4 when it is in the Abelian phase and a 3-fold degenerate ground state when it is in the non-Abelian phase. We let E_{min} denote the lowest fermionic ground state energy out of the 4 homology sectors. In Fig. 2.10, we plot the energy of the fermionic ground states and first excited states in each of the 4 homology sectors after subtracting E_{min} as a function of $J = J_x = J_y$. The other couplings of the Hamiltonian are fixed to be $J_z = 1$ and $\kappa = 0.2$. We see in Fig. 2.10a that, for the system with even dimensions N_x and N_y, in the Abelian phase ($J < 0.5$) all 4 homology sectors are degenerate but as the system crosses the phase transition at $J = 0.5$ one of these sectors splits from the others to become an excited state while the other 3 sectors form the degenerate ground state in the non-Abelian phase ($J > 0.5$).

Now we consider the model on a $N_x \times N_y$ lattice where both N_x and N_y are **odd** numbers by fixing $N_x = N_y = 15$. Applying the same analysis we find the system has a 2-fold degenerate ground state degeneracy when it is in the Abelian phase and a 3-fold degenerate ground state in the non-Abelian phase. The different degeneracies we find in the Abelian phase are a result of (2.26). For lattices where both N_x and N_y are even, the parity of fermions in the ground state is the same for each homology sector. However, for lattices where either N_x or N_y are odd, the parity of fermions in the ground state is odd in half of the homology sectors and even in the other half. This leads to a splitting in the fermionic ground state energies between one half of the homology sectors from the other half. As there are 4 homology sectors in total, this results in a degeneracy of 2. In Fig. 2.10b, we see that the system with odd dimensions N_x and N_y has two of its homology sectors forming the ground state in the Abelian phase while the other two form excited states. As the system approaches the

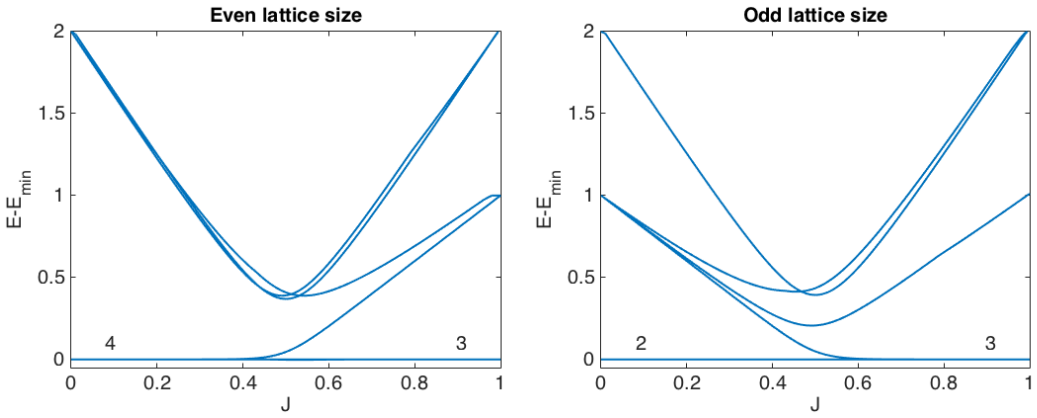

(a) (b)

Figure 2.10: Shown in (a) is the difference between E_{min} and the energy E of fermionic ground states and first excited states in each homology sector as a function of $J_x = J_y = J$ for $N_x = N_y = 16$ and $\kappa = 0.2$. In (b) the same energy difference is plotted for $N_x = N_y = 15$. The number of degenerate ground states is included just above the lowest curves in both the Abelian and non-Abelian phases.

phase transition, the sectors forming excited states begin to split with one of them dropping in energy to join the other two sectors forming the 3 fold degenerate ground state in the non-Abelian phase. In both the even and odd cases, the first excited state in each homology sector remains an excited state of the model, as the system crosses the phase transition, without any of them dropping in energy to contribute to the ground state degeneracy.

The dependence of the ground state degeneracy on the parity of N_x and N_y in the Abelian phase can be understood by considering the system when the x and y couplings are much weaker than the z coupling: $J_x, J_y << J_z$. By treating the terms in the Hamiltonian with J_x or J_y for coefficients as a perturbation of the system when $J_x, J_y = 0$, the first non-constant term in the perturbed Hamiltonian is given by

$$H_{\text{eff}} = -\frac{J_x^2 J_y^2}{16|J_z|^3} \sum_P Q_P, \tag{2.66}$$

where the sum is over all plaquettes of the system and Q_P is the operator appearing in the hardcore-boson/fermion representation of the vortex operator for the plaquette P (2.21). This Hamiltonian can be shown to be equivalent to the toric code Hamiltonian [13]. The ground states of this perturbed system are

those basis states from our chosen complete set of commuting observables (2.27) whose quantum numbers consist of all the hardcore-boson/fermion numbers being zero, $\eta_q = 0$, and the vortex and loop eigenvalues being such that the above Hamiltonian is minimised. For a state to minimise (2.66) we clearly want it to be a common eigenstate of all the Q_P operators with eigenvalues all equal to 1.

We note again that not all of the Q_P operators are independent. Given that the states we are considering have $\eta_q = 0$ for all q, (2.26) can be rewritten to give the following relation satisfied by the Q_P operators.

$$(-1)^{N_x N_y}(-L_x)^{N_y}(-L_y)^{N_x} \prod_{coloured} Q_P = 1. \tag{2.67}$$

The product in the above relation can either be over the coloured plaquettes or the uncoloured plaquettes of the appropriate checkerboard pattern giving us two relations satisfied by the Q_P operators. Hence, if we let b denote one of the coloured plaquettes and w denote one of the uncoloured plaquettes, we can write both Q_b and Q_w in terms of the loop operators and the other Q_P operators.

If we are considering a lattice where both N_x and N_y are even, then the effective Hamiltonian becomes

$$\begin{aligned} H_{\text{eff}} &= a\Big(- Q_b - Q_w - \sum_P Q_P \Big), \\ &= a\Big(- \prod_{coloured} Q_P - \prod_{uncoloured} Q_P - \sum_P Q_P \Big), \end{aligned} \tag{2.68}$$

where $a = \dfrac{J_x^2 J_y^2}{16|J_z|^3}$ and the products and sum are over the independent Q_P operators. Clearly any state in the vortex free sector minimises the above Hamiltonian and so the four homology sectors are degenerate in this case.

However, if we are considering a lattice where both N_x and N_y are odd, then the effective Hamiltonian becomes

$$H_{\text{eff}} = a\Big(L_x L_y \prod_{coloured} Q_P + L_x L_y \prod_{uncoloured} Q_P - \sum_P Q_P\Big). \tag{2.69}$$

States from the vortex free sector will minimise the sum in this Hamiltonian, however they must be from either the $(l_x = 1, l_y = -1)$ or $(l_x = -1, l_y = 1)$ homology sectors to minimise the first two terms. Hence, the fermionic ground states in these two homology sectors form a two fold degenerate ground state while the other two homology sectors are now excited states. In fact, the fermionic ground states from these excited homology sectors are not even in the sector where $\eta_q = 0$ for all q and so they do not satisfy the condition (2.67).

Similarly, when N_x is odd and N_y is even the Hamiltonian becomes

$$H_{\text{eff}} = a\Big(L_y \prod_{coloured} Q_P + L_y \prod_{uncoloured} Q_P - \sum_P Q_P\Big). \tag{2.70}$$

States that minimise this Hamiltonian are from the vortex free sector and are either in the $(l_x = 1, l_y = -1)$ or $(l_x = -1, l_y = -1)$ homology sectors. The Hamiltonian has a similar form when N_y is odd and N_x is even with the factor of L_y in the above expression replaced by L_x. So when one of the dimensions (N_x or N_y) is odd and the other one is even, the effect on the ground state degeneracy is essentially the same as when both are odd. The only difference between these cases and the case where both N_x and N_y are odd is that a different pair of homology sectors contain the ground states.

2.6 Zero-modes attached to vortices

We can study the spectrum of the single particle modes by diagonalising the single particle Hamiltonian H_{sing} appearing in the BdG formalism.

$$H_{\text{sing}} = \begin{bmatrix} \xi + \kappa\bar{\xi} & \Delta + \kappa\bar{\Delta} \\ \Delta^\dagger + \kappa\bar{\Delta}^\dagger & -\xi^T - \kappa\bar{\xi}^T \end{bmatrix}. \tag{2.71}$$

In particular we can observe the behaviour of single particle modes in the presence of vortices in the non-Abelian phase. It is known that the low energy excitations of the Kitaev honeycomb model in the non-Abelian phase are formed by zero-energy fermions attached to vortices known as Ising anyons and exhibit non-Abelian fractional statistics [18, 31]. We took a 16×16 lattice and considered the system in a sector with two vortices separated by 6 plaquettes and calculated the four energy levels closest to zero. We plot these levels in Fig. 2.11 as a function of $J = J_x = J_y$ (we fix $J_z = 1$, $l_x = l_y = 1$ and $\kappa = 0.2$). We observe the formation of zero-modes as the two energy levels closest to zero in the Abelian phase tend zero when the model transitions into the non-Abelian phase. The spectrum is altered by the presence of the vortices in the same way in the other homology sectors. Recall that the spectrum of the single particle Hamiltonian is symmetric about zero as discussed in section 2.4. A pair of energy levels E_i and $-E_i$ correspond to the presence and absence of a single quasiparticle excitation whose creation operator we denote by $\gamma_i^\dagger$. Namely, E_i is how much the energy of an eigenstate of the Hamiltonian is increased after $\gamma_i^\dagger$ is applied to it, provided it is not annihilated. Similarly, $-E_i$ is how much the energy of an eigenstate is changed after γ_i is applied to it. Hence the presence of the two zero energy levels in the spectrum of H_{sing} shows that one of the $\gamma^\dagger$ fermions has zero energy when two well separated vortices occupy the system.

We can also look at the behaviour of the wave functions associated with these zero-modes. If we act on the c-fermion vacuum with the creation operator associated with any quasiparticle mode $\gamma_i^\dagger$, we obtain a superposition of states with a single fermion localised on a particular site.

$$\begin{aligned} \gamma_i^\dagger|-\rangle &= \left(\sum_q U_{qi}c_r^\dagger + V_{qi}c_r\right)|-\rangle, \\ &= \sum_q U_{qi}c_q^\dagger|-\rangle. \end{aligned} \tag{2.72}$$

Here, the sum is over the sites of the lattice. Hence, we can plot the amplitudes

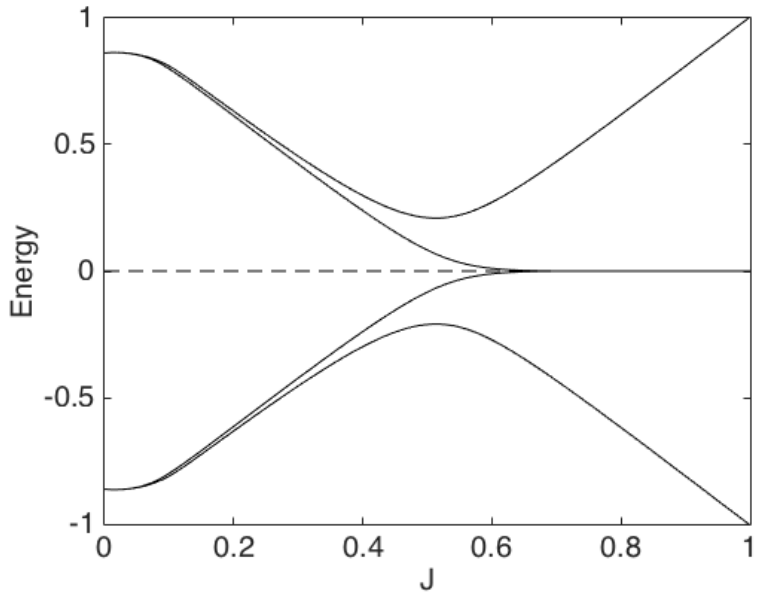

Figure 2.11: Here we plot the four energy levels closest to zero for a 16×16 lattice as a function of $J = J_x = J_y$. The model is tuned to a sector with two vortices separated by 6 plaquettes (we fix $J_z = 1$, $l_x = l_y = 1$ and $\kappa = 0.2$). The formation of zero-modes is clear as two energy levels in the Abelian phase tend zero when the model transitions into the non-Abelian phase.

contained in U_i over a $N_x \times N_y$ grid representing the lattice to visualise the wave function of the corresponding quasiparticle. In Fig. 2.12 we plot the wave function of the eigenstate corresponding to the lowest positive energy level appearing in Fig. 2.11 in the non-Abelian phase with ($J_x = J_y = J_z = 1$). We calculated this state for a 40×40 lattice with $\kappa = 0.1$ in the two vortex sector described above and in the homology sector with $l_x = l_y = 1$. We see this state is localised in the vicinity of the vortices.

Introducing a second pair of vortices affects the single particle spectrum in a similar way by changing the four energy levels closest to zero so that they all converge to zero in the non-Abelian phase. In general, if we consider the model in the non-Abelian phase in a sector which includes $2M$ well separated vortices, the spectrum will include $2M$ zero modes. So for $2M$ well separated vortices, there are M quasiparticles $\gamma_i^\dagger$ which have zero energy [32].

The number of well separated vortices in a particular sector of the Hilbert space affects the fermionic ground state degeneracy via the presence of these zero energy single particle modes. Clearly, if $|gs\rangle$ is the ground state, we can

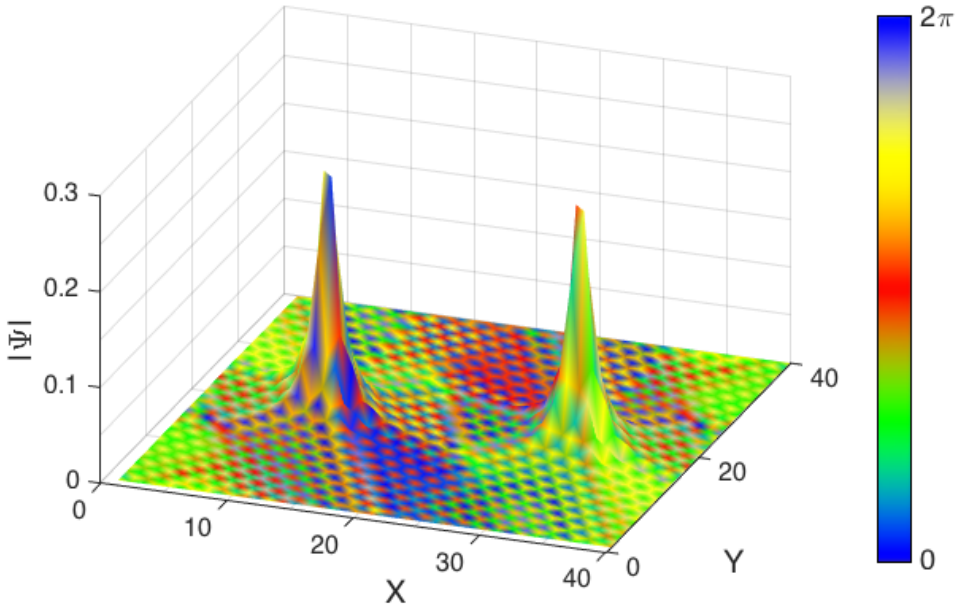

Figure 2.12: Here we plot the eigenstate corresponding to the lowest positive energy level appearing in Fig. 2.11 in the non-Abelian phase with $J_x = J_y = J_z = 1, l_x = l_y = 1$ and $\kappa = 0.1$ on a 40×40 lattice in the two vortex sector described above. On the z-axis we plot the modulus of the state. The colour bar shows how colours are assigned to the plot depending on the phase of the eigenstate at any one site.

apply a single zero energy quasiparticle creation operator to it to create an orthogonal state with the same energy. However, since the parity of fermions in the system is restricted to being either odd or even only, we can only apply such operators in pairs in order to ensure the resultant state is a physical one. So for a system occupied by two well separated vortices the fermionic ground state is unique since there is only one zero energy quasiparticle. However, for a system with four well separated vortices, we have two such quasiparticles, which we denote by $\gamma_1^\dagger$ and $\gamma_2^\dagger$, and we have two orthogonal fermionic ground states, namely $|gs\rangle$ and $\gamma_1^\dagger\gamma_2^\dagger|gs\rangle$. In general, for a system in a particular homology sector occupied by $2M$ well separated vortices we have M zero energy quasiparticles and hence a 2^{M-1} fold degenerate fermionic ground state.

It is known that these quasiparticle excitations formed by low energy fermions attached to vortices are anyons of Ising type and their non-Abelian braid statistics have been demonstrated in [31]. It was proposed by Kitaev in [17] that a system with $2M$ well separated vortices could be used to implement

a method of fault tolerant quantum computation known as topological quantum computation. From a quantum computation perspective, the degenerate fermionic ground state discussed above could be used as a computational space and unitary gates could be implemented via the braiding of vortices.

Chapter 3

Lattice Defects in the Kitaev Honeycomb Model

3.1 The model with a defect

In this chapter we will be interested in lattice defects of the Kitaev honeycomb model, specifically in its non-Abelian phase. Unlike quasiparticle defects of the model's topological order which emerge as excitations of the model, lattice defects are introduced by rearranging a number of edges of the underlying lattice such that the model is no longer on a perfect hexagonal lattice. While there is a wide range of possible lattice defects we could study, the defect we have chosen to investigate is a non-trivial dislocation of the lattice which, when tuned to the Abelian phase, is equivalent to the toric code defect string, or domain wall, presented by Kitaev and Kong [33]. Their work stems from the earlier study of boundaries in toric code models by Bravyi and Kitaev [34]. Generalizations of the toric code model with boundaries and domain walls have also been investigated by Bombin and Martin-Delgado and Beigi and co-workers [35, 36]. Defects of the honeycomb model have also been studied by Petrova et al [37] who found that some defects carry Majorana fermions. However, this work has focused on the Abelian phase of the model. To study the model with a lattice defect, we will require a non-trivial generalization of the exact solution of the model presented in the last chapter. After modifying the solution to

accommodate lattice defects, we will use it to calculate the energy eigenstates of the model with a defect numerically and confirm that the defect alters the fermionic spectrum of the model in much the same way a pair of vortices do. Specifically, in the non-Abelian phase, the defect is accompanied by zero-energy modes that are similar to the Majorana zero modes bound to vortices in the model. This is expected as vortices are also defects in the model's topological order [38].

The defect is introduced to the honeycomb model by decoupling a line of spin pairs, connected by z-links, from their nearest neighbours and then recoupling them as illustrated in Fig. 3.1. The interaction between spins along these new links depend on the orientation of the new links, just as the interactions along the old links did. The orientation of these new links are also shown in Fig. 3.1. The spins which are decoupled from the rest of the system are no longer considered to be part of the system and so their degrees of freedom are projected out of the original Hilbert space. The number of pairs of spins removed from the system in this way will be referred to as the length of the defect. We continue to consider the model on a torus and the Hamiltonian is still given by summing over all the link interactions.

$$H_0 = -J_x \sum_{x-links} \sigma_i^x \sigma_j^x - J_y \sum_{y-links} \sigma_i^y \sigma_j^y - J_z \sum_{z-links} \sigma_i^z \sigma_j^z. \tag{3.1}$$

This rearrangement of links alters the shape of some of the plaquettes of the lattice. The plaquettes along the defect line, not including the ends, still have six vertices coupled to each other in the same way the vertices of the original plaquettes were. This means we can number the vertices of these plaquettes as we did with the original ones. At either end of the defect line, however, we now have a plaquette with eight vertices and eight edges. We will refer to these plaquettes as the top and bottom defect plaquettes. The way we number the vertices of these plaquettes is shown in Fig. 3.2. We note that the lattice is no longer trivalent as both the top and bottom defect plaquettes have one

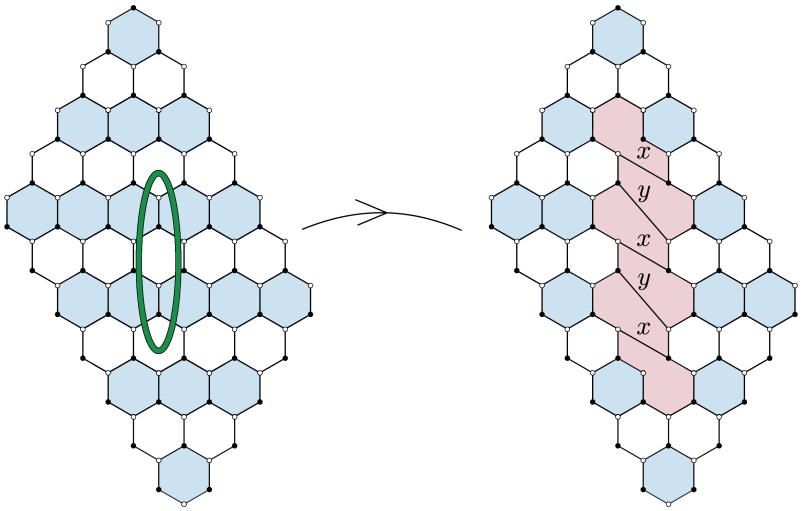

Figure 3.1: Each spin is coupled to its neighbours by one of three links, (x, y, z), depending on its orientation. The orientation of the new links created along the defect are labelled on the right. Also on the left, the line of spins to be deleted in order to create the defect is encircled. The number of z-links deleted along this line is what we will call the length of the defect.

vertex which is only coupled to two links while every other vertex of the lattice is coupled to three. We also note that, as a consequence of this dislocation in the lattice, the total number of plaquettes has been reduced by one. If we introduce a defect of length L to a $N_x \times N_y$ lattice on a torus the system will have $N_x \times N_y - 2L$ vertices and $N_x \times N_y - 2L - 1$ plaquettes.

The contribution to the time-reversal and parity-breaking potential of the plaquettes along the defect line, excluding the top and bottom defects, is given by the same expression as for the original plaquettes (2.3). The contribution to the potential from the bottom defect plaquette is given by

$$\begin{aligned} V_P = \sigma_8^y \sigma_1^z \sigma_2^x + \sigma_1^x \sigma_2^y \sigma_3^z + \sigma_2^z \sigma_3^x \sigma_4^y + \sigma_3^y \sigma_4^z \sigma_5^x \\ + \sigma_4^x \sigma_5^y \sigma_6^z + \sigma_5^z \sigma_6^x \sigma_7^y + \sigma_6^x \sigma_7^x \sigma_8^z + \sigma_7^z \sigma_8^x \sigma_1^y, \end{aligned} \tag{3.2}$$

while that of the top defect plaquette is

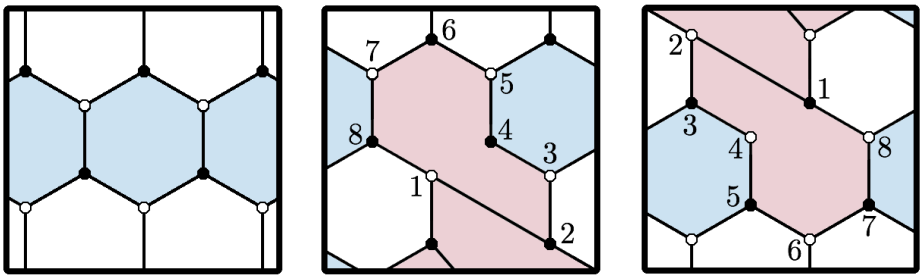

(a) (b) (c)

Figure 3.2: We still number the sites of hexagonal plaquettes as depicted in Fig. 2.1. Note that the plaquettes along the defect line, not including the ends, all have six edges and so the sites of these plaquettes are numbered in the same way. The sites of the plaquettes at the top and bottom of the defect line are numbered as depicted in the centre and on the right.

$$\begin{aligned} V_P = \sigma_8^y\sigma_1^z\sigma_2^x + \sigma_1^x\sigma_2^y\sigma_3^z + \sigma_2^z\sigma_3^x\sigma_4^y + \sigma_3^y\sigma_4^x\sigma_5^z \\ + \sigma_4^z\sigma_5^x\sigma_6^y + \sigma_5^y\sigma_6^z\sigma_7^x + \sigma_6^x\sigma_7^y\sigma_8^z + \sigma_7^z\sigma_8^x\sigma_1^y. \end{aligned} \tag{3.3}$$

Hence, the full Hamiltonian for the system can still be written as

$$H = H_0 + \kappa \sum_P V_P, \tag{3.4}$$

where κ is the magnetic coupling constant and the sum is over all plaquettes of the system, including both defect plaquettes.

Like the model without a defect, this Hamiltonian also has a symmetry for every 1-cycle of the underlying lattice. We continue to use the boundaries of individual plaquettes and the two homologically non-trivial cycles C_x and C_y as generators for Z_1 and regard the associated operators via K as the elementary symmetries of the system. So we can still define vortex operators for every six sided plaquette, including plaquettes along the defect line. The symmetries assigned to the top and bottom defect plaquettes are also referred to as vortex operators and are also denoted by W_P. We retain our interpretation of vortex operator eigenvalues for the defect plaquettes and say a defect plaquette is occupied by a vortex if the state of the system is an eigenstate of the corresponding vortex operator with eigenvalue -1. So if P denotes either the

top or bottom defect plaquette, we have

$$\begin{aligned} W_P &\equiv K(dP), \\ &= K_1^x K_2^z K_3^y K_4^x K_5^z K_6^y K_7^z K_8^y, \\ &= \sigma_1^z \sigma_2^y \sigma_3^x \sigma_4^x \sigma_5^x \sigma_6^z \sigma_7^y \sigma_8^x. \end{aligned} \tag{3.5}$$

Unlike the model without a defect, however, this Hamiltonian also has a symmetry which is not associated with a 1-cycle, but can be associated with a 1-chain whose boundary is given by the two vertices that are only connected to two links. Consider the 1-chain depicted in Fig. 3.3. We can assign an operator to this 1-chain by composing the link interactions associated with the links that constitute the 1-chain, similar to the way K assigns operators to 1-cycles, and then applying a σ^x operator to both the top and bottom boundary vertices. We will refer to this operator as the defect string operator and denote it by S_d. While we may have chosen any other 1-chain with the same boundary to define S_d, the operator assigned to it in this way will be equivalent to the one we have just defined up to some product of vortex and loop operators.

As well as being a symmetry, the defect string operator also commutes with all vortex and loop operators, so the Hilbert space can be decomposed as follows. (We again use $\{w_p\}$ to denote a particular configuration of vortex operator eigenvalues and l_x and l_y to denote the eigenvalues of L_x and L_y respectively. We denote the eigenvalue of S_d by s_d and use $\{\{w_p\}, s_d, l_x, l_y\}$ to denote the set of all configurations of these eigenvalues.)

$$\mathcal{H} = \bigoplus_{\{\{w_p\},s_d,l_x,l_y\}} \mathcal{H}_{\{w_p\},s_d,l_x,l_y}. \tag{3.6}$$

Here we have used $\mathcal{H}_{\{w_p\},s_d,l_x,l_y}$ to denote the common eigenspace of all vortex, loop and string defect operators corresponding to the configuration of eigenvalues $\{w_p\}, s_d, l_x, l_y$.

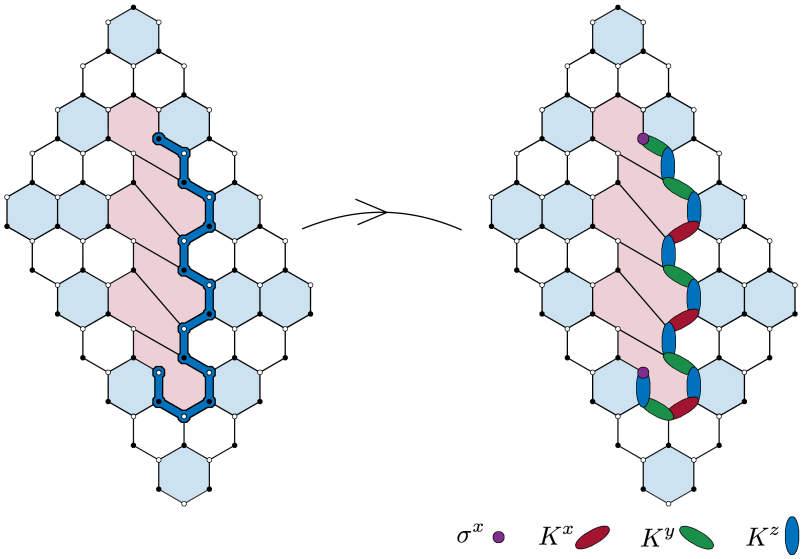

Figure 3.3: To the 1-chain highlighted on the left we can assign an operator which commutes with the vortex operators, loop operators and the Hamiltonian. This operator is represented graphically on the right using the representation described in Fig. 2.2.

3.2 The solution of the model with a defect

We now map the system with a defect onto a square lattice as we did in the last chapter to form the hardcore boson/effective spin representation of the model. The resultant square lattice will also have a defect in it as depicted in Fig. 3.4. The spin degrees of freedom of the defected honeycomb lattice are still represented by the effective spin and hardcore boson degrees of freedom of the square lattice as in (2.13). We still define creation and annihilation operators for hardcore bosons and Pauli operators for the spins in terms of the Pauli operators or the original spins of the honeycomb lattice as in (2.14) and (2.16). In terms of these operators the Hamiltonian is of the same form as when the defect was not introduced to the system, only now the summations include terms for the new x and y-links.

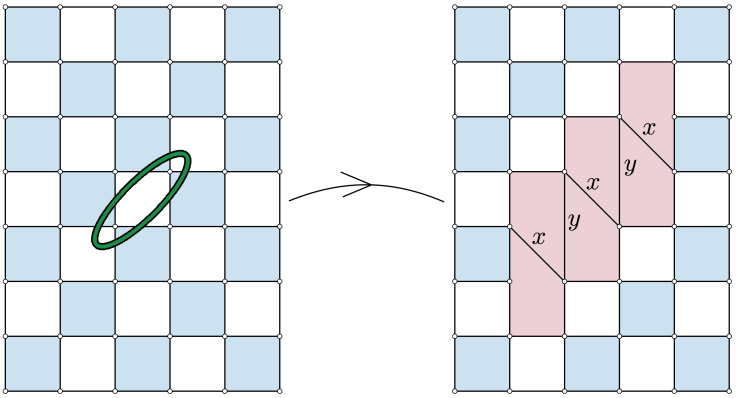

Figure 3.4: Mapping the honeycomb lattice can be visualised as shrinking the z-links of the lattice to a point, creating a square lattice. The degrees of freedom of each of the z-links are mapped to the degrees of freedom of the sites of the square lattice according to (2.13). The resultant defect in the square lattice is equivalent to the toric code defect introduced in [33] via a unitary transformation of the vortex operators described in [13]. The z-links that are deleted from the model are mapped to the sites of the square lattice encircled on the left while the orientation of the new links along the defect are shown on the right.

$$\begin{aligned} H_0 = &- J_x \sum_{x-links} (b_{q1}^\dagger + b_{q1})\tau_{q2}^x (b_{q2}^\dagger + b_{q2}) \\ &- J_y \sum_{y-links} i\tau_{q1}^z (b_{q1}^\dagger - b_{q1})\tau_{q2}^y (b_{q2}^\dagger + b_{q2}) \\ &- J_z \sum_q (I - 2N_q), \end{aligned} \tag{3.7}$$

where $q1$ and $q2$ denote the sites on the left and right hand side of a x-link respectively, and the sites at the bottom and top of a y-link respectively.

If we label the vertices of the bottom defect plaquette as shown in Fig. 3.5c, the contribution to the time-reversal and parity-breaking potential from the bottom defect plaquette can be expressed as follows:

$$\begin{aligned} V_p = \tau_e^y \tau_a^z \tau_b^x (I - 2N_a)(b_e^\dagger + b_e)(b_b^\dagger + b_b) \quad &+ i\tau_b^x (b_a^\dagger + b_a)(b_b^\dagger - b_b) \\ + \tau_b^z \tau_c^y (b_b^\dagger + b_b)(b_c^\dagger + b_c) \quad &+ i\tau_b^z \tau_c^z (b_b^\dagger - b_b)(b_d^\dagger + b_d) \\ + i\tau_c^x (b_c^\dagger + b_c)(b_d^\dagger - b_d) \quad &+ \tau_d^y \tau_e^z (b_d^\dagger - b_d)(b_e^\dagger - b_e) \end{aligned} \tag{3.8}$$

$$+ \tau_e^z \tau_d^y (b_e^\dagger + b_e)(b_d^\dagger + b_d) \qquad + \tau_e^y \tau_a^z (b_e^\dagger - b_e)(b_a^\dagger - b_a),$$

while the contribution from the top defect plaquette is given by:

$$\begin{aligned} V_p = \tau_e^y \tau_a^z \tau_b^x (I - 2N_a)(b_e^\dagger + b_e)(b_b^\dagger + b_b) \quad & + i\tau_b^x (b_a^\dagger + b_a)(b_b^\dagger - b_b) \\ + \tau_b^z \tau_c^y (b_b^\dagger + b_b)(b_c^\dagger + b_c) \quad & + \tau_c^y \tau_b^z (b_c^\dagger - b_c)(b_b^\dagger - b_b) \\ + \tau_c^z \tau_d^y (b_c^\dagger + b_c)(b_d^\dagger + b_d) \quad & + i\tau_c^z \tau_d^z (b_c^\dagger - b_c)(b_e^\dagger + b_e) \\ + i\tau_d^x (b_d^\dagger + b_d)(b_e^\dagger - b_e) \quad & + \tau_e^y \tau_a^z (b_e^\dagger - b_e)(b_a^\dagger - b_a), \end{aligned} \tag{3.9}$$

where the vertices of the top defect plaquette are labelled as in Fig. 3.5b. The contribution from every other plaquette is still given by (2.20).

We now want to express the symmetries of the model in terms of the bosonic creation and annihilation operators and the Pauli operators for the effective spins. The vortex operators in the hardcore boson/effective spin representation are given by the following expression. (We label the sites of normal and defect plaquettes as shown in Fig. 3.5.)

$$W_p = \begin{cases} (I - 2N_a)(I - 2N_e)(\tau_a^z \tau_b^y \tau_c^x \tau_d^z \tau_e^y) & \text{if p is at the top defect plaquette,} \\ (I - 2N_a)(I - 2N_d)(\tau_a^z \tau_b^y \tau_c^z \tau_d^y \tau_e^x) & \text{if p is at the bottom defect plaquette,} \\ (I - 2N_a)(I - 2N_d)(\tau_a^z \tau_b^y \tau_c^z \tau_d^y) & \text{otherwise.} \end{cases} \tag{3.10}$$

The 1-chain we used to define the defect string operator translates to the 1-chain depicted in Fig. 3.6a when the honeycomb model is mapped onto the square lattice. In Fig. 3.6b we graphically present the defect string operator in the hardcore boson/effective spin representation. The loop operators L_x and L_y are still defined by (2.22).

Now, we change to a basis in the Hilbert space which reflects the decomposition (3.6). We will use the common eigenstates of the complete set of commuting observables consisting of all the independent vortex and single site

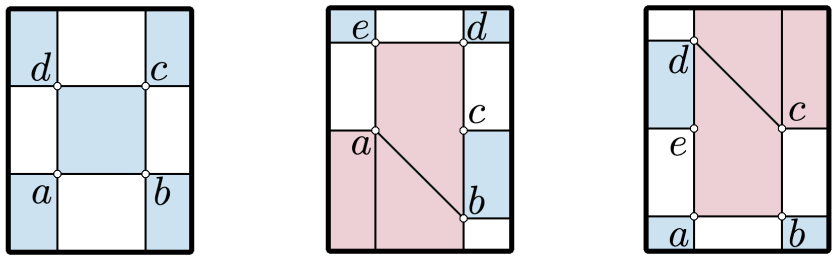

(a) (b) (c)

Figure 3.5: After mapping the z-links of the honeycomb to the sites of the square lattice, we label the sites of the normal plaquettes as in (a). The sites of the top and bottom defect plaquettes are labelled as in (b) and (c) respectively.

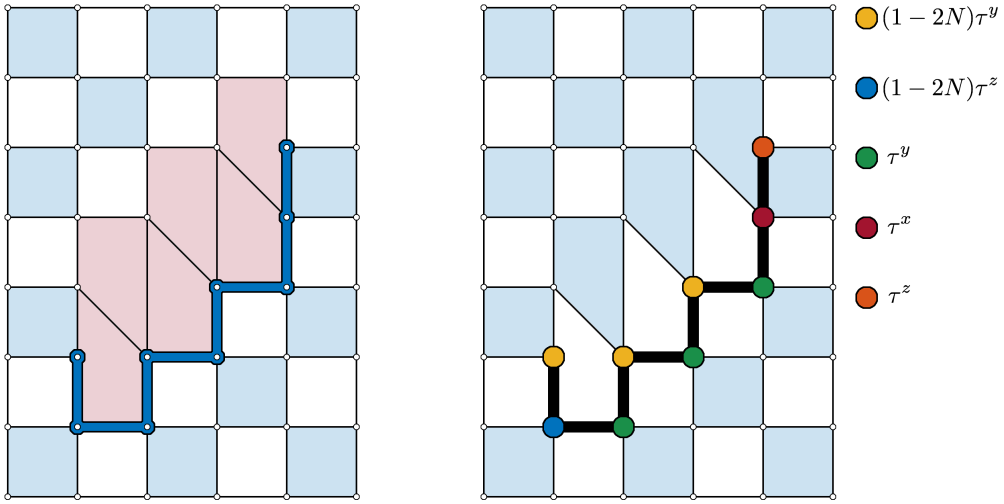

(a) (b)

Figure 3.6: The 1-chain used to define the defect string operator is shown in (a). The defect string operator in the hardcore boson/effective spin representation is given by the composition of the operators illustrated in (b).

boson number operators as well as the defect string operator and the two loop operators. We note that due to the presence of the defect, we cannot colour the plaquettes of the lattice with a checkerboard pattern like we did when the defect was absent. However, similar to case of a lattice with odd dimensions N_x or N_y, we can colour the plaquettes with a checkerboard pattern that is misaligned along the defect as in Fig. 3.6b. This allows us to write the boson parity operator as a product of vortex operators over the coloured plaquettes times the defect string operator. The composition of all vortex operators is still equivalent to the identity. So the defined symmetries of the model satisfy the following two relations

$$\prod_P W_P = 1, \tag{3.11}$$

$$\prod_q (1 - 2N_q) = (-1)^{N_x N_y} (-L_x)^{N_y} (-L_y)^{N_x} S_d \prod_{coloured} W_P, \tag{3.12}$$

where the product in (3.11) is over all vortex operators and the product in (3.12) is over all the vortex operators corresponding to coloured plaquettes of the checkerboard pattern in Fig. 3.6b.

A system of size $N_x \times N_y$ with a defect of length L has $4^{N_x \times N_y - L}$ degrees of freedom while we have defined $N_x \times N_y - L$ boson number operators and $N_x \times N_y - L - 1$ vortex operators. The relations (3.11) and (3.12) mean we can choose to ignore one vortex operator and one single site boson number operator and regard the rest as forming a complete set of commuting observables with the two loop operators and the defect string operator. As before, we identify a plaquette of the square lattice by the coordinates of the site in the lower left hand corner of the plaquette. We choose to exclude both the vortex operator and number operator that are identified by the origin $q = (0, 0)$ and change to the basis of common eigenvectors of this set of observables which we can write as follows:

$$B = \Big\{ |\{\omega_q, \eta_q : q \neq (0,0)\}, s_d, l_x, l_y\rangle \ : \ \omega_q, \eta_q, s_d, l_x, l_y \in \{1, -1\}, \ \forall q \Big\}. \tag{3.13}$$

To fermionize the bosons, we will proceed as before by defining a Jordan-Wigner type string operator for each site q of the lattice. The string operator for a site q is still denoted by S_q. We begin by first picking a particular site of the lattice as a reference point, labelled O. Due to the presence of the defect, strictly speaking our model is no longer a lattice model and so we can not use lattice basis vectors in the usual way. That is, not all combinations of the form $(q_x, q_y) \equiv q_x e_x + q_y e_y$, where q_x and q_y are integers and e_x and e_y are basis vectors for the square lattice, represent sites that are still considered to be part of the model since they may have been removed when the defect was

introduced. However, for the purpose of notation, we will continue to identify sites of the model by the integers (q_x, q_y) bearing in mind that not all pairs of integers represent physical sites.

We again choose the origin of this coordinate system $(q_x, q_y) = (0, 0)$ as the reference site O needed to define the string operators. The string operator S_q is still defined by considering a string of sites connecting the reference site to the site $q = (q_x, q_y)$ which is made up of a horizontal part (sites (x, y) with $x < q_x - 1$ and $y = 0$), a corner part ($(x, y) = (q_x, 0)$), a vertical part (sites (x, y) with $x = q_x$ and $0 < y < q_y 0$) and an end point which coincides with q as shown in Fig. 3.7. On the sites making up the horizontal part, S_q acts like the operator $-(1 - 2N_i)\tau_i^x$ while on the sites making up the vertical part, the corner and the end point, S_q acts like $\tau_i^x, -\tau^y$ and τ^y respectively. So we have

$$S_q = \overbrace{[\prod_i -(1-2N_i)\tau_i^x]}^{\text{Horizontal}} \overbrace{[-\tau^y]}^{\text{Corner}} \overbrace{[\prod_i \tau_i^x]}^{\text{Vertical}} \overbrace{[\tau^y]}^{\text{End point}} . \tag{3.14}$$

We can now define fermionic creation and annihilation operators for a site q by composing S_q with the boson operators associated with q as follows:

$$\begin{aligned} &c_q^\dagger \equiv b_q^\dagger S_q, && c_q \equiv b_q S_q. \\ &\{c_q^\dagger, c_q'\} = \delta_{q,q'}, \quad \{c_q^\dagger, c_{q'}^\dagger\} = 0, \quad \{c_q, c_{q'}\} = 0, \end{aligned} \tag{3.15}$$

Expressing the basic Hamiltonian in terms of these fermionic creation and annihilation operators yields,

$$\begin{aligned} H_0 =& J_x \sum_{x-links} X_{q_1,q_2}(c_{q_1}^\dagger - c_{q_1})(c_{q_2}^\dagger + c_{q_2}) \\ &+ J_y \sum_{y-links} Y_{q_1,q_2}(c_{q_1}^\dagger - c_{q_1})(c_{q_2}^\dagger + c_{q_2}) \\ &+ J_z \sum_q (2N_q - I), \end{aligned} \tag{3.16}$$

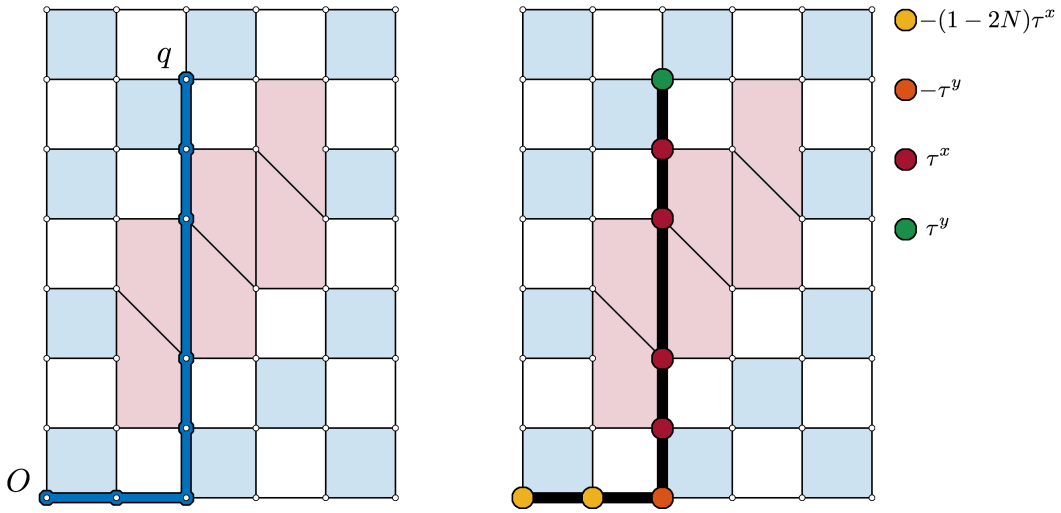

(a) (b)

Figure 3.7: In (a) we depict a string connecting the reference site O to the site q. The string operator S_q is defined as acting on the sites that this string passes through as shown in (b).

where, if q_1 and q_2 are sites on the left and right hand side of a x-link respectively, $X_{q_1,q_2} = -(I - 2N_{q_1})S_{q_1}\tau^x_{q_2}S_{q_2}$ and if q_1 and q_2 are sites at the bottom and top of a y-link respectively, $Y_{q_1,q_2} = i\tau^z_{q_1}S_{q_1}\tau^y_{q_2}S_{q_2}$. These X and Y operators, for the same reason when the defect was absent, are again proportional to a certain product of vortex and loop operators depending on the associated link the X or Y operator corresponds to and are still given by (2.37) and (2.38).

Both the basic Hamiltonian and the potential are quadratic in fermionic operators and can be written as

$$H = \frac{1}{2}\sum_{q,q'} \begin{bmatrix} c_q^\dagger & c_q \end{bmatrix} \begin{bmatrix} \xi_{q,q'} + \kappa\bar{\xi}_{q,q'} & \Delta_{q,q'} + \kappa\bar{\Delta}_{q,q'} \\ \Delta^\dagger_{q,q'} + \kappa\bar{\Delta}^\dagger_{q,q'} & -\xi^T_{q,q'} - \kappa\bar{\xi}^T_{q,q'} \end{bmatrix} \begin{bmatrix} c_{q'} \\ c^\dagger_{q'} \end{bmatrix}. \tag{3.17}$$

where the matrix elements coming from the basic Hamiltonian are

$$\begin{aligned} \xi_{q,q'} &= J_z\delta_{q,q'} + J_xX_{q,q'}\left(\delta^{(x)}_{q,q'} + \delta^{(x)}_{q',q}\right) + J_yY_{q,q'}\left(\delta^{(y)}_{q,q'} + \delta^{(y)}_{q',q}\right), \\ \Delta_{q,q'} &= J_xX_{q,q'}\left(\delta^{(x)}_{q,q'} - \delta^{(x)}_{q',q}\right) + J_yY_{q,q'}\left(\delta^{(y)}_{q,q'} - \delta^{(y)}_{q',q}\right). \end{aligned} \tag{3.18}$$

The matrix elements coming from the potential are

$$\bar{\xi}_{q,q'} = i \sum_{\rho} X_{q,\rho} Y_{q',\rho} \left(-\delta^{(x)}_{q,\rho}\delta^{(y)}_{q',\rho} + \delta^{(x)}_{q',\rho}\delta^{(y)}_{q,\rho} + \delta^{(x)}_{\rho,q'}\delta^{(y)}_{\rho,q} - \delta^{(x)}_{\rho,q}\delta^{(y)}_{\rho,q'} \right), \tag{3.19}$$

and

$$\begin{aligned} \bar{\Delta}_{q,q'} = i \sum_{\rho} X_{q,\rho} Y_{q',\rho} \left(\delta^{(x)}_{q,\rho}\delta^{(y)}_{q',\rho} - \delta^{(x)}_{q',\rho}\delta^{(y)}_{q,\rho} + \delta^{(x)}_{\rho,q'}\delta^{(y)}_{\rho,q} - \delta^{(x)}_{\rho,q}\delta^{(y)}_{\rho,q'} \right) \\ - 2iX_{q,q'} \left(\delta^{(x)}_{q,q'} - \delta^{(x)}_{q',q} \right) + 2iY_{q,q'} \left(\delta^{(y)}_{q,q'} - \delta^{(y)}_{q',q} \right). \end{aligned} \tag{3.20}$$

Here, $\delta_{q,q'}$ is the usual Kronecker delta and $\delta^{(x)}_{q,q'}$ is defined to be 1 if q and q' are the sites on the left and right hand side of an x-link respectively and zero otherwise. Similarly, $\delta^{(y)}_{q,q'}$ is 1 if q and q' are the sites on the bottom and top side of a y-link respectively and zero otherwise.

We now have a recipe for studying the spectrum of the model with a defect numerically. Restricting to a particular common eigenspace of the vortex and loop operators appearing in (3.6) means we can replace the X and Y operators appearing in Hamiltonian by their eigenvalues for that subspace. As with the case when the defect was absent, this results in a matrix which can be diagonalised numerically to find the fermionic ground state and excited states within the subspace we have restricted to as described in section 2.4.

3.3 Ground state degeneracy

We can apply the analysis described in section 2.4 to calculate the ground state degeneracy of the model with a defect. Unlike the model without a defect, we no longer expect the true ground state of the system to be in the vortex free sector. To see why we can fix $J_z = 1$ and take $J_x, J_y \ll 1$ to treat the x and y-link interactions as a perturbation of the system. The first non-constant effective Hamiltonian given at fourth order of perturbation theory is

$$H_{\text{eff}}^{(4)} = -\frac{J_x^2 J_y^2}{16 J_z^3} \sum_p Q_p, \tag{3.21}$$

where the Q_p operators the same operators appearing in (2.21) and the summation is over all the square plaquettes of the system, excluding the two defect plaquettes. However, the operators for the defect plaquettes are present in the Hamiltonian given at fifth order of perturbation theory:

$$H_{\text{eff}}^{(5)} = \frac{3 J_x^2 J_y^3}{64 J_z^4} (Q_t + Q_b), \tag{3.22}$$

where Q_t and Q_b are the analogue of Q_p operators for the top and bottom defect plaquettes respectively. Explicitly, these operators are given by

$$Q_p = \begin{cases} \tau_a^z \tau_b^y \tau_c^x \tau_d^z \tau_e^y & \text{if p is at the top defect plaquette,} \\ \tau_a^z \tau_b^y \tau_c^z \tau_d^y \tau_e^x & \text{if p is at the bottom defect plaquette.} \end{cases} \tag{3.23}$$

Here, we label the vertices of the defect plaquettes as in Fig. 3.5.

Clearly the effective Hamiltonian $H_{\text{eff}}^{(4)} + H_{\text{eff}}^{(5)}$ is minimised in the sector where the Q_p operators corresponding to square plaquettes all have eigenvalue 1 while the operators Q_t and Q_b have eigenvalue -1. In this setting where $J_x, J_y \ll J_z$, we expect the ground state to be vacant of fermions, so when acting on the ground state with a vortex operator, the single site fermion/boson parity factors appearing in (3.10) can be ignored meaning the actions of the vortex operators W_p and the Q_p operators are really equivalent on the ground state. Hence we expect the true ground state of the system to be in the sector where all the square plaquettes of the lattice are unoccupied by vortices but the two defect plaquettes are occupied.

This two-vortex sector is composed of eight sectors: four homology sectors with even parity and four homology sectors with odd parity. These correspond to the eight configurations of eigenvalues associated to two loop operators and the defect string operator. The defect string operator does not appear

in the Hamiltonian of the system via the X and Y operators like the vortex and loop operators do. Instead, choosing to restrict our attention to a sector corresponding to a particular eigenvalue of S_d influences the spectrum via the parity of fermions (3.12). For this reason, we refer to the different eigenspaces of S_d as the even and odd parity sectors. The particular eigenvalue of S_d that corresponds to even parity sector and which one corresponds to the odd parity sector is determined by the vortex and loop configuration via (3.12).

We calculated the fermionic ground state energy for the eight sectors in both the Abelian and non-Abelian phase and found a four fold degeneracy of the ground state in both phases. In Fig. 3.8 we plot, as a function of $J = J_x = J_y$, the energy of the fermionic ground states and first excited states in each of the 8 homology and parity sectors, after subtracting the lowest fermionic ground state energy out of the 8 sectors E_{min}. We fix $J_z = 1$ and $\kappa = 0.2$. The calculation was done with a 16×16 lattice which had a defect of length $L = 10$. We see from the figure, in the Abelian phase ($J < 0.5$) the four homology sectors with even parity form the ground state while the fermionic ground states from the four homology sectors with odd parity are all excited states. As the system crosses the phase transition with increasing J, one of the homology sectors with even parity becomes excited. At the same time, the same homology sector with odd parity drops in energy to form part of the ground state leading to the four fold degeneracy in the non-Abelian phase. The first excited state in each homology/parity sector never drops in energy, as the system crosses the phase transition, so it does not contribute to the ground state degeneracy.

We do not observe a different ground state degeneracy in the Abelian phase for lattices with odd sizes N_x or N_y like we did with a regular lattice without a defect. This is because, unlike the lattice without a defect, states of the system with either odd or even parity in a particular vortex/homology sector represent true states of the system. For instance, for a lattice with a defect and with both N_x and N_y even, the four homology sectors within the two vortex sector and with even parity form the ground state degeneracy in the Abelian phase

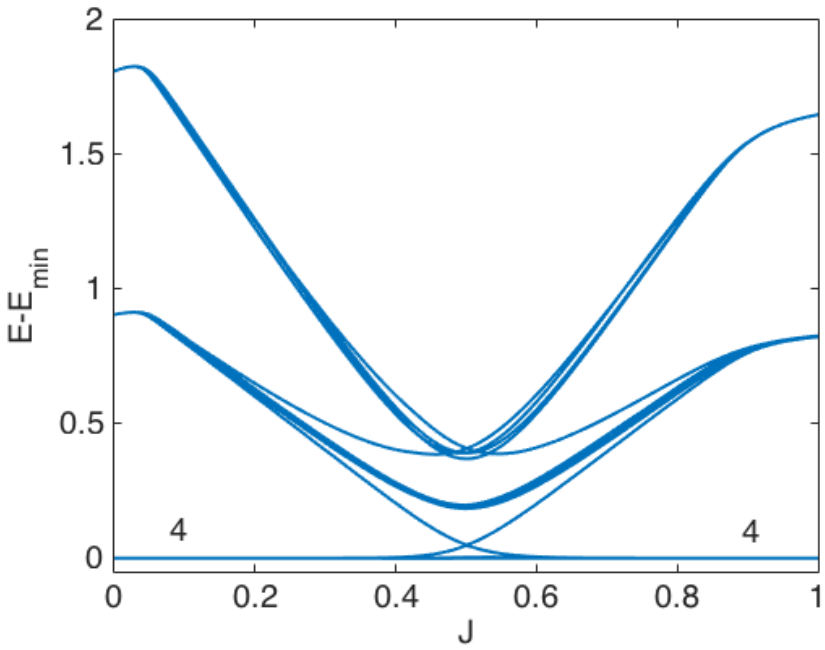

Figure 3.8: Here we plot the difference between E_{min} and the energy E of fermionic ground states and first excited states in each homology and parity sector as a function of $J_x = J_y = J$ for $N_x = N_y = 16$ and $\kappa = 0.2$. The number of degenerate ground states is included in both the Abelian ($J < 0.5$) and non-Abelian ($J > 0.5$) phases.

of the model. Altering the size of the lattice so that either N_x or N_y are odd will change the parity of two of those sectors via (3.12). This will increase the fermionic ground state energy of those sectors and turn them into excited states. However, at the same time the same sectors with odd parity also change parity which will decrease their fermionic ground state energy to replace the original sectors and so the system retains its four fold degenerate ground state.

3.4 Zero-modes attached to defect plaquettes

Calculating the single particle spectrum, as discussed in section 2.6, for a system with a defect in the vortex free sector reveals the formation of two zero-modes in the non-Abelian phase. In Fig. 3.9, we plot the four energy levels closest to zero as a function of $J = J_x = J_y$. This calculation was done with a 16×16 lattice with a defect of length 10, $\kappa = 0.2$ and $l_x = l_y = -1$ in the sector with no vortices. We see the two levels closest to zero tend to zero as

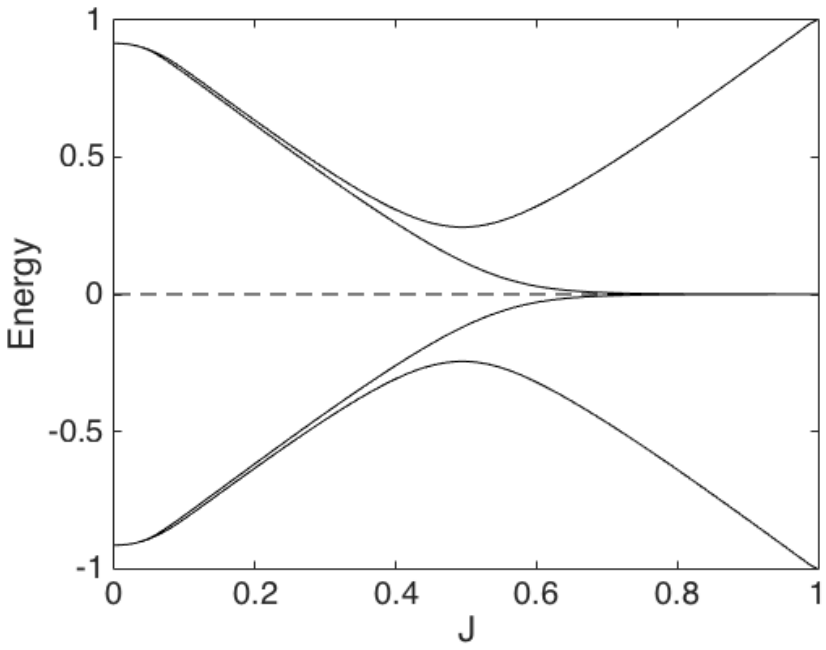

Figure 3.9: Here we plot the four single particle energy levels closest to zero for a 16×16 lattice, in a sector the vortex free sector, as a function of $J = J_x = J_y$ (we fix $J_z = 1$, $l_x = l_y = 1$ and $\kappa = 0.2$). The formation of zero-modes when the model transitions into the non-Abelian phase resembles the formation of zero-modes when the defect is absent and the model is occupied by two vortices shown in Fig. 2.11.

the model transitions from the Abelian phase to the non-Abelian phase. The same behaviour occurs in the other homology sectors.

The energy of these zero modes are not exactly zero for a $N_x \times N_y$ lattice with a defect of length L_d due a finite separation L_d between the defect plaquettes. Calculating the energy of these modes for various defect lengths shows the energy of these fermionic modes decrease exponentially as the defect length is increased. In Fig. 3.10 we plot this dependence for different values of κ. Each calculation for a system with a defect of length L_d was done using a $2L_d \times 2L_d$ lattice in the $(1, 1)$ homology sector.

In Fig. 3.11 we plot the wave function of the quasiparticle corresponding to these energy levels for a 40×40 system with a defect of length $L = 20$ in the non-Abelian phase $J_x = J_y = J_z = 1$. We note, in order to visualise the wave function over a 40×40 lattice, like we did in section 2.6, we set the value of the wave function to zero over the sites that were deleted when the defect was

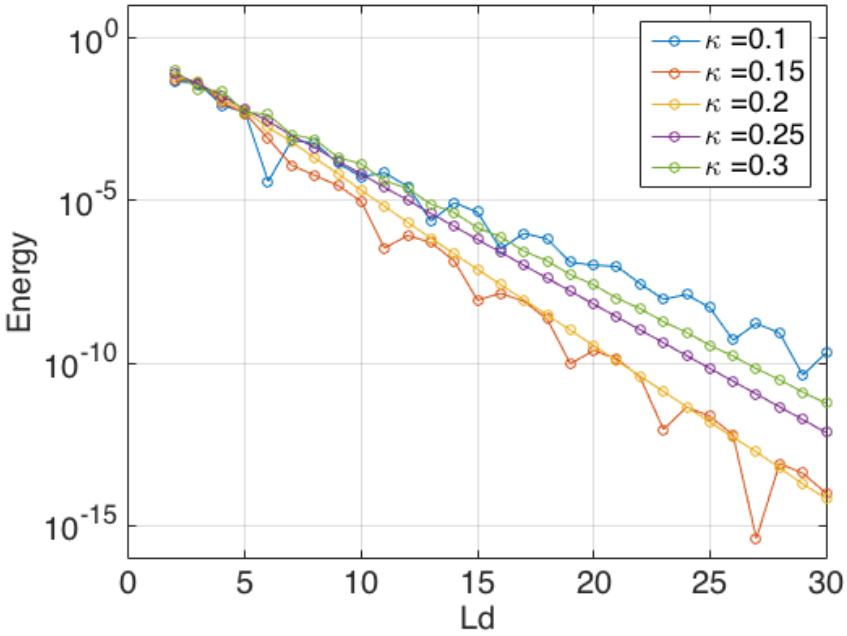

Figure 3.10: Here we plot the energy of the positive single particle energy level closest to zero as a function of the length of the defect L_d for different values of κ. We see the energy tends to zero as the length of the defect increases, confirming zero-modes exist in the model with well separated defect plaquettes.

introduced. We see the wave function of this quasiparticle is localised about the top and bottom defect plaquettes. This behaviour is essentially identical to the situation where the zero modes are localized around vortices discussed in section 2.6.

These zero energy quasiparticles attached to well separated defect plaquettes affect the fermionic ground state degeneracy in much the same way as pairs of vortices do. For $2M$ well separated vortices and defect plaquettes in a particular homology and parity sector, the fermionic ground state is 2^{M-1} fold degenerate. Unlike vortices, however, the defect plaquettes cannot be moved around the system without constantly decoupling and re-coupling the underlying lattice and so cannot be braided with one another.

On the other hand, one can consider braiding vortices with the defect plaquettes which differs from the braiding of vortices amongst themselves due to the presence of the defect string symmetry. If we consider braiding in a system with a single defect and some number of vortices well separated from each other and the defect plaquettes, the evolution operator that permutes the

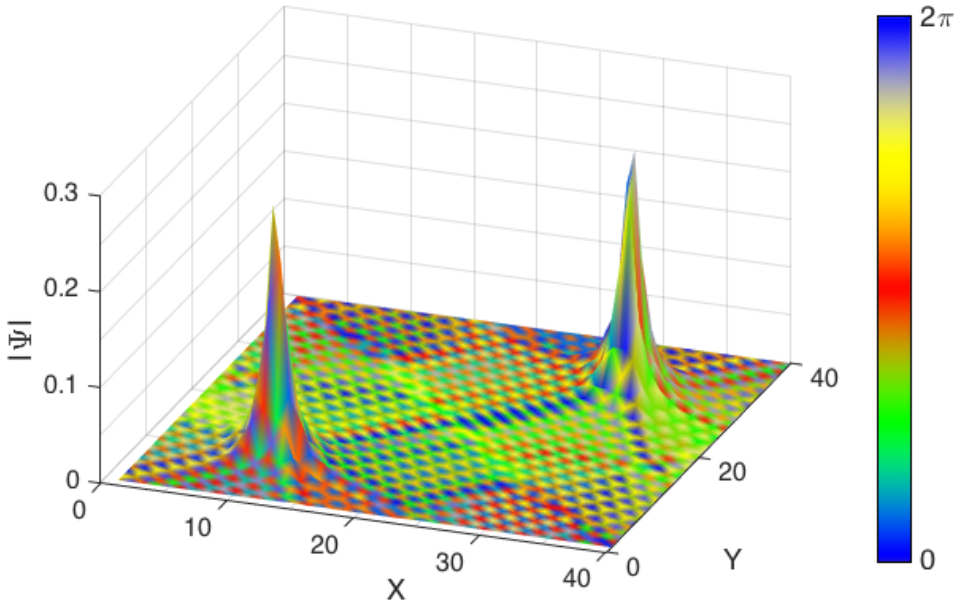

Figure 3.11: Plotted is the eigenstate corresponding to the lowest positive single particle energy level appearing in Fig. 3.9 in the non-Abelian phase. This plot was calculated with $J_x = J_y = J_z = l_x = l_y = 1$ and $\kappa = 0.1$ on a 40×40 lattice with a defect length of 20 in the vortex free sector. On the z-axis we plot the modulus of the state. The colour bar shows how colours are assigned to the plot depending on the phase of the eigenstate at any one site.

vortices about the defect plaquettes may not commute with the defect string operator and so may change the parity of the state it acts on. Hence, in terms of quantum computation, if we have M zero energy quasiparticles and unitary gates are implemented via braiding, the computational space associated with a particular homology sector of a system with a defect is 2^M dimensional instead of 2^{M-1} dimensional like it is for a system without a defect.

Being able to alter the parity of fermions in the system by braiding excitations with end points of a defect is how Petrova et al were able to show that excitations in the Abelian phase of the model exhibit non-Abelian statistics [37]. Defect plaquettes like the ones we have studied are also known as twist defects. It has been pointed out by You and Wen that unlike the excitations of the Hamiltonian, twist defects have projective non-Abelian statistics [39, 40]. It has also been shown by Brown et al, by calculating topological entanglement entropy, that twist defects have the same quantum dimension and fusion rules as Ising anyons [41].

3.5 Conclusions

We introduced a lattice defect into the Kitaev honeycomb model by removing a line of z-links from the lattice and coupling their neighbours together. We then accordingly generalised the solution of the model to be able to facilitate the lattice defect. An important part of this effort was the accommodation of new symmetries of the model associated with five sided plaquettes created by the defect and particularly the defect itself.

The symmetry associated with the defect plays a central role in the dependence of fermionic parity on the symmetries of the model and allows us to represent physical states of the hexagonal lattice model by states of the square lattice model with both odd and even parity. This inevitably results in a ground state degeneracy of four regardless of which phase the model is tuned to and regardless of the size of the lattice.

Also, the five sided plaquettes manifest themselves through the formation of fermionic zero energy modes localised around these plaquettes. This implies the ground state of the model is no longer in the vortex free sector when the defect is introduced but in a sector where two vortices occupy the five sided plaquettes.

Moreover, since states of both even and odd parity are now allowed, the dimension of the degenerate subspace associated with $2M$ well separated excitations is now twice what it was before the defect (i.e. 2^M rather than 2^{M-1}). Thus, with a such a defected lattice, a qubit may now be realised by just two excitations rather than four.

We believe that introducing dislocation defects into the non-Abelian topological phase opens up interesting opportunities. For example, they enable a more complex fractional statistics as suggested by Kitaev [18] and shown by Petrova et al. [37] in the Abelian phase of the honeycomb model. They are also related to interesting algebraic structures that generalize the braid group like those in [42] for example. On a more abstract level, they are also connected with extended topological quantum field theories [43].

Chapter 4

The Kitaev Model with Higher Genus

4.1 Lattices of genus $g \geq 2$

In this chapter we will discuss how to realise the Kitaev honeycomb model on lattices that tile closed surfaces of genus greater than one and extend the solution of the model used thus far to be able to study the model on such surfaces. A key aspect of the solution we have been using is a mapping of the honeycomb lattice onto a square lattice with spins and hardcore bosons living on the vertices. However, a square lattice can only be realised on two surfaces with distinct topologies, namely the plane and the torus. This is because the Euler characteristic of a square lattice is zero, as is that of the original hexagonal lattice. Our aim is to modify the solution so that we can numerically calculate the spectrum of the model on higher genus lattices, in different vortex/homology sectors, as was done in the previous chapter to study a lattice defect. We will do this by introducing a lattice which can be realised on such surfaces and adjust any definitions or relations used by the solution to fit the context of this new lattice. We will then use the solution to calculate the ground state degeneracy of the model in both the Abelian and non-Abelian phases on a number of different surfaces of genus greater than one.

To put the model on a closed surface of genus $g > 1$ we necessarily have to

consider a lattice with a negative Euler characteristic due to the well known relation between the Euler characteristic and genus: $\chi = 2 - 2g$. This rules out using a perfect square lattice because for such a lattice with N vertices, there are N plaquettes and $2N$ edges and so $\chi = V - E + F = N - 2N + N = 0$, where V is the number of vertices of the lattice, E is the number of edges and F is the number of plaquettes (faces). We can create a lattice with negative Euler characteristic by taking a square lattice and altering some of its vertices or plaquettes. For example, these alterations may include increasing or decreasing the number of edges connected to some vertices or increasing/decreasing the number of edges surrounding a number of plaquettes so that they are no longer square. We will refer to such alterations as defects. We would like to avoid non-local defects such as lines of dislocation defects [44, 37, 38] and keep any defects introduced to the lattice localised to some degree (we can think of them as particles, called genons [40, 45]). We will first introduce a lattice with genus $g = 2$ before considering lattices with genus $g > 2$.

We can create a surface with genus $g = 2$ by taking an octagon and identifying its opposing boundaries in a way similar to creating a torus by taking a rectangle and gluing the opposing boundary edges together. The construction is illustrated in Fig. 4.1. If we tessellate an octagon with a square lattice and identify the sites and edges residing on the boundary as indicated in Fig. 4.2, the resultant lattice will have genus $g = 2$. The square lattice will then have a defect plaquette with twelve edges centred around the corners of the original octagon, all of which are identified once the boundary edges are glued together. Clearly we could tessellate an octagon with a variety of square lattices of different sizes. The particular lattice we use can be characterised by three numbers $\{N_a, N_b, N_c\}$ which specify the number of vertices or edges along the vertical, diagonal and horizontal edges respectively as shown in the Fig. 4.2. The total number of vertices on such a lattice with dimensions $\{N_a, N_b, N_c\}$ is $N_{tot} = 2N_b(N_a + N_b + N_c) + N_a N_c$. We can calculate the Euler characteristic by noticing that there are exactly $2N_{tot}$ edges and $N_{tot} - 2$ plaquettes including the

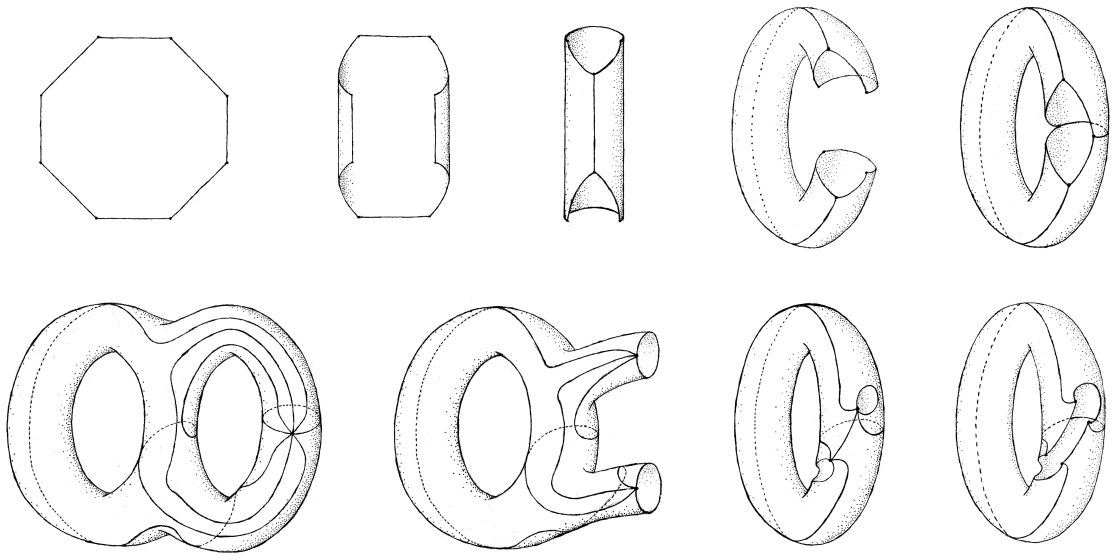

Figure 4.1: To construct a genus 2 surface we can identify the diametrically opposed edges of an octagon.

defect plaquette. Hence we have $\chi = N_{tot} - 2N_{tot} + N_{tot} - 2 = -2$ as desired. We note for completeness that there are other ways of gluing the edges of an octagon together in order to produce a $g = 2$ surface but these may lead to emergence of undesired line defects. Our approach described above avoids this issue.

Alternatively, we could consider a similar construction using the dual lattice. While the original lattice has each vertex four-valent and all plaquettes are square except the defect plaquette, the dual lattice has all plaquettes square and all vertices four-valent except one defect vertex which is twelve-valent. However, this would require changes of the Hamiltonian of the model. We therefore prefer to work with the original lattice which preserves the form of the Hamiltonian. We will, nevertheless, need to define the vortex operator for the defect plaquette and also its magnetic contribution.

We now consider the construction of lattices on surfaces with genus $g > 2$. One approach to generalise the construction developed for the $g = 2$ surfaces above would be to start with a polygon with a greater number of sides (e.g. dodecagon for a g=3 surface) and then glue the opposite sides accordingly. Here we prefer a different and more modular approach which lends itself more

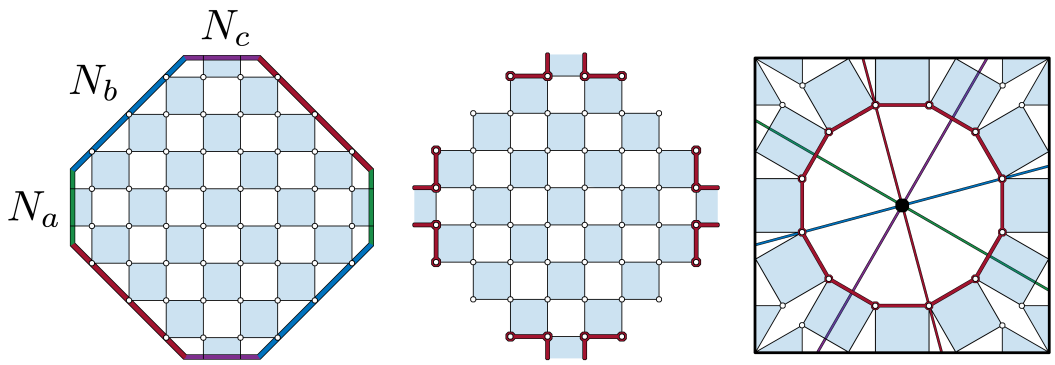

Figure 4.2: The lattices we will be considering on genus 2 surfaces will tessellate an octagon as depicted on the left. They are characterised by three numbers N_a, N_b and N_c. N_a is the number of links crossing the vertical (green) edge of the octagon. N_b is the number of sites living on a diagonal (blue or red) edge. N_c is the number of links crossing the horizontal (purple) edge of the octagon. When the edges have been identified appropriately, the links coloured red in the centre image form a closed chain depicted in the image on the right. The corners of the octagon are all meet at a common point represented by the black dot at the centre of the right image. The corresponding plaquette, centred around this point, will have twelve edges and we will refer to it as the defect plaquette.

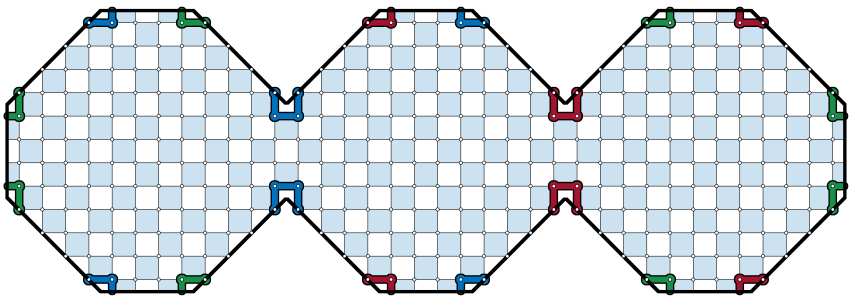

Figure 4.3: Joining three copies of the octagonal piece of lattice as depicted and imposing the same boundary conditions on the diagonal and horizontal edges as described in Fig. 4.2 on each octagon results in a lattice tiling a surface of genus $g = 4$ after the vertical edges have been identified.

naturally to a numerical implementation.

Regarding an octagon, once all but two of the edges have been glued together, we are left with a surface with the topology of a torus with two punctures in it. We can use this as a building block for constructing surfaces with higher genus. If we take $g-1$ copies of a torus with two punctures, we can always glue the punctures together in such a way that results in a closed connected surface of genus g. With regards to the lattice, this means we can start with $g-1$ copies of the octagonal piece of square lattice described above and stitch them together to form a chain of octagons as depicted in Fig.4.3. We then form a lattice on a surface of the desired topology by identifying the remaining opposing edges of each octagon as well as by gluing together the remaining edges of the first and the last octagon of the chain. The resultant lattice will have $g-1$ defect plaquettes, identical to the one described above, located where two octagons are joined together.

We now verify the Euler characteristic for our higher genus lattices. If each octagonal piece has dimensions N_a, N_b and N_c then the total number of vertices on this lattice is $(g-1)N_{tot}$. We can still uniquely associate every vertex to two edges so the lattice has $2(g-1)N_{tot}$ edges. To write down the number of plaquettes as a function of the lattice dimensions $\{N_a, N_b, N_c\}$, we can associate every vertex to the upper right hand plaquette it forms a corner of. Every square plaquette will be assigned a unique vertex while the defect plaquettes will be assigned three. So the number of plaquettes on the lattice is equal to the number of vertices minus 2 for every defect: $(g-1)N_{tot} - 2(g-1)$. Hence the Euler characteristic of the lattice is $\chi = (g-1)N_{tot} - 2(g-1)N_{tot} + (g-1)N_{tot} - 2(g-1) = 2-2g$ as expected.

4.2 The model on surfaces of genus $g \geq 2$

4.2.1 The effective spin/hardcore boson representation

We will now consider the model on the lattices constructed in the last section. We first write down and discuss the Hamiltonian for the system and its symmetries in the effective spin/hardcore-boson representation of the model. We then fermionize the bosons to obtain a Hamiltonian quadratic in fermionic operators. Since the lattices we will be considering do not have any translational symmetries, we will not be able to write down the ground state in closed form as was done in [21] for the model on a torus. However, the formalism allows one to efficiently diagonalise the Hamiltonian numerically within any particular common eigen-subspace of the model's symmetries.

The Hamiltonian in the effective spin/hardcore-boson representation on the lattice described above is of the same form as that on a lattice without defects (2.19). In both cases, every vertex is four-valent with two horizontal (x-links) and two vertical (y-links) edges attached. If we denote a site of the lattice by q, then by $q + n_x$ we denote the neighbour to the right of q that is connected to it by an x-link. Similarly, we use the notation $q + n_y$ to denote the neighbour above q that is connected to it by a y-link. The bare Hamiltonian can then be written as follows:

$$\begin{aligned} H_0 = &- J_x \sum_q (b_q^\dagger + b_q)\tau^x_{q+n_x}(b^\dagger_{q+n_x} + b_{q+nx}) \\ &- J_y \sum_q i\tau^z_q (b_q^\dagger - b_q)\tau^y_{q+n_y}(b^\dagger_{q+n_y} + b_{q+ny}) \\ &- J_z \sum_q (I - 2b_q^\dagger b_q). \end{aligned} \tag{4.1}$$

Regarding the potential $V = \sum_p V_p$, the contribution from the square plaquettes are still given by the expression (2.20). On the other hand, the contribution of the defect plaquettes to the potential are more complicated and are given by:

$$
\begin{aligned}
V_p = \tau_l^y \tau_a^z \tau_b^x (I - 2N_a)(b_l^\dagger + b_l)(b_b^\dagger + b_b) \quad & + i\tau_b^x (b_a^\dagger + b_a)(b_b^\dagger - b_b) \\
+ \tau_b^z \tau_c^y (b_b^\dagger + b_b)(b_c^\dagger + b_c) \quad & + i\tau_b^z \tau_c^z (b_b^\dagger - b_b)(b_d^\dagger + b_d) \\
+ i\tau_c^x (b_c^\dagger + b_c)(b_d^\dagger - b_d) \quad & + \tau_d^y \tau_e^z (b_d^\dagger - b_d)(b_e^\dagger - b_e) \\
+ \tau_d^y \tau_e^z \tau_f^x (I - 2N_e)(b_d^\dagger + b_d)(b_f^\dagger + b_f) \quad & + i\tau_f^x (b_e^\dagger + b_e)(b_f^\dagger - b_f) \\
+ \tau_f^z \tau_g^y (b_f^\dagger + b_f)(b_g^\dagger + b_g) \quad & + i\tau_f^z \tau_g^z (b_f^\dagger - b_f)(b_h^\dagger + b_h) \\
+ i\tau_g^x (b_g^\dagger + b_g)(b_h^\dagger - b_h) \quad & + \tau_h^y \tau_i^z (b_h^\dagger - b_h)(b_i^\dagger - b_i) \\
+ \tau_h^y \tau_i^z \tau_j^x (I - 2N_i)(b_h^\dagger + b_h)(b_j^\dagger + b_j) \quad & + i\tau_j^x (b_i^\dagger + b_i)(b_j^\dagger - b_j) \\
+ \tau_j^z \tau_k^y (b_j^\dagger + b_j)(b_k^\dagger + b_k) \quad & + i\tau_j^z \tau_k^z (b_j^\dagger - b_j)(b_l^\dagger + b_l) \\
+ i\tau_k^x (b_k^\dagger + b_k)(b_l^\dagger - b_l) \quad & + \tau_l^y \tau_a^z (b_l^\dagger - b_l)(b_a^\dagger - b_a)
\end{aligned}
\tag{4.2}
$$

Here, we label the vertices of the defect plaquette as in Fig. 4.4. This expression follows from translating the three-body spin terms, linked at the third order of perturbation theory to the weak magnetic field, into the effective spin/hardcore-boson representation. In the original honeycomb picture, the defect corresponds to a plaquette with eighteen edges and its contribution to the potential is the following sum of three-body spin terms:

$$
\begin{aligned}
V_p \; = \sigma_{18}^y \sigma_1^z \sigma_2^x \; + \sigma_1^x \sigma_2^y \sigma_3^z \; + \sigma_2^z \sigma_3^x \sigma_4^y \; + \sigma_3^y \sigma_4^z \sigma_5^x \; + \sigma_4^x \sigma_5^y \sigma_6^z \; + \sigma_5^z \sigma_6^x \sigma_7^y \\
+ \sigma_6^y \sigma_7^z \sigma_8^x \; + \sigma_7^x \sigma_8^y \sigma_9^z \; + \sigma_8^z \sigma_9^x \sigma_{10}^y \; + \sigma_9^y \sigma_{10}^z \sigma_{11}^x \; + \sigma_{10}^x \sigma_{11}^y \sigma_{12}^z + \sigma_{11}^z \sigma_{12}^x \sigma_{13}^y \\
+ \sigma_{12}^y \sigma_{13}^z \sigma_{14}^x + \sigma_{13}^x \sigma_{14}^y \sigma_{15}^z + \sigma_{14}^z \sigma_{15}^x \sigma_{16}^y + \sigma_{15}^y \sigma_{16}^z \sigma_{17}^x + \sigma_{16}^x \sigma_{17}^y \sigma_{18}^z + \sigma_{17}^z \sigma_{18}^x \sigma_1^y
\end{aligned}
\tag{4.3}
$$

We can still define a vortex operator which commutes with the full Hamiltonian $H = H_0 + \sum_p V_p$ for every plaquette. For square plaquettes the vortex operator is still defined as (2.21). For the defect plaquettes however we define the vortex operator as follows:

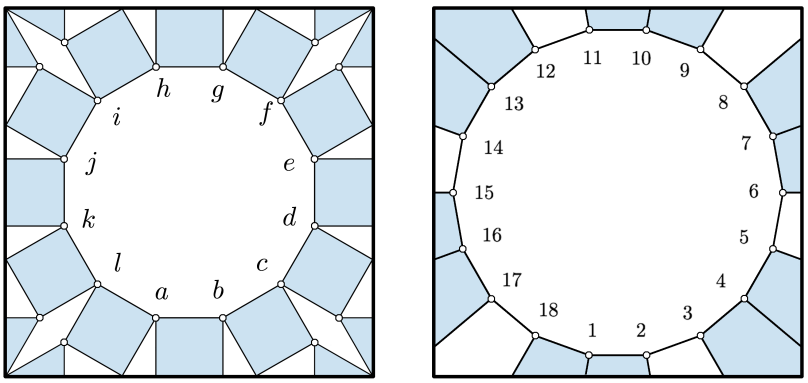

Figure 4.4: The twelve sided defect of the square lattice (left) becomes an eighteen sided defect plaquette (right) in the honeycomb lattice picture.

$$W_p = (1-2N_a)(1-2N_d)(1-2N_e)(1-2N_h)(1-2N_i)(1-2N_l)\tau_a^z\tau_b^y\tau_c^z\tau_d^y\tau_e^z\tau_f^y\tau_g^z\tau_h^y\tau_i^z\tau_j^y\tau_k^z\tau_l^y. \tag{4.4}$$

This definition of the vortex operator for the defect plaquette is equivalent to the following product of Pauli operators in the original honeycomb picture of the model:

$$W_p = \sigma_1^z\sigma_2^y\sigma_3^x\sigma_4^z\sigma_5^y\sigma_6^x\sigma_7^z\sigma_8^y\sigma_9^x\sigma_{10}^z\sigma_{11}^y\sigma_{12}^x\sigma_{13}^z\sigma_{14}^y\sigma_{15}^x\sigma_{16}^z\sigma_{17}^y\sigma_{18}^x. \tag{4.5}$$

In addition to the vortex operators, we can also define an operator, which commutes with the Hamiltonian, for every generator in a basis for the 1st $\mathbb{Z}_2$-homology group H_1 of the lattice. We will call these operators loop operators and to define them we will need to choose a basis for H_1 and a particular representative from each homology class in that basis. For a lattice of genus $g \geq 2$ the rank of H_1 is $2g$ so we will need to choose $2g$ homologically distinct cycles. We choose the cycles depicted in Fig. 4.5 and their associated homology classes as the representatives and basis respectively. As depicted, for a lattice with $g-1$ copies of an octagonal piece of lattice we will choose three cycles on the first copy, two cycles on every other copy (reflecting the fact that every additional copy increases the genus by 1 and the rank of H_1 by 2) and one horizontal cycle that spans each octagon. The loop operators we will define

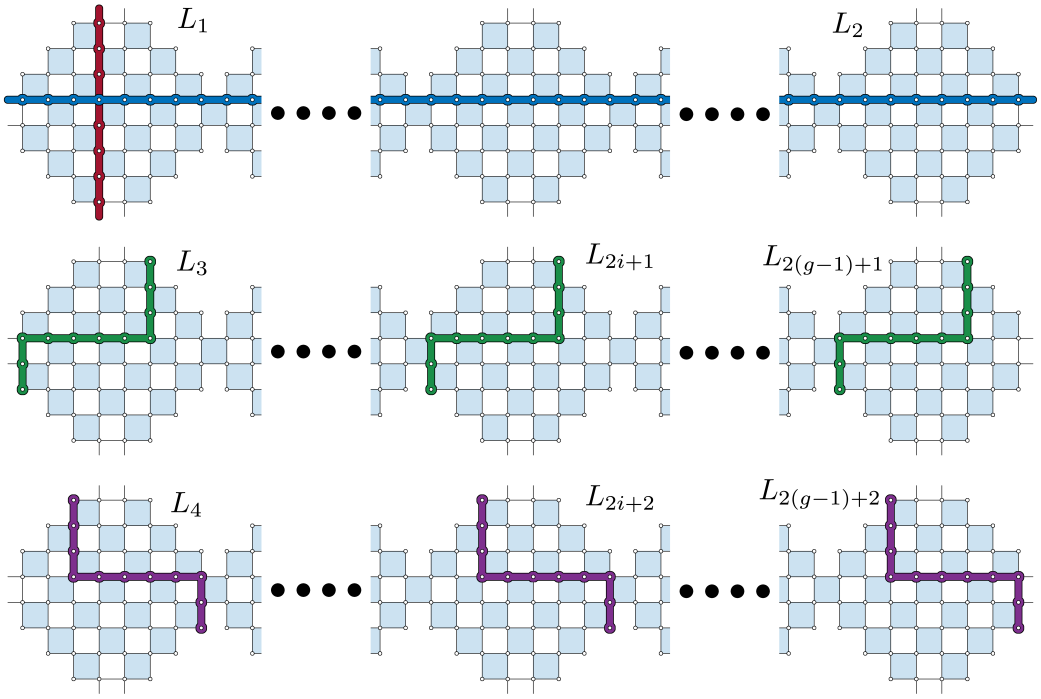

Figure 4.5: The first two cycles we choose, denoted L_1 and L_2, wrap vertically around the first octagonal part of the lattice and horizontally around the entire lattice as depicted. Also, for each octagonal part $i = 1 \cdots (g-1)$, we choose the two cycles labelled by L_{2i+1} and L_{2i+2}. There are $2g$ cycles in total.

for these cycles will act on the sites of the lattice that are connected to the links that constitute these cycles. How a loop operator acts on a particular site is determined by the way the associated cycle passes through it. There are six ways a cycle can pass through a site as depicted in Fig. 4.6 and we will associate a single site operator with each of them as follows:

$$\begin{aligned} &\text{Horizontal:} && -(1-2N)\tau^x \\ &\text{Vertical:} && \tau^x \\ &\text{Corner 1:} && -(1-2N)\tau^y \\ &\text{Corner 2:} && i\tau^z \\ &\text{Corner 3:} && -i(1-2N)\tau^z \\ &\text{Corner 4:} && -\tau^y \end{aligned} \tag{4.6}$$

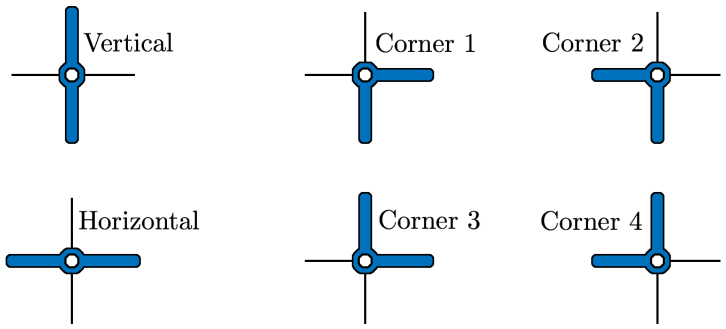

Figure 4.6: If a 1-chain passes through a site once, it can only do so in one of six ways as depicted.

We define the loop operator for a particular cycle as the composition of all the single site operators associated with the sites it passes through times a minus sign. For example, the cycle numbered 3 has a horizontal part, a vertical part and two corners and so the loop operator for this cycle can be written as follows:

$$L_3 = -\overbrace{[-(1-2N)\tau^y]}^{\text{Corner 1}}\overbrace{[\prod_i -(1-2N_i)\tau_i^x]}^{\text{Horizontal}}\overbrace{[-\tau^y]}^{\text{Corner 4}}\overbrace{[\prod_i \tau_i^x]}^{\text{Vertical}} \tag{4.7}$$

One can in principle define a different set of loop operators that commute with the Hamiltonian. However, following from (2.9), these will in general be equivalent to a product of the loop operators already defined times a product of vortex operators [46].

The vortex and loop operators form a set of commuting observables, allowing us to decompose the Hilbert space as follows

$$\mathcal{H} = \bigoplus_{\{w_p,\ l_i\}} \mathcal{H}_{\{w_p,\ l_i\}}. \tag{4.8}$$

Here $\{w_p\}$ and $\{l_i\}$ denote particular configurations of eigenvalues of all the vortex and loop operators respectively. $\mathcal{H}_{\{w_p,\ l_i\}}$ is the common eigen-subspace of all vortex and loop operators corresponding to the configuration $\{w_p, l_i\}$. The method we use to solve the model involves restricting the Hamiltonian to one of these subspaces where it can be expressed as a combination of terms

that are quadratic in fermionic operators. The restricted Hamiltonian can then be diagonalized by an appropriate Bogoliubov transformation.

We now want to change to a basis in the Hilbert space which reflects the decomposition (4.8). As we did when the model was on a torus, we will come up with a complete set of commuting observables, which include the vortex and loop operators, and use the corresponding set of common eigenvectors as our basis. We encounter the same issue for such choosing such a set of observables where it seems natural to consider the common eigenstates of the vortex and loop operators along with the boson number operator ($N_q = b_q^\dagger b_q$) for each site q of the square lattice. However, the basis so defined would be overcomplete. If there are $(g-1)N_{tot}$ sites in the lattice, the model clearly has $2^{2(g-1)N_{tot}}$ configurations of spins and bosons. Yet there are $(g-1)N_{tot}-2(g-1)$ vortex operators, $(g-1)N_{tot}$ boson number operators (one for each site of the square lattice) and $2g$ loop operators, all of which have eigenvalues ± 1. So there appears to be $2^{(g-1)N_{tot}-2(g-1)} \times 2^{(g-1)N_{tot}} \times 2^{2g} = 2^{2(g-1)N_{tot}+2}$ distinct combinations of eigenvalues a common eigenvector of this set of observables might have. This issue is again resolved by the fact the vortex and number operators satisfy two conditions and so are not completely independent.

The first condition is the fact that the product of all vortex operators is equivalent to the identity operator. That is,

$$\prod_P W_P = 1, \tag{4.9}$$

where the product is over all the plaquettes of the lattice. Since a product of vortex operators can be thought of as counting the parity of vortices occupying the associated plaquettes, this essentially means there can only be an even number of vortices in total in the model. So the number of independent vortex operators is $(g-1)N_{tot} - 2(g-1) - 1$ and hence the number of configurations of vortices in the model is $2^{(g-1)N_{tot}-2(g-1)-1}$.

The second condition is a relation between the parity of bosons in the system and a certain product of vortex operators. For a lattice where the

numbers N_a and N_b are both even, we can consider a set of plaquettes forming a checkerboard pattern as depicted in the top left image of Fig. 4.7 by the coloured squares. It is easy to check that since the Pauli operators square to the identity, the product of the vortex operators associated with the coloured (or uncoloured) plaquettes is equivalent to the boson parity operator.

$$\prod_{coloured} W_P = \prod_q (1 - 2N_q), \tag{4.10}$$

where q runs over all the sites of the lattice. In other words, the parity of the number of bosons must be the same as the parity of the number of vortices on coloured plaquettes (or equivalently uncoloured plaquettes). Since the parity of bosons is fixed to be 1 or -1 depending on the configuration of vortices, the number of independent boson number operators N_q is $(g-1)N_{tot} - 1$ and hence the number of configurations of bosons in the model is $2^{(g-1)N_{tot}-1}$.

For lattices where N_a or N_b are odd numbers, there is a similar dependence of the boson parity on the configuration of vortices in the system. For such lattices, we can not colour the plaquettes with a perfect checkerboard pattern but we can consider sets of plaquettes as depicted in Fig. 4.7, such that the checkerboard pattern is misaligned along a 1-cycle of links that separate plaquettes of the same colour. The exact pattern we choose to colour the plaquettes in and the associated cycle along which the checkerboard pattern is misaligned depends on the parity of the numbers N_a, N_b and g for the lattice and is described in Fig. 4.7. If we compose the corresponding vortex operators, the Pauli operators for sites away from this cycle will cancel out as they did before but along the cycle, the resultant operator will act with a string of Pauli operators and may not act with the parity operator $(1 - 2N_q)$ for some sites. However, we can cancel the action of these Pauli operators, and replace any missing single site parity operators we need to obtain the full boson parity operator, by composing this product of vortex operators with a product of loop operators that act on the sites connected to the links of the cycle. The desired product of loop

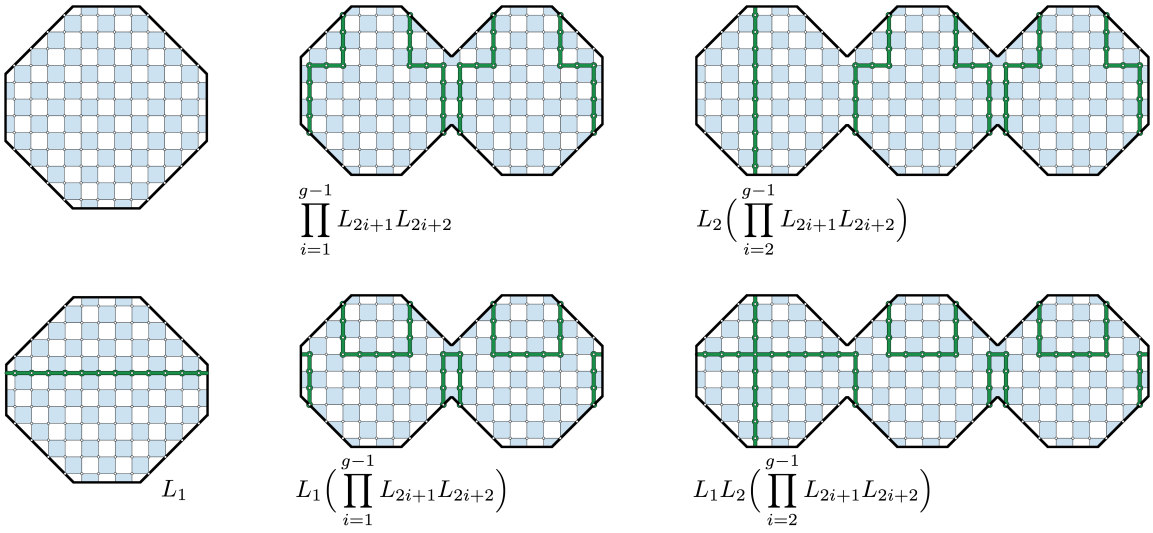

Figure 4.7: If both N_a and N_b are even numbers, then the plaquettes of each octagonal part of the lattice can be coloured in a checkerboard pattern as depicted in the top left image. If N_a is odd but N_b is even we can colour the plaquettes of each octagonal part as depicted in the bottom left image. In this case the checkerboard pattern is misaligned along the cycle associated with the loop operator L_1. If N_b is odd, then the pattern we colour the plaquettes in depends on the parity of g. If g is odd then the plaquettes of each octagonal part can be coloured like one of the octagonal parts of the top centre image if N_a is even or the bottom centre image if N_a is odd. If both g and N_a are even then the plaquettes of the first octagonal part can coloured as depicted in the top right image while those of the other octagonal parts are coloured like the other octagonal parts of the top right image. If g is even and N_a is odd then the plaquettes of the first octagonal part can coloured as depicted in the bottom right image while those of the other octagonal parts are coloured like the other octagonal parts of the bottom right image.

operators that act on the sites connected to the links of the cycle are shown in Fig. 4.7. In general, the boson parity operator can be written as

$$\prod_q (1-2N_q) = (-1)^{N_a N_c (g-1)} L_1^{N_a} (L_2 L_3 L_4)^{N_c (g-1)} \Big(\prod_{i=1}^{g-1} L_{2i+1}L_{2i+2}\Big)^{N_c} \prod_{coloured} W_P, \tag{4.11}$$

where the product of vortex operators is over the corresponding set of coloured plaquettes. These conditions mean we can form a complete set of commuting observables reflecting the decomposition (4.8) by taking all vortex and loop operators with every single site boson number operator and then excluding one vortex operator and one number operator.

4.2.2 Fermionization

The next step of the solution is to use the 'Jordan-Wigner' type transformation to fermionize the bosons of the model. To fermionize the bosons, we will again define a Jordan-Wigner type string operator for each site q of the lattice, denoted by S_q. The composition of these string operators with the boson creation and annihilation operators will be fermionic creation and annihilation operators. Expressing the Hamiltonian and other observables in terms of these new operators will effectively transform the hardcore bosons of the model into fermions.

To define a string operator for a site q of the lattice we consider the following: If we had a particle located at the reference site (as in Fig.4.8(a)) we can always move that particle to any site q by first moving it to the right an appropriate number of sites and then up an appropriate number of sites. Even the sites below the level of the reference site can be reached in this way by making use of the boundary conditions as shown in Fig.4.8(b). We can associate a single site operator for every site traversed in the path just described connecting the reference site to the site q. The string operator for q will be defined as the composition of these operators. To every site i crossed by the horizontal part of the path we associate the operator $-(1-2N_i)\tau_i^x$, to the corner of the path we associate the operator $-\tau_i^y$, to every site i crossed by the vertical part of the path we associate the operator τ_i^x and to the last site of the path we associate the operator τ_i^y. Since each of these operators act on different sites, they all commute with each other and so we are free to define S_q as the composition of these operators without worrying about the order of composition. If we let q_x denote the number of sites that need to be traversed in the horizontal part of the path with the site at the corner and q_y the number of sites that need to be traversed in the vertical part of the path with the site at the end, then we can number the sites of the path from 1 to $q_x + q_y$, beginning at the reference site and ending at q and we can write the string operator for q as follows:

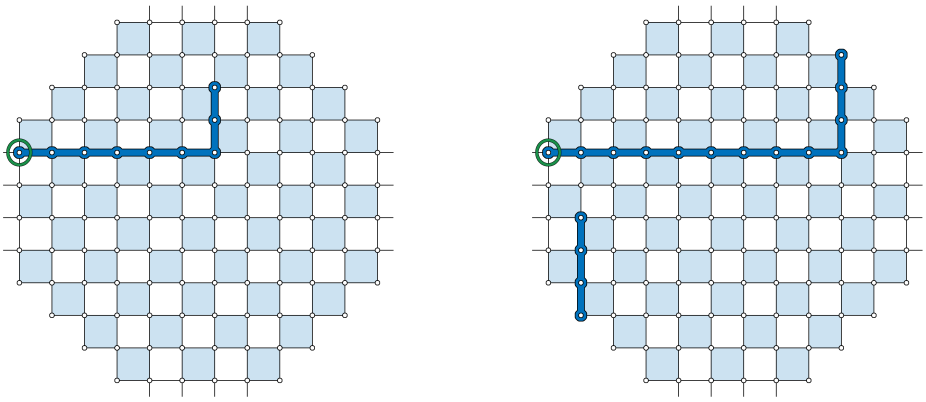

(a) (b)

Figure 4.8: The reference site we have chosen in defining string operators for each site of the lattice is encircled in green. Any site can be reached from the reference site by moving to the right a number of sites and then moving up a number of sites as shown in (a). Sites beneath the reference site can be reached in this way if the boundary conditions of the lattice are utilised as shown in (b).

$$\begin{aligned} S_q &= [-(1-2N_1)\tau_1^x] \times \cdots \times [-(1-2N_{q_x-1})\tau_{q_x-1}^x] && \text{horizontal part} \\ &\times -\tau_{q_x}^y && \text{corner} \\ &\times \tau_{q_x+1}^x \times \cdots \times \tau_{q_x+q_y-1}^x && \text{vertical part} \\ &\times \tau_{q_x+q_y}^y && \text{end} \end{aligned} \tag{4.12}$$

If we consider two string operators S_q and $S_{q'}$ such that $q \neq q'$ there will be a single site, shared by the paths defining the string operators, where the action of S_q anti-commutes with the action of $S_{q'}$. It follows that composing the string operator S_q with the bosonic creation and annihilation operators for the site q defines fermionic creation and annihilation operators for q which we denote by $c_q^\dagger$ and c_q.

$$\begin{aligned} &c_q^\dagger \equiv b_q^\dagger S_q, && c_q \equiv b_q S_q. \\ &\{c_q^\dagger, c_{q'}\} = \delta_{q,q'}, \quad \{c_q^\dagger, c_{q'}^\dagger\} = 0, \quad \{c_q, c_{q'}\} = 0, \end{aligned} \tag{4.13}$$

Expressing the basic Hamiltonian in terms of these fermionic creation and annihilation operators yields the following sum of quadratic fermionic terms:

$$\begin{aligned} H_0 =& J_x \sum_{x-links} X_{q1,q2}(c^\dagger_{q1} - c_{q1})(c^\dagger_{q2} + c_{q2}) \\ &+ J_y \sum_{y-links} Y_{q1,q2}(c^\dagger_{q1} - c_{q1})(c^\dagger_{q2} + c_{q2}) \\ &+ J_z \sum_q (2N_q - I), \end{aligned} \tag{4.14}$$

where, if $q1$ and $q2$ are sites on the left and right hand side of a x-link respectively, $X_{q1,q2} = -(I - 2N_{q1})S_{q1}\tau^x_{q2}S_{q2}$ and, if $q1$ and $q2$ are sites at the bottom and top of a y-link respectively, $Y_{q1,q2} = i\tau^z_{q1}S_{q1}\tau^y_{q2}S_{q2}$.

Noting that both the $X_{q,q'}$ and $Y_{q,q'}$ operators, being products of string operators, act on a closed loop of sites, we can associate a 1-cycle with each of the $X_{q,q'}$ and $Y_{q,q'}$ operators as we did when the model was on a torus. Namely 1-cycle consisting of the set of links joining the sites being acted on. These operators will always be equivalent to a product of loop operators, which is determined by the homology class of this cycle, and a product of vortex operators which is determined by a certain 2-chain related to the cycle and the representatives of the homology classes we have chosen as a basis for H_1. So whatever the homology class may be for the cycle a associated with an X or Y operator, we can always create a unique cycle b which will be homologous to a by adding some combination of the cycles associated with the loop operators. A particular X or Y operator is proportional to a product of the loop operators corresponding to the cycles used in the combination forming b.

There will also be a 2-chain, which we will denote by ς, which will have $a + b$ as a boundary. A particular X or Y operator will also be proportional to a product of the vortex operators associated with the plaquettes which constitute ς. This is a result of (2.9). We note that while such a 2-chain ς is not unique, the operator obtained by composing the vortex operators associated with the plaquettes of ς is unique. For example, if we cut out a cylinder with

boundaries a and b from a torus, the product of the vortex operators inside of the cylinder is the same as in its complement. This follows from the fact that vortex operators square to the identity and the relation (4.9). In general, when expressed in terms of loop and vortex operators, the X and Y operators are of the similar form. We will use a notation to reflect this by letting Z_q denote X_q if q is a x-link and Y_q if q is a y-link. Explicitly we have

$$Z_q = L_1^{a_1} \cdots L_{2g}^{a_{2g}} \prod_{P \in \varsigma(q)} W_P \tag{4.15}$$

where $(a_1, \cdots, a_{2g}) \in H_1$ is the homology class of the cycle associated with the link q in our chosen basis for H_1. The expression (4.15) highlights the dependence of the Z_q operators, and by extension the Hamiltonian, on the first homology group of the underlying lattice. The Hamiltonian can be written as follows:

$$\begin{aligned} H_0 =& J_x \sum_{x-links} Z_{q1,q2}(c_{q1}^\dagger - c_{q1})(c_{q2}^\dagger + c_{q2}) \\ &+ J_y \sum_{y-links} Z_{q1,q2}(c_{q1}^\dagger - c_{q1})(c_{q2}^\dagger + c_{q2}) \\ &+ J_z \sum_q (2N_q - I), \end{aligned} \tag{4.16}$$

Since the basic Hamiltonian is quadratic in fermionic operators, it can be written using the BdG formalism:

$$H = \frac{1}{2} \begin{bmatrix} c^\dagger & c \end{bmatrix} \begin{bmatrix} \xi & \Delta \\ \Delta^\dagger & -\xi^T \end{bmatrix} \begin{bmatrix} c \\ c^\dagger \end{bmatrix} \tag{4.17}$$

where the elements of the $(g-1)N_{tot} \times (g-1)N_{tot}$ matrices ξ and Δ are given by

$$\begin{aligned}\xi_{q,q'} &= J_z\delta_{q,q'} + J_x Z_{q,q'}\left(\delta^{(x)}_{q,q'} + \delta^{(x)}_{q',q}\right) + J_y Z_{q,q'}\left(\delta^{(y)}_{q,q'} + \delta^{(y)}_{q',q}\right), \\ \Delta_{q,q'} &= J_x Z_{q,q'}\left(\delta^{(x)}_{q,q'} - \delta^{(x)}_{q',q}\right) + J_y Z_{q,q'}\left(\delta^{(y)}_{q,q'} - \delta^{(y)}_{q',q}\right).\end{aligned} \tag{4.18}$$

Here, $\delta_{q,q'}$ is the usual Kronecker delta and $\delta^{(x)}_{q,q'}$ is defined to be 1 if q and q' are the sites on the left and right hand side of an x-link respectively and zero otherwise. Similarly, $\delta^{(y)}_{q,q'}$ is 1 if q and q' are the sites on the bottom and top side of a y-link respectively and zero otherwise.

Regarding the potential, when expressed in terms of the fermionic creation and annihilation operators, each term appearing in the sum defining the contribution from a plaquette inherits a product of string operators similar to the X and Y operators. The potential also becomes quadratic in fermionic operators and can be written as

$$V = \sum_p V_p = \frac{1}{2}\begin{bmatrix} c^\dagger & c \end{bmatrix}\begin{bmatrix} \bar{\xi} & \bar{\Delta} \\ \bar{\Delta}^\dagger & \bar{\xi}^T \end{bmatrix}\begin{bmatrix} c \\ c^\dagger \end{bmatrix}, \tag{4.19}$$

where the elements of the matrices $\bar{\xi}$ and $\bar{\Delta}$ are given by

$$\bar{\xi}_{q,q'} = i\sum_\rho Z_{q,\rho}Z_{\rho,q'}\left(-\delta^{(x)}_{q,\rho}\delta^{(y)}_{q',\rho} + \delta^{(x)}_{q',\rho}\delta^{(y)}_{q,\rho} + \delta^{(x)}_{\rho,q'}\delta^{(y)}_{\rho,q} - \delta^{(x)}_{\rho,q}\delta^{(y)}_{\rho,q'}\right), \tag{4.20}$$

and

$$\begin{aligned}\bar{\Delta}_{q,q'} = i\sum_\rho Z_{q,\rho}Z_{\rho,q'}&\left(\delta^{(x)}_{q,\rho}\delta^{(y)}_{q',\rho} - \delta^{(x)}_{q',\rho}\delta^{(y)}_{q,\rho} + \delta^{(x)}_{\rho,q'}\delta^{(y)}_{\rho,q} - \delta^{(x)}_{\rho,q}\delta^{(y)}_{\rho,q'}\right) \\ &- 2iZ_{q,q'}\left(\delta^{(x)}_{q,q'} - \delta^{(x)}_{q',q}\right) + 2iZ_{q,q'}\left(\delta^{(y)}_{q,q'} - \delta^{(y)}_{q',q}\right).\end{aligned} \tag{4.21}$$

Hence, the full Hamiltonian is

$$H = \frac{1}{2}\begin{bmatrix} c^\dagger & c \end{bmatrix}\begin{bmatrix} \xi + \kappa\bar{\xi} & \Delta + \kappa\bar{\Delta} \\ \Delta^\dagger + \kappa\bar{\Delta}^\dagger & -\xi^T - \kappa\bar{\xi}^T \end{bmatrix}\begin{bmatrix} c \\ c^\dagger \end{bmatrix} \tag{4.22}$$

Now, if we were to choose to restrict our attention a particular common eigenspace of the vortex and loop operators appearing in (4.8), we may replace the vortex and loop operators appearing in the definition of the Z operators by their eigenvalues. This would result in replacing the Z operators appearing in the Hamiltonian by their eigenvalues and we could diagonalise the square matrix appearing (4.22) numerically to study the spectrum in that subspace.

4.3 Ground state degeneracy

We can use the formalism developed so far to numerically calculate the ground state degeneracy of the model on a surface of arbitrary genus g, given enough computational resources to handle $(g-1) \times N_{tot}$ sites. As we are now able to restrict to a particular common eigenspace of the vortex and loop operators we can obtain an effective Hamiltonian for the fermions within that subspace. The unique ground state of this effective Hamiltonian can be found using the BdG formalism and we call it the fermionic ground state for the associated subspace.

According to the generalised flux phase conjecture the ground state of the model is in the common eigenspace of the vortex operators where all the corresponding eigenvalues are 1 (the vortex free sector of the Hilbert space). This was verified by Lieb [30] for lattices with certain periodicity. As the defect plaquettes break the translational symmetry of the lattices we are considering, the same periodicity cannot be realized and so the proof of Lieb is not applicable for our purposes. However, calculating the ground state energy of the model with different vortex configurations shows the introduction of vortices in or around the defect plaquettes increases the energy of the model. We thus assume the conjecture to be true for the lattices we are considering.

As discussed in section 2.5, the degeneracy arises from the different homology

sectors having fermionic ground states with the same energy. Hence, to calculate the ground state degeneracy of the system we need to calculate the fermionic ground state energy in each homology sector of the vortex free sector and see which ones have ground states with the same energy.

We considered the case of a genus $g = 2$ lattice, with both N_a and N_c being even numbers, and applied the analysis described above. We found that the system has a ground state degeneracy of 16 in the Abelian phase and 10 in the non-Abelian phase. In Fig.4.9a, we plot the difference in energy between the fermionic ground states in each of the 16 homology sectors and the homology sector with the lowest ground state energy as a function of $J = J_x = J_y$ while we fix $J_z = 1$, $\kappa = 0.2$ and $N_a = N_b = N_c = 4$. We see that the system with even dimensions N_a and N_c in the Abelian phase ($J < 0.5$) all 16 homology sectors are degenerate but as the system approaches the phase transition at $J = 0.5$ these sectors split with 6 of them becoming excited states in the non-Abelian phase ($J > 0.5$) while the other 10 sectors form the degenerate ground state.

When both N_a and N_c are odd numbers we find a eight-fold degeneracy of the ground state n the Abelian phase and ten in the non-Abelian phase. The different degeneracies we find in the Abelian phase are a result of (4.11). For lattices where both N_a and N_c are even, the parity of fermions in the ground state is the same for each homology sector. However, for lattices where either N_a or N_c are odd, the parity of fermions in the ground state is odd in half of the homology sectors and even in the other half. This leads to a splitting in the energy between fermionic ground states in half of the homology sectors from the other half resulting in the degree of degeneracy $d = 8$. In Fig. 4.9b, we see that the system with odd dimensions N_a and N_c has half of its homology sectors forming the ground state in the Abelian phase while the other half are excited states. As the system approaches the phase transition, the sectors forming the ground state begin to split with two of them becoming excited in the non-Abelian phase while four of the excited sectors drop in energy to join

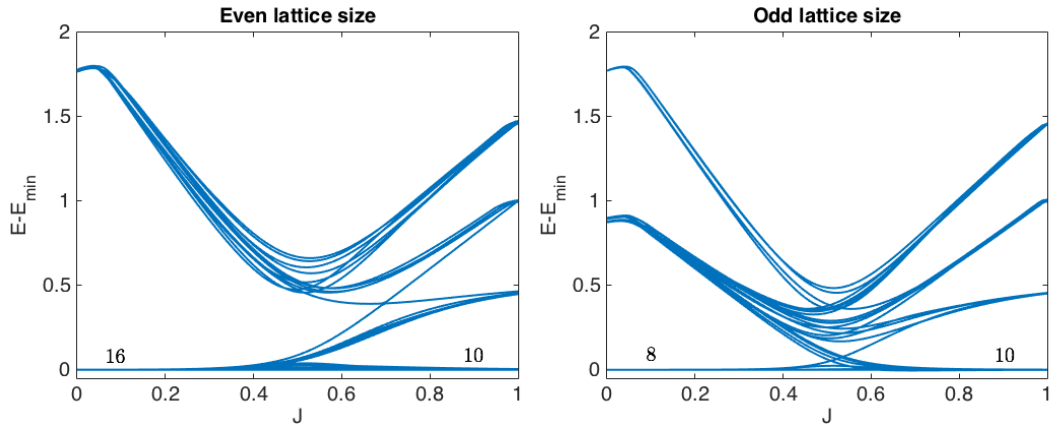

(a) (b)

Figure 4.9: In (a) we show the difference between E_{min} and the energy E of fermionic ground states and first excited states in each homology sector as a function of $J_x = J_y = J$ for $N_a = N_b = N_c = 4$ and $k = 0.2$ on a genus 2 lattice. In (b) the same energy difference is plotted for $N_a = N_b = N_c = 5$. The number of degenerate ground states is included just above the lowest curves in both the Abelian and non-Abelian phases.

the remaining six non-excited sectors to form the ten-fold degenerate ground state in the non-Abelian phase.

Due to finite size effects, there is a small splitting in the energy between the degenerate homology sectors that form the ground state. We expect this splitting to vanish in the thermodynamic limit. We measure this splitting by the difference in energy between the sector with the highest energy and the sector with the lowest energy. In Fig.4.10 we plot the splitting between the degenerate states as a function of $N = N_a = N_b = N_c$ for the two Abelian cases (even and odd sizes) and the non-Abelian case. As shown in the figure, we find the splitting between the sectors forming the ground state approaches zero exponentially as N grows. This calculation was done with $\kappa = 0.2$ in each case and with $J = 0.1$ for both of the Abelian cases and $J = 1$ for the non-Abelian case.

We used this method to calculate the degeneracy of the system on lattices with genus $g = 2, 3, 4, 5$ and 6 in both the Abelian (for even and odd sizes) and non-Abelian phases. We have summarized the results in Table (4.1) and we see the expected dependence of the ground state degeneracy on the topology of the underlying lattice. Namely, the model in the Abelian phase on a lattice with

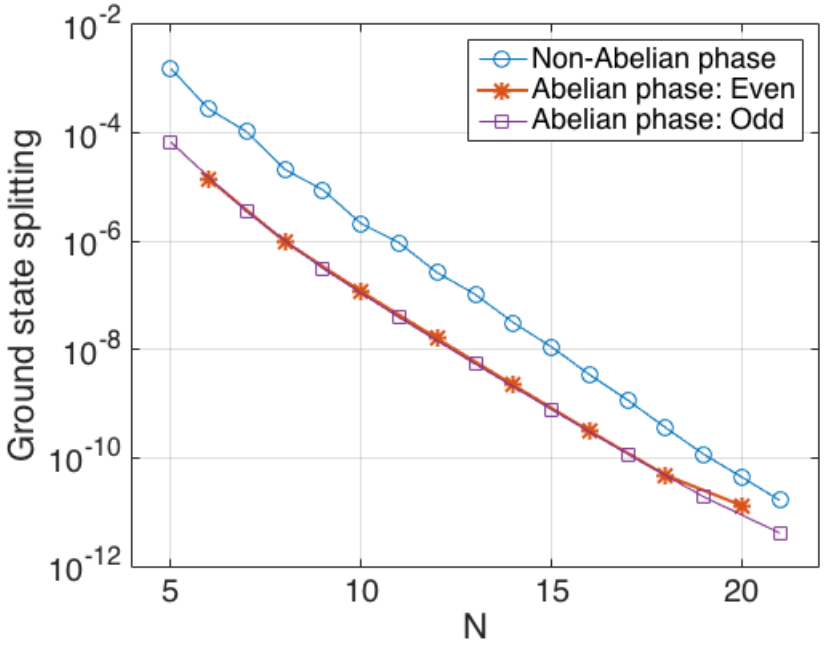

Figure 4.10: The splitting in energy between the degenerate homology sectors, measured by the difference between the sector with the highest energy and the sector with lowest energy, vanishes exponentially as the system size $N = N_a = N_c$ increases.

even size, which is equivalent to the toric code, has a ground state degeneracy that grows like 4^g with genus g. For systems where either N_a or N_c are odd we find the degeneracy is exactly half of 4^g. This can be attributed to the fact that the equivalent toric code in this case has a line defect in it like the one discussed in [33]. In the non-Abelian phase, which is equivalent to the Ising topological phase, we see the degeneracy is given by $2^{g-1}(2^g + 1)$ which is the number of even spin structures on a surface of genus g [47]. Graphs similar to those in Fig.4.9 were also calculated for these cases and can be found in appendix B.

Phase	$g = 2$	$g = 3$	$g = 4$	$g = 5$	$g = 6$
Abelian: Odd	8	32	128	512	2048
Abelian: Even	16	64	256	1024	4096
non-Abelian	10	36	136	528	2080

Table 4.1: The ground state degeneracy for lattices of genus g

As mentioned, these degeneracies are to be expected according to the relevant

topological quantum field theories (the toric code and Ising TQFTs). The formulae 4^g and $2^{g-1}(2^g+1)$ for the degeneracy in the Abelian and non-Abelian phases respectively can be derived using the general argument presented by Oshikawa et al [48] and by Einarsson [49]. We will briefly outline the derivation of the formula for the degeneracy in the Abelian phase and then repeat the argument for the non-Abelian case.

First, we consider the model in the Abelian phase on a torus. The quasi-particle excitations here are the toric code's electric and magnetic charges e and m. If we identify the torus with a square patch of the xy-plane in the usual way, we can consider a loop which wraps around the torus in the x direction and another loop that wraps around it in the y direction. We denote these two homologically non-trivial loops by C_x and C_y respectively. We can define two operators A_γ and B_γ ($\gamma = x, y$) for each of these loops as follows: we define A_γ by the process of creating a pair of electric charges and then moving one of the charges along the loop C_γ before annihilating the pair. Similarly, we define B_γ by the process of creating a pair of magnetic charges and then moving one of the them along the loop C_γ before annihilating the pair. These operators map ground states to ground states and satisfy the following relations which follow from the particles' exchange statistics:

$$[A_x, A_y] = [B_x, B_y] = [A_x, B_x] = [A_y, B_y] = 0$$

$$\{A_x, B_y\} = \{A_y, B_x\} = 0$$

We choose to use the eigenvalues of the commuting observables A_x and A_y to label the ground states of the system. Letting $|a_x, a_y\rangle$ denote a ground state, where a_x and a_y are eigenvalues of A_x and A_y respectively, we can generate three other ground states by applying the operators B_x and B_y. Namely the following states are also ground states:

$$B_x|a_x, a_y\rangle = |a_x, -a_y\rangle \qquad B_y|a_x, a_y\rangle = |-a_x, a_y\rangle \qquad B_yB_x|a_x, a_y\rangle = |-a_x, -a_y\rangle$$

So we have at least 4 ground states on a torus.

On a surface of genus g we can consider a pair of loops similar to C_x and C_y for each handle of the surface. Specifically, if we number the g handles of the surface, for the i-th handle we can consider two loops, C_x^i and C_y^i, that wrap around and through the i-th handle respectively. Moreover, we can choose such a set of loops such that the loops associated with one handle do not intersect with those of another handle. We can define operators A_γ^i and B_γ^i, as we did above, for each of these loops. Since the set of A operators is a commuting set of observables, we label the ground states by their eigenvalues. As the loops C_α^i and C_β^j $(i \neq j)$ do not intersect, the operators A_α^i and B_α^i commute with the operators A_β^j and B_β^j. Assuming we have a four fold degenerate ground state on a torus, it clearly follows that we can expect a 4^g fold degenerate ground state for a surface of genus g.

The non-Abelian phase of the model is equivalent to the Ising topological phase where the allowed topological charges are the vacuum 1, a half-flux quantum quasi-particle σ and a neutral fermion ψ. For a given surface of genus g we can consider the same set of homologically non-trivial loops as before. For each pair of loops associated with a particular handle we can similarly define operators A_γ^i and B_γ^i. A_γ^i is defined as the evolution operator that creates a pair of neutral fermions (c-fermions in our model) and then moves one of the fermions around the loop C_γ^i before annihilating the pair. B_γ^i is defined as the evolution operator that creates a pair of σ particles (which in our model are vortex excitations with majorana bound states attached) and then moves one of the particles around the loop C_γ^i before annihilating the pair. The A operators still commute with one another and so we again use their eigenvalues to label the ground states.

Considering first the system, on a torus, in a ground state with anti-periodic boundary conditions for the fermions in both the x and y directions (i.e. the state $|-1,-1\rangle$ as the boundary conditions correspond to the eigenvalues of the A operators). We can generate other ground states by applying B operators.

Namely $B_x|-1,-1\rangle$ and $B_y|-1,-1\rangle$. However, if we apply the operator B_x to a ground state, we also change the boundary condition in the y direction from anti-periodic to periodic. As a consequence, applying the operator B_y to the state $B_x|-1,-1\rangle$ produces an excited state. This is because if we create two σ particles and wrap them through the hole, they cannot be fused to form the vacuum due to the blocking mechanism discussed in [48]. Instead they fuse to a fermion. Thus, for a torus we have only three ground states and one state where a pair of σ particles are blocked from fusing to the vacuum.

Since, for a genus g surface, the A and B operators for a particular handle commute with those for every other handle we can immediately conclude we have at least 3^g ground states. However, if we create a left over pair of σ particles from one of the handles as described above, we can still form a ground state provided we create another left over pair out of another handle as both pairs fuse to a fermion and we can always fuse two fermions to the vacuum. Hence the total number of ground states on a genus g surface is the number of states we can create with an even number of left over σ pairs:

$$\begin{aligned}
N_g &= \sum_{k \text{ is even, } k=0}^{g} \binom{g}{k} 3^{g-k} \\
&= \sum_{k=0}^{g} \left(\frac{1+(-1)^k}{2}\right) \binom{g}{k} 3^{g-k} \\
&= \frac{1}{2}\sum_{k=0}^{g} \binom{g}{k} 3^{g-k} + \frac{1}{2}\sum_{k=0}^{g} \binom{g}{k} 3^{g-k}(-1)^k \\
&= \frac{1}{2}\left[(3+1)^g + (3-1)^g\right] \\
&= 2^{g-1}(2^g+1).
\end{aligned}$$

Here, the binomial theorem was used in going from line 3 to line 4.

4.4 Conclusion

In this chapter we realised the Kitaev honeycomb model on surfaces with genus $g \geq 2$ by considering the model on flat, octagonal pieces of lattice and gluing the boundaries together in a way that creates a lattice with the correct topology. Any such gluing necessarily introduces extrinsic defects to the underlying lattice. Solving the model on these higher genus lattices required a non-trivial generalization of the exact solution of the model to include extra loop symmetries associated with the homologically non-trivial loops of the lattice. We also highlighted the non-trivial dependence of the parity of fermions on both the vortex and loop symmetries of the model for even and odd lattice dimensions. The generalized solution was then used to calculate the ground states in both the Abelian and non-Abelian phases of the model. The degree of degeneracy of these ground states in both topological phases are in accord with available theoretical predictions based on topological quantum field theory.

Our work provides a direct realization of two distinct topological quantum field theories, specifically the Abelian doubled-$\mathbb{Z}_2$ and non-Abelian Ising theory, on closed surfaces of higher genus. As such it provides a solid basis for further investigation of the model on various manifolds, including also manifolds with boundaries which would extend previous studies of the Kitaev model [50]. Recent works on time-dependent simulation of creation and annihilation of vortex-like excitation on defects in the Kitaev model on torus [44] suggest the possibility of a dynamical process where creation and annihilation of extrinsic defects would result in dynamical change of the model genus and thus its topology. Interestingly this incarnation of topological field theory would be close to its axiomatic definition as a modular functor from a monoidal category of cobordisms to that of vector spaces [14, 16].

Other works have also considered topological models on higher genus surfaces [45, 51, 52, 53]. While our work involves creating lattices by gluing octagonal pieces of lattice together, these works consider two layers of a lattice with periodic boundary conditions and lattice dislocations are introduced to

effectively change the topology by creating ‘wormholes’ between the two layers.

Chapter 5

Conclusions and outlook

We introduced topologically ordered matter and illustrated its properties using the toric code model as an example. Namely, we demonstrated the toric code has a ground state degeneracy which depends on the topology of its lattice and that the model's quasiparticle excitations exhibit fractional statistics. We also mentioned the relevance of topological order to current research areas of modern mathematics in the context of TQFTs and highlighted the importance of topological order for the development of quantum technologies.

The Kitaev honeycomb model was then formally introduced. This model is a hexagonal lattice model that exhibits two distinct topological phases (The toric code phase and the Ising phase). We described the solution of the model developed by Kells et al [21] which first maps the model onto a square lattice with spin one half particles and hardcore bosons living on its vertices and then uses a Jordan-Wigner type transformation to turn the bosons of the model into fermions resulting in a Hamiltonian which is quadratic in fermionic operators. The model can then be expressed in the BdG formalism which allows us to numerically calculate the eigenvalues and eigenvectors of the Hamiltonian. This allows us to numerically calculate the ground state of the model and its degeneracy in either of its two phases. The solution also allows for the numerical simulation of the model's quasiparticle excitations undergoing braiding [31].

This solution was then altered to study the model with a lattice defect. We chose to study a lattice dislocation defect which is equivalent to the defect line

discussed by Kitaev and Kong in [33] when the model is tuned to its Abelian phase. The defect is introduced to the model by removing a line of sites from the model and recoupling their neighbours together in such a way that creates two plaquettes at the ends of the line which have eight edges and vertices while every other plaquette of the lattice has six edges and vertices. We found that the model with this defect has a symmetry associated with the defect which differs from the other symmetries of the model. We refer to this symmetry as the defect string operator. Unlike the regular symmetries of the model which act on chains of sites forming closed loops, the defect string operator acts on an open string of sites whose end points coincide with the defect end points. The defect string operator does not appear in the Hamiltonian like the plaquette and loop symmetries. Instead it appears as a factor in a product of plaquette and loop operators to form the boson/fermion parity operator. In the absence of the defect, the model can only be occupied by either an even or an odd number of fermions depending on the configuration of vortices occupying the model. However, as a result of the fermion parity operator's dependence on the defect string operator, both even and odd parity sectors represent physical states of the system with the defect.

A consequence of this is that introducing the defect to the model on a torus increases the ground state degeneracy from three to four in the non-Abelian phase of the model. We also confirm the expectation that zero energy fermions form in the presence of the defect, when the model is tuned to the non-Abelian phase. These zero energy fermions are localised around the defect plaquettes at both ends of the defect line. This is identical to how the presence of vortex pairs affect the model's spectrum. In fact the true ground state of the model is in the two vortex sector where both of the defect plaquettes at the ends of the defect line are occupied by vortices. The presence of the vortex pair cancels the effect of the defect plaquettes on the spectrum, in much the same way vortices on the same plaquette annihilate each other, thereby minimising the energy. We also briefly discussed how the presence of the defect affects the braiding of

anyons in the model.

We note we would expect the same results in other Kitaev like models which can be solved using an Jordan-Wigner transformation such as the Yao-Kivelson model and the square-octagon model [54, 55]. Namely, on a four-valent lattice, introducing a defect that reduces the number of plaquettes to be less than the number of sites will introduce a symmetry associated with the defect. For example, on a torus, the Euler characteristic of the lattice must be 0 regardless of the exact geometry of the lattice. If the lattice has N sites and the presence of a defect meant the number of plaquettes is $N-1$, then we must have:

$$\begin{aligned} \chi &= V - E + F, \\ \implies 0 &= (N) - E + (N-1), \\ \implies E &= 2N - 1. \end{aligned}$$

This means there are not enough edges to link the sites such that the resulting lattice is four-valent. We are one short. If there are no sites that are linked to more than four edges, this implies there are exactly two sites that are trivalent (one for each end of the missing edge). For a Kitaev like Hamiltonian we would expect a symmetry of the model associated with a string connecting these two sites. Such a symmetry would be constructed by composing the link interactions going along the string.

We would also expect to find a dependence of fermion parity on loop symmetries, for lattices with odd length, and on the defect symmetry when the model has a lattice defect. Where the fermion parity is given by a product of plaquette symmetries associated with some pattern covering the whole lattice, a lattice with an odd length or with a lattice defect may break the pattern along a string. In that case the parity will be given by a product of plaquette symmetries associated with the broken pattern and a symmetry associated with the string the pattern is broken along. This symmetry should be expressible in terms of the defect, loop and plaquette symmetries.

We extended the solution of the model to lattices with different topologies.

We began the chapter with a discussion of lattices tiling surfaces of genus two and introduced a hexagonal piece of square lattice which we can use as a building block to construct lattices tiling surfaces of higher genus. Specifically, to create a lattice of of genus $g > 2$ we need to combine $g - 1$ copies of the hexagon piece and implement the appropriate boundary conditions. Then we described how the model on such a lattice can be solved using the solution from the previous chapters. This involved defining a procedure for assigning Jordan-Wigner type string operators to each site of the lattice and defining vortex operators for defect plaquettes, that are required to be present in the lattice to give it the required Euler characteristic. The contribution of these defect plaquettes to the model's time-reversal and parity-breaking potential was also defined. We then identified $2g$ homologically non-trivial 1-chains of the lattice to be used for defining loop symmetries of the model. Expressing the Hamiltonian in terms of products of loop symmetries and vortex operators involved identifying the homology class of loops assigned to links by terms in the Hamiltonian involving products of string operators. The resultant expression for the Hamiltonian highlights the dependence of the model on the first homology group of the underlying lattice.

This solution was then used to calculate the ground state degeneracy of the model on lattices of genus two up to six and found our results match with theoretical expectations. The main result of this chapter is that it presents a tool for conducting numerical experiments involving properties of the Kitaev honeycomb model and its excitations on surfaces of genus $g \geq 2$. This work provides a direct realisation of two distinct topological quantum field theories, specifically the Abelian doubled-$\mathbb{Z}_2$ and non-Abelian Ising theory, on closed surfaces of higher genus. As such it provides a solid basis for further investigation of the model on various manifolds, including manifolds with boundaries which would extend previous studies of the Kitaev model [50]. Following recent work on the time-dependent simulation of the annihilation of vortex-like excitations on defects in the Kitaev model [44], an interesting

direction for further investigation is the possibility of a dynamical process where the creation and annihilation of extrinsic defects would result in the dynamical change of the model's genus and thus its topology. Interestingly this incarnation of topological field theory would be close to its axiomatic definition as a modular functor from a monoidal category of cobordisms to that of vector spaces [14, 16].

Another direction would be the time-dependent simulation of braiding vortex excitations with the ends of the line defect introduced in chapter 3. As suggested by Kitaev [18] and shown by Petrova et al. [37], introducing dislocation defects in the Abelian phase of the honeycomb model enables more complex fractional statistics. It would be interesting to see how one could facilitate braiding using our description of the model, especially in the non-Abelian phase. One potential issue in this direction is the dynamics of the parity of fermions. Consider a system with a defect and a pair of vortices such that the parity of fermions in the model is even. Taking one of the vortices and braiding it around one of the ends of the defect by moving it through the defect changes the parity of fermions. This is because the parity of branch cuts going through the defect is changed meaning the eigenvalue of the string defect operator appearing in the parity operator changes sign. However, if one were able to braid vortices and defects, it would be interesting to identify what the braiding statistics of the defect end points are, to see what qubit gates could be implemented by such braiding and if the allowed gates meant that universal quantum computation was achievable in the system with a defect.

Combining the results of chapters 3 and 4 and looking at line defects in lattices with higher genus, we can predict the ground state degeneracy of the model in such a scenario. Recall, the line defect has a symmetry associated with it. This symmetry appears as a factor in the parity operator for fermions which means states of both odd and even parity represent physical states of the model. It is, therefore, easy to see why one would expect the ground state degeneracy for the model on such a lattice to be equal to the number of homology sectors

(4^g) regardless of what phase the model is tuned to or if the lattice size is even or odd. However, the presence of different homologically non-trivial loops and two (or possibly more) different types of defect plaquettes could enable one to perform very complex and curious braids between vortices and defects. So studying such lattices is still a promising possibility for future research.

Systematically investigating the existence of zero modes in the presence of different defect plaquettes would also be intriguing. When we introduced a line defect into the model, we found zero energy fermions, in the vortex free sector, localised around the five sided defect plaquettes at either end of the line. On the other hand, when we put the model on a lattice with genus $g > 1$, we did not find any zero energy fermions in the vortex free sector associated with the twelve sided plaquettes of the lattice. This might be understood using perturbation theory in the $J_x, J_y << J_z$ limit. In this limit, the vortex operator of a plaquette with n sides contributes to the Hamiltonian at n-th order of perturbation theory. The perturbative expansion of the Hamiltonian turns out to be an alternating sum where the even order terms appear with a negative sign and odd terms appear with a positive sign. This indicates which plaquettes need to by occupied by vortices in order to calculate the ground state. Namely, the odd sized plaquettes need to be occupied. We used precisely this in chapter 3 to identify which vortex sector contained the ground state of the model with a line defect. Hence, in the vortex free sector one may expect to find excitations associated with the odd sized plaquettes in the form of zero energy fermions attached to them. In the honeycomb picture of the model however, both types of defect plaquettes we have discussed have an even number of edges (an eight sided plaquette at either end of the line defect and an eighteen sided plaquette on a lattice with genus $g > 1$) and the relationship between the existence of zero energy fermions and the geometry of certain plaquettes is not immediately clear. A deeper understanding of this relationship may lead to a very useful generalisation of Lieb's theorem which could identify which sector the ground state of the model is in for any given lattice.

Appendix A: Homology

Here we give a brief overview of the basic concepts, terminology and notation borrowed from the field of homology and used in the main body of this thesis. For a more complete description of homology theory and its relevance to lattice systems see [56, 57]. When we talk about the homology of a lattice in this thesis, we are specifically talking about a certain brand of homology known as $\mathbb{Z}_2$-homology. The central idea behind the homology of a lattice is to use the lattice to construct a family of vector spaces known as the homology groups. These homology groups contain information about the topology of the lattice they were constructed from.

In order to construct the homology groups from a lattice we first need to construct an auxiliary set of vector spaces known as the p-chain groups. A p-chain group is a vector space of p-dimensional objects which make up the defining lattice. We will only be considering two dimensional lattices here. Therefore, the only non-trivial p-chain groups we will discuss are the 0-chain, 1-chain and 2-chain groups related to the vertices, edges and faces of the lattice respectively.

The p-chain groups are defined as follows: Given a lattice, we can consider the set of all vertices V, the set of all edges E, and the set of all faces (plaquettes) of the lattice F. The power set of E can be given a vector space structure over the field $\mathbb{Z}_2$ by defining addition and scalar multiplication as follows. If $a, b \in P(E)$, we define the addition of a and b as follows (see Fig. 5.1).

$$a + b = a \cup b \setminus a \cap b.$$

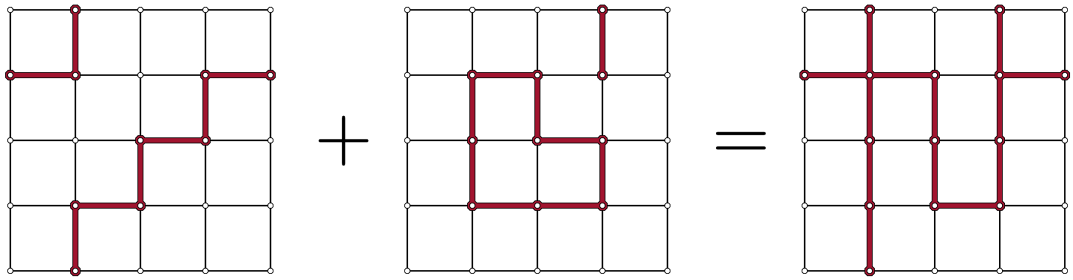

Figure 5.1: Depicted above is a graphical representation of the addition of two 1-chains. As a 1-chain is a subset of E, we can represent it by colouring each edge which is an element of the 1-chain. Here, we have coloured an edge red if it is an element of the 1-chain and black if it not.

If $\lambda \in \mathbb{Z}_2$, we define scalar multiplication as:

$$\lambda \cdot a = \begin{cases} a & \text{if } \lambda = 1 \\ \emptyset & \text{if } \lambda = 0 \end{cases}$$

It is straight forward to check that the tuple $(P(E), +, \cdot)$ forms a vector space with the empty set playing the role of the zero vector. As edges are one dimensional objects, an element of this vector space is known as a 1-chain and we denote the vector space by C_1. The power sets of V and F can also be given a vector space structure in the same way. Since vertices are zero dimensional objects, the vector space $(P(V), +, \cdot)$ is denoted by C_0, elements of which are called 0-chains. Similarly, as a lattice face is a two dimensional object, C_2 denotes the vector space $(P(F), +, \cdot)$ whose elements are called 2-chains.

The next step in constructing the homology groups is to define the boundary operator d_p for p-chains. The operator d_p is defined to map a p-chain to the $(p-1)$-chain representing its boundary. For example, if a is a 2-chain then $d_2 a$ is the 1-chain that borders that 2-chain (See Fig. 5.2). For p-chains with no boundary, the application of the boundary operator yields the zero vector in C_{p-1}. As of yet, there is no C_{-1} group. However, it is clear that every 0-chain has no boundary and so the application of d_0, as defined, should yield the zero vector in C_{-1}. Hence, for d_0 to be well defined, it is usual to define C_{-1} as a trivial vector space consisting of only a zero vector. It is an easy exercise to

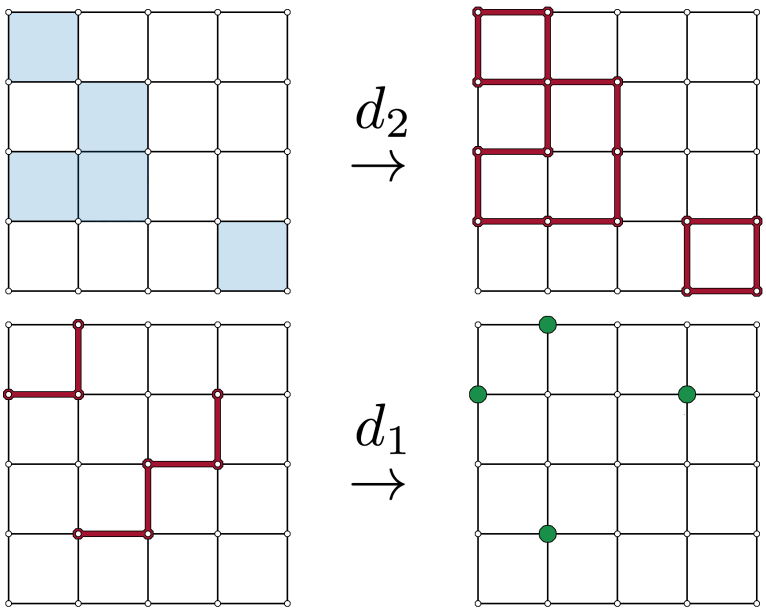

Figure 5.2: Here, we show a graphical representation of the action the the boundary operator on 2-chains and 1-chains. We graphically represent 1-chains as we did in Fig. 5.1. Similarly, as 2-chains are subsets of faces, we represent a 2-chain on a picture of the lattice by colouring its elements in blue. Likewise, we represent a 0-chain by colouring its elements in green. In the top two images we show an example of a 2-chain and its image under the boundary operator. In the bottom two images we show an example of a 1-chain and the 0-chain representing its boundary.

show the boundary operator is a linear operator. An obvious yet important property of the boundary operators is the following:

$$d_{p-1}d_p = 0.$$

where zero here is the operator which maps all p-chains to the zero vector in C_{p-2}. This simply states that a $(p-1)$-chain representing the boundary of a p-chain has no boundary. The subscript of the operator d_p is often omitted in the literature as it is usually clear from context which boundary operator is being used.

Within C_1 are two subspaces which will define the first homology group of the lattice. These are $Z_1 \equiv \ker(d_1)$ and $B_1 \equiv \mathrm{Im}(d_2)$. The first subspace, Z_1, is the vector space of 1-chains which have no boundary, known as 1-cycles. The second subspace, B_1, is the space of 1-chains which are the boundary of some

2-chain. We note that the subspace B_1 must also be a subspace of Z_1 since the following statements are equivalent:

$$\mathrm{Im}(d_2) \subset \ker(d_1) \quad \text{and} \quad d_1 d_2 = 0.$$

We can define an equivalence relation $\sim$ on the space of 1-cycles using the space of boundaries by saying two 1-cycles are equivalent if their sum is the boundary of some 2-chain. That is, if $a, b \in Z_1$,

$$a \sim b \iff a + b \in B_1, \tag{5.1}$$

in which case the cycles a and b are said to be homologous. The first homology group is then defined as the group of equivalence classes (or homology classes) under $\sim$, namely, the quotient space of Z_1 and B_1.

$$H_1 = {}^{Z_1}\!/_{B_1}. \tag{5.2}$$

As both Z_1 and B_1 are vector spaces, H_1 is also a vector space. The equivalence class containing the zero 1-chain plays the role of the zero vector. Elements of this class represent the boundaries of 2-chains and are called homologically trivial. Non-zero elements of H_1 contain 1-cycles which are not the boundary of a 2-chain. Such 1-cycles can only exist if the underlying lattice has a one dimensional hole and in this way the first homology group H_1 of the lattice holds information about its topology.

Appendix B: Higher Genus Calculations

In Fig. 5.3 we present the results of the calculations described in section 4.3 for odd and even sized lattices with genus $g = 3, 4, 5, 6$. Namely, we plot the difference in energy between the fermionic ground states in each of the homology sectors (of which there are 4^g) and the homology sector with the lowest ground state energy as a function of $J = J_x = J_y$ while we fix $J_z = 1$, $\kappa = 0.2$. We also plot the difference in energy bewtween the first excited state in each of the homology sectors and the lowest ground state energy to show the energy gap bewteen the ground states and the first excited states. The odd sized lattices have $N_a = N_b = N_c = 5$ while the even sized lattices have $N_a = N_b = N_c = 6$. We see that, for the system with even dimensions in the Abelian phase ($J < 0.5$), the fermionic ground states from all homology sectors are degenerate while for systems with odd dimensions, only half of these states are degenerate. However, as the system approaches the phase transition at $J = 0.5$ these states split with some of them becoming excited states in the non-Abelian phase ($J > 0.5$) while the rest of the states join some of the first excited states, which drop in energy at the phase transition, to form the degenerate ground state. The degeneracy in the non-Abelian phase does not depend on the lattice size.

Calculating the ground state energy of the model in a particular vortex/homolgy sector, and for a particular set of values for J_x,J_y,J_z and κ, involved the full diagonalisation of the single particle Hamiltonian of the model (i.e. the matrix appearing in (4.22)). The size of the single particle Hamiltonian matrix

ranged from 175×175 for odd sized lattices on a genus 2 surface to 1260×1260 for even sized lattices on a genus 6 surface. Once the spectrum of the single particle Hamiltonian has been calculated, the ground state energy was calculated using (2.51). These computations were done using MATLAB and its interface with the Fortran library ARPACK to diagonalise matrices using Arnoldi iteration. All numerical results presented in this thesis were calculated on a MacBook Pro with a 2.6 GHz Intel Core i7 processor and 8 GB 1600 MHz DDR3 memory. The code used to calculate the results in chapter 4 can be found at: https://github.com/johnb90/KitaevHoneycombHigherGenus. The code used to calculate the results in chapter 3 can be found at: https://github.com/johnb90/KitaevHoneycombDefect.

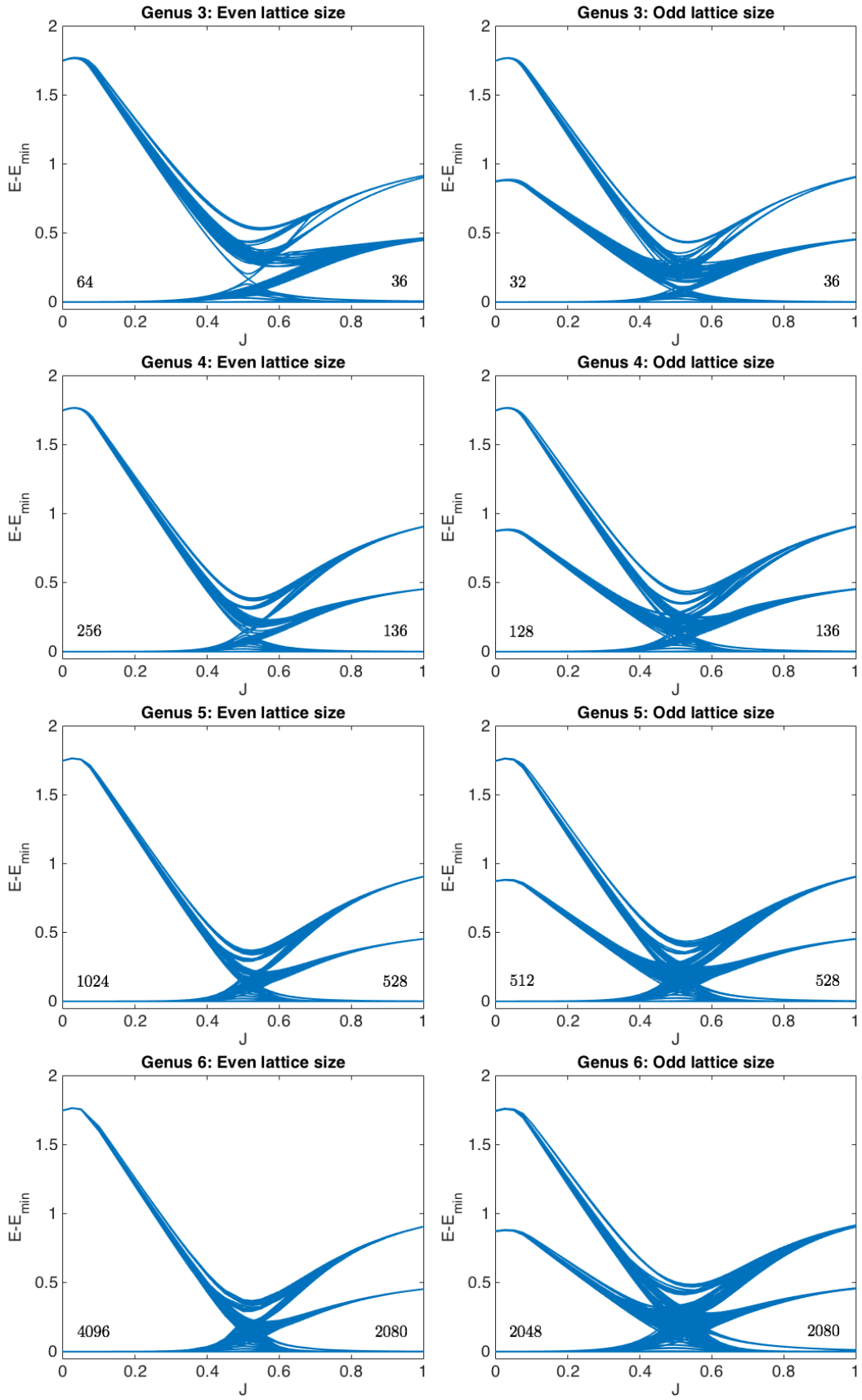

Figure 5.3: Here we plot the difference in energy between the fermionic ground states in each of the homology sectors and the homology sector with the lowest ground state energy as a function of $J = J_x = J_y$ while we fix $J_z = 1$, $\kappa = 0.2$. We do this for both odd and even sized lattices with genus $g = 3, 4, 5, 6$. The number of degenerate ground states is included just above the lowest curves in both the Abelian and non-Abelian phases.

Bibliography

[1] V. L. Ginzburg and L. D. Landau. On the theory of superconductivity, 1950.

[2] D. C. Tsui, H. L. Störmer, and A. C. Gossard. Two-dimensional magnetotransport in the extreme quantum limit. *Phys. Rev. Lett.* **48**, *1559*, 1982.

[3] X. G. Wen. *Quantum Field Theory of Many-body Systems.* Oxford University Press, 2007.

[4] X. G. Wen. An introduction of topological orders. *http://dao.mit.edu/˜wen.*

[5] X. G. Wen. Topological order in rigid states. *Int. J. Mod. Phys. B4, 239*, 1990.

[6] X. G. Wen and Q. Niu. Ground-state degeneracy of the fractional quantum hall states in the presence of a random potential and on high-genus riemann surfaces. *Phys. Rev. B* **41**, *9377*, 1990.

[7] X. G. Wen. Vacuum degeneracy of chiral spin states in compactified space. *Phys. Rev. B* **40**, *7387*, 1989.

[8] H. K. Onnes. *Leiden Comm. 122b, 124c*, 1911.

[9] X. G. Wen. Colloquium: Zoo of quantum-topological phases of matter, 2017.

[10] V. G. Turaev. *Quantum Invariants of Knots and 3-Manifolds.* De Gruyter, 2 edition, 2010.

[11] B. Bakalov and Jr. A. Kirillov. *Lectures on Tensor Categories and Modular Functors*. American Math. Society, 2001.

[12] E. Witten. Quantum field theory and the jones polynomial. *Comm. Math. Phys. 121, 351*, 1989.

[13] P. Watts, G. Kells, and J. Vala. From topological quantum field theories to topological materials. In S. Kais, editor, *Quantum Information and Computation for Chemistry*. John Wiley & Sons, Inc., 2014.

[14] M. Atiyah. Topological quantum field theories. *Publications Mathmatiques de l'IHS, 68 (68)*, 1988.

[15] M. Atiyah. *The Geometry and Physics of Knots*. Cambridge University Press, 1990.

[16] J. Koch. *Frobenius Algebras and 2D Topological Quantum Field Theories*. Cambridge University Press, 2003.

[17] A. Kitaev. Fault-tolerant quantum computation by anyons. *Ann. Phys.* **303**, *2*, 2003.

[18] A. Kitaev. Anyons in an exactly solved model and beyond. *Ann. Phys.* **321**, *2*, 2006.

[19] M. H. Freedman, A. Kitaev, M. J. Larsen, and Z. Wang. Topological quantum computation. *Bull. Amer. Math. Soc.*. **40**, *31*, 2002.

[20] M. Z. Hasan and C.L. Kane. Topological insulators. *Rev. Mod. Phys.* **82** *3045*, 2010.

[21] G. Kells, J. K. Slingerland, and J. Vala. Description of Kitaev's honeycomb model with toric-code stabilizers. *Phys. Rev. B* **80**, *125415*, 2009.

[22] J. K. Pachos. The wavefunction of an anyon. *Ann. Phys.* **322**, *2*, 2007.

[23] V. Lahtinen, G. Kells, A. Carollo, T. Stitt, J. Vala, and J. K. Pachos. Spectrum of the non-abelian phase in Kitaev's honeycomb lattice model. *Ann. Phys.* **323**, *2286*, 2008.

[24] Y. Yu and Z. Wang. An exactly soluble model with tunable p-wave paired fermion ground states. *Europhys. Lett..* **84**, *57002*, 2008.

[25] G. Baskaran, D. Sen, and R. Shankar. Spin-s kitaev model: Classical ground states, order by disorder and exact correlation functions. *Phys. Rev. B* **76** *115116*, 2008.

[26] S. Yang, S.-J. Gu, C.-P. Sun, and H.-Q. Lin. Fidelity susceptibility and long-range correlation in the Kitaev honeycomb model. *Phys. Rev. A* **78** *012304*, 2008.

[27] K. Sengupta, D. Sen, and S. Mondal. Exact results for quench dynamics and defect production in a two-dimensional model. *Phys. Rev. Lett.* **100** *077204*, 2008.

[28] P. Ring and P. Schuck. *The Nuclear Many-Body Problem.* Springer, 3 edition, 2004.

[29] C. Bloch and A. Messiah. The flux phase of the half-filled band. *Nucl. Phys.* **39**, *95.*

[30] E. Lieb. The flux phase of the half-filled band. *Phys. Rev. Lett* **73***(16) 2158*, 1994.

[31] A. Bolukbasi and J. Vala. Rigorous calculations of non-abelian statistics in the Kitaev honeycomb model. *New J. Phys.* **14**, *045007*, 2012.

[32] D. A. Ivanov. Non-abelian statistics of half-quantum vortices in p-wave superconductors. *Phys. Rev. Lett.* **86** *268*, 2001.

[33] A. Kitaev and L. Kong. Models for gapped boundaries and domain walls. *Commun. Math. Phys.* **313**, *351*, 2012.

[34] S. B. Bravyi and A. Kitaev. Quantum codes on a lattice with boundary. *arXiv:quant-ph/9811052*.

[35] H. Bombin and M. A. Martin-Delgado. Family of non-abelian Kitaev models on a lattice: Topological condensation and confinement. *Phys. Rev. B* **78**, *115421*, 2008.

[36] S. Beigi, P. S. Shore, and D. Whalen. The quantum double model with boundary: condensations and symmetries. *Commun. Math. Phys.* **306**, *663*, 2011.

[37] O. Petrova, P. Mellado, and O. Tchernyshyov. Unpaired Majorana modes on dislocations and string defects in Kitaev's honeycomb model. *Phys. Rev. B* **90**, *134404*, 2014.

[38] H. Zheng, A. Dua, and L. Jiang. Demonstrating non-abelian statistics of Majorana fermions using twist defects. *Phys. Rev. B* **92**, *245139*, 2015.

[39] Y.-Z. You and X. Wen. Projective non-abelian statistics of dislocation defects in a $\mathbb{Z}_n$ rotor model. *Phys. Rev. B* **86**, *161107(R)*, 2012.

[40] M. Barkeshli, Chao-Ming Jian, and Xiao-Liang Qi. Genons, twist defects, and projective non-abelian braiding statistics. *Phys. Rev. B* **87**, *045130*, 2013.

[41] B. Brown, S. Bartlett, A. Doherty, and S. Barrett. Topological entanglement entropy with a twist. *Phys. Rev. Lett.* **111** *220402*, 2013.

[42] G. Burella, P. Watts, V. Pasquier, and J. Vala. Graphical calculus for the double affine q-dependent braid group. *Ann. Henri Poincare* **15**, *2177*, 2014.

[43] A. Kapustin. Topological field theory, higher categories, and their applications, 2010.

[44] J. Brennan and J. Vala. Lattice defects in the Kitaev honeycomb model. *J. Phys. Chem. A* **2016** *120(19), pp 33263334*, 2016.

[45] Z. Liu, G. Möller, and E. J. Bergholtz. Lattice genons. *arXiv:1702.05115*, 2017.

[46] G. Kells, A. Bolukbasi, V. Lahtinen, J. K. Slingerland, J. K. Pachos, and J. Vala. Topological degeneracy and vortex dynamics in the Kitaev honeycomb model. *Phys. Rev. Lett.* **101** *240404*, 2008.

[47] N. Read and D. Green. Paired states of fermions in two dimensions with breaking of parity and time-reversal symmetries and the fractional quantum hall effect. *Phys. Rev. B* **61** *10267*, 2000.

[48] M. Oshikawa, Y. B. Kim, K. Shtengel, C. Nayak, and S. Tewari. Topological degeneracy of non-abelian states. *Ann. Phys.* **322***, 6*, 2007.

[49] T. Einarsson. Fractional statistics on a torus. *Phys. Rev. Lett.* **64**, 1995.

[50] G. Kells and J. Vala A. Zero energy and chiral modes in a p-wave magnetic spin model. *Phys. Rev. B* **82** *125122*, 2010.

[51] M. Barkeshli and X. Qi. Topological nematic states and non-abelian lattice dislocations. *Phys. Rev. X* **2** *031013*, 2012.

[52] M. Barkeshli, C. Jian, and X. Qi. Twist defects and projective non-abelian braiding statistics. *Phys. Rev. B* **87** *045130*, 2013.

[53] M. Barkeshli, H. Jiang, R. Thomale, and X. Qi. Twist defects and projective non-abelian braiding statistics. *Phys. Rev. Lett.* **114** *026401*, 2015.

[54] G. Kells, D. Mehta, J. K. Slingerland, and J. Vala. Exact results for the star lattice chiral spin liquid. *Phys. Rev. B* **81** *104429*, 2010.

[55] G. Kells, J. Kailasvuori, J. K. Slingerland, and J. Vala. Kaleidoscope of topological phases with multiple Majorana species. *New J. Phys.* **13***, 095014*, 2011.

[56] H. Bombin. Topological codes. In D. A. Lidar and T. A. Brun, editors, *Quantum Error Correction*. Cambridge University Press, 2013.

[57] D. Browne. Lectures on topological codes and quantum computation, 2014.